Influence of Temperature on Deterioration Process

of Reinforced Concrete Members

Due to Steel Corrosion

July 2005

Takahiro Nishida

Abstract

In recent years, the maintenance of reinforced concrete has been becoming major concern around the world. Especially steel corrosion induced by Cl^- or CO_2 is the main cause of deterioration progress of reinforced concrete. When above deterioration is discussed, the rates of diffusion of substance, especially diffusion coefficient of the Cl^- or carbonation coefficient, and steel corrosion are very important factors. Moreover, it is generally said that the rates of diffusion of substance and steel corrosion rise up with the temperature rising. Therefore, there is a high possibility that the deterioration progress of reinforced concrete becomes faster with the temperature rising. However, the research related to above matter is inadequate. Especially, there are few researches which explain the deterioration progress of reinforced concrete structures using Arrhenius theory, although the influence of temperature on the material diffusion and the chemical reaction can be explained by this theory.

From above backgrounds, the main objectives of this study became as follows;

1) To investigate the influence of temperature on the rate of diffusion of substance and steel corrosion in concrete induced by Cl^- or CO_2,

2) To study the influence of temperature on deterioration of reinforced concrete using the activation energy calculated by Arrhenius theory using the result of the objective (1),

3) To predict the deterioration progress of reinforced concrete considering the temperature effect.

As a result of this study, it was confirmed that the Cl^- diffusivity and carbonation coefficient of concrete increased with the temperature rising. Also the rate of macrocell and microcell steel corrosion in concrete induced by Cl^- and CO_2 increased with the temperature rising. Additionally it was confirmed that the logarithms of this phenomenon, diffusion of substance or steel corrosion in concrete, were proportional to the reciprocal of absolute temperature. This fact indicated that the deterioration of reinforced concrete due to the steel corrosion induced by Cl^- or CO_2 apparently agreed with the Arrhenius theory.

After considering the above results, the activation energies of deterioration phenomenon of reinforced concrete were calculated based on Arrhenius theory. As a result, the activation energies of diffusion of harmful substance against steel corrosion in concrete such as Cl^-, CO_2 and O_2 obtained were 12.0 to 32.2kcal/mol, 3.1 to 3.9kcal/mol and 10.5 to 23.8kcal/mol respectively. It was also confirmed that these values were largely influenced by the property of concrete, especially the pore structure of concrete derived from mix proportion. On the other hand, the activation energy of steel corrosion in concrete induced by Cl^- and CO_2 obtained were 5.2 to 19.4 kcal/mol and 7.2 to 44.5 kcal/mol respectively. These activation energies seemed to be changed with the property of concrete or the kind of substance. And it was confirmed that the rates of macrocell corrosion and the microcell corrosion had different temperature dependency. Especially, it was considered that the rate of macrocell corrosion seemed to be easily influenced by concrete resistance and the activation energy increased with the concrete resistance increasing. Also it was confirmed that the activation energy of corrosion of steel bar was almost same with that of oxygen permeability when the corrosion rate of steel bar in concrete controlled by oxygen permeability.

Finally, the deterioration progress of reinforced concrete due to steel corrosion induced by Cl^- was discussed using the data of temperature of various cities in the world. According to the results, it was confirmed that the period of incubation, propagation and acceleration varied with the regional and seasonal temperature, and the life time of reinforced concrete exponentially decreased with the temperature of the city increasing. Especially it was indicated that the environment in the cities of South-East Asian countries was the most severe environment against steel corrosion in concrete from the viewpoint of temperature effect. The life time of reinforced concrete in South-East Asia became 70% of that in mild temperature environment (20ºC). Moreover it was confirmed that the influence of temperature on the incubation period was lager than that on the propagation period or acceleration period.

Acknowledgements

~ **Contents** ~

Abstract

Acknowledgements

Contents

Chapter 1 Introduction

Chapter 2 Influence of Temperature on Cl^- Induced Corrosion in Concrete

Chapter 3 Influence of Temperature on CO_2 Induced Corrosion in Concrete

Chapter 1

Introduction.

1.1   Backgrounds
1.2   Literature Review
1.3   Objectives
1.4   Significance and Originality
1.5   Flow of This Study
Reference of Chapter 1

1.1 Backgrounds

Now the maintenance of reinforced concrete is becoming major concern around the world because of (a) the lack of good and cheap materials used for construction, (b) limitation of construction cost or (c) the lack of funds to construct new infrastructures. Therefore huge numbers of researches related to deterioration or maintenance of reinforced concrete structure were reported.

Steel corrosion induced by Cl^- or CO_2 is the main cause of deterioration of reinforced concrete. Normally the alkalinity of concrete around steel bar provides a passive environment. This passive state can be broken down by the presence of Cl^- and/or by carbonation of concrete. If O_2 and H_2O are present there, the steel bar easily starts to corrode. As the corrosion product (rust) occupies a greater volume than the original steel, the expansive pressure causes concrete to crack or spall. Especially in coastal and marine works, Cl^- induced corrosion is the most important durability issue. The basic lines for maintenance of reinforced concrete structures are, however, similar for both Cl^- induced corrosion and CO_2 induced corrosion, involving the use of high quality impermeable concrete of adequate thickness as steel protection.

Hence, it is generally said that most of the diffusions of substance and the chemical reactions are speeded up with the increase of the temperature. As the deteriorations of concrete are also based on diffusion or chemical reaction, it is considered that the deterioration progress also has the temperature dependency.

Additionally some developed countries such as USA, EU or JAPAN has individual standard for construction materials or construction methods of reinforced concrete from their experience under the mild temperature condition (almost 20ºC). Now some developing countries follow the above standards without enough local investigations. When they have investigations for the applying the standard made in another country to their country, temperature becomes one of the most important parameters as well as materials used.

In view of the above it is necessary to know the influence of temperature on the deterioration progress of reinforced concrete due to steel corrosion and discuss about the appropriate maintenance method under the several temperature conditions.

1.2 Literature Review

This study was preceded based on the literature surveys related to (a) the steel corrosion in concrete, (b) influence of temperature on deterioration of reinforced concrete, and (c) deterioration progress in concrete due to steel corrosion induced by Cl^- or CO_2. In this section, the various information dealing with the above subjects were reviewed.

1.2.1 Steel Corrosion in Concrete

(1) Mechanism of steel corrosion in concrete[1-1), 1-2), 1-3)]

The steel corrosion in concrete occurs mainly due to the existence of Cl^- or carbonation of concrete, with the co-existence O_2 of and H_2O. This corrosion mechanism can be explained based on electrochemical concept as explained below. When metals corrode, the electrochemical corrosion cell is generated in the surrounding electrolyte as shown in **Fig.1.2.1**[1-2)]. In this corrosion cell, cathode is the

pole that receives an electron and the anode pole releases an electron to the electrolyte. Generally, the corrosion product (rust) occurs at anode. The anodic metal releases electrons and turn to be metal ions that solved in an electrolyte. Considering these anodic and cathodic reactions as one system, it is clear that the metal surface in the electrolyte has a different electrical potential. The steel corrosion in concrete can be described as the reaction shown in Equation (1-1) to (1-3).

$$Fe \rightarrow Fe^{2+} + 2e^- \qquad\qquad\qquad (1-1)$$

$$O_2 + 2H_2O + 4e^- \rightarrow 4OH^- \qquad\qquad\qquad (1-2)$$

$$2Fe + O_2 + H_2O \rightarrow 2Fe(OH)_2 \qquad\qquad\qquad (1-3)$$
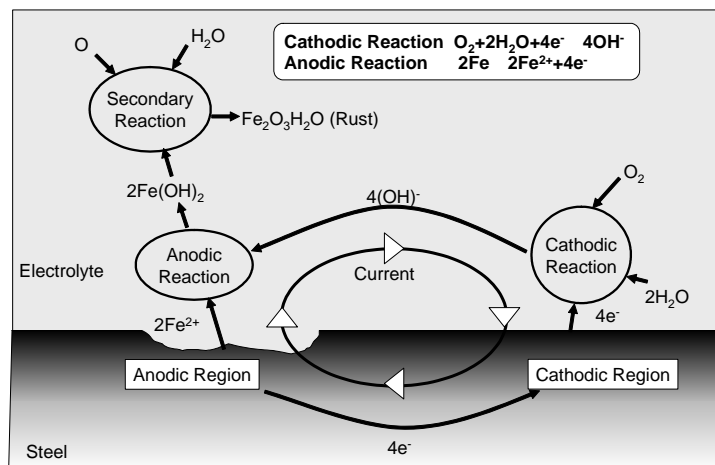
Fig.1.2.1 Corrosion Reaction in Concrete

Based on the reaction formula above, the electrical current density of 100 μA/cm^2 can be translated to corrosion rate of 1.16mm/year as shown in Equation (1-4) [1-4].

$$\frac{100 \times 10^{-6}(A/cm^2)}{96500(C)} \cdot \frac{55.85(g/mol)}{7.86(g/cm^3) \cdot 2} \cdot 3.1536 \times 10^7 = 1.16(mm/year) \qquad (1-4)$$

The formation of corrosion cells may be generated in two ways as (a) due to significant variations exist in surface characteristics of the steel and (b) due to the concentration cell formed with the variation of dissolved ions in the vicinity of steel, such as Cl^- and O_2. And the steel corrosion in concrete is almost divided into two patterns as macrocell corrosion and microcell corrosion. And the below here macrocell and microcell will be further discussed.

(2) Macrocell corrosion and microcell corrosion

Macrocell corrosion occurs when anode and cathode are absolutely separated by several centimeters. This macrocell corrosion likely occurs when different parts of the steel are subjected to different environment. The anodic region and the cathodic region may be visibly separated due to the difference of Cl^- concentration, O_2 concentration, and local depassivation due to materials segregation, the cracks or the construction defects such as cold-joint and so on. For example, the parts with the relatively high Cl^- or the relatively low pH have a high potency to be an anode. As the anode parts and the cathode pars are completely separated, the steel corrosion in concrete occurred is very locally harsh.

On the other hand, microcell corrosion occurs when anode and cathode are uniformly distributed. And the completely uniformed corrosion is produced. Compared to the macrocell corrosion, microcell corrosion relatively occurs in a low rate and in a long term.

As mentioned above, the steel corrosion in concrete occurs with the presence of O_2 and H_2O condition. However the steel in normal concrete is protected to corrode with the formation of passivity film with the thickness of 10^{-3} to 10^{-1} μm as shown in **Fig.1.2.2**. And the passivity film can be broken due to two reasons as from the effect of the sufficient concentration of Cl^- or carbonation of concrete.
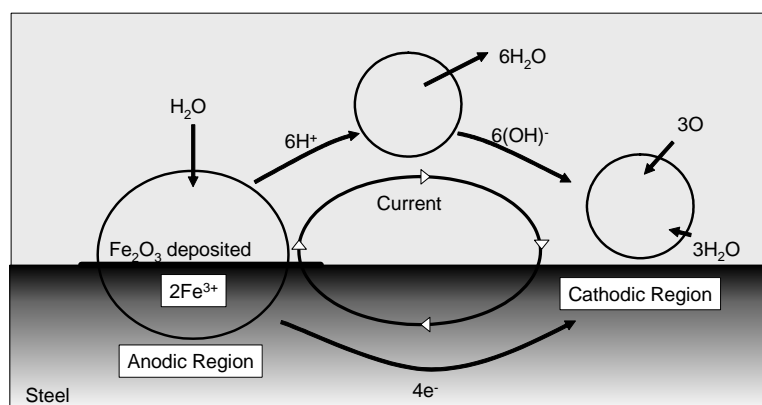
Fig. 1.2.2 Passivating Reaction in Concrete

(3) Cl^- induced corrosion

As the Cl^- reaches to the steel surface, the passivity film is dissolved and the steel is exposed directly to O_2 and H_2O, which then lead the steel corrosion to take place. Several theories have been proposed to explain the apparent catalytic role of Cl^-, notably the "Adsorption theory" and "oxide film theory" [1-5]. The former theory suggests that Cl^- are preferentially adsorbed with metals instead of O_2 and OH^-, while the later suggests that Cl^- penetrate the oxide film much more readily than other anions. Thus Cl^- causes the passivation layer to loss material by forming soluble chloro-complexes at its outer boundary. Glasser et. al.[1-6] reported that even low bulk level of Cl^-, 0.01 wt.% of cement, could initiate the process of depassivation. This suggestion that the pH is lowered by the presence of Cl^{-}[1-7] appears improbable, it would require extensive replacement of OH^- by Cl^- to lower pH sufficiently to create acidic pits in an otherwise highly buffered alkaline medium of pH 13.0 to 14.0. K.K. Sagoe[1-8] concluded the breaking of the passivation film as semi passive and the active state of steel corrosion as follows;

The semi passive state, which is considered to be representative of the condition of most real concrete structures, has a duplex interfacial structure comprising an inner spinel layer and an outer mixture of goethite and spinel. Low Cl^- concentration as 0.01%wt of cement accelerates corrosion rates and changes the mineralogy of the film to favor the development of akageneite. Preliminary studies indicate that Cl^- accelerate depassivation by forming intermediary iron-chloro complexes rather than by direct attack of the substrate steel.

(4) CO_2 induced corrosion

The hydration reaction of cement produced a calcium hydrate that then remained as a pore solution. The existence of this pore solution assures the high alkalinity in the pH levels of 12.0 to 13.0 of cement paste in concrete. However the penetration of CO_2 into concrete neutralizes this pore solution and gradually reaches the steel surface. Evans reported that the steel corrosion in concrete begins as the pre solution pH downgraded until below 10 because in this range of pH the passivity film was broken down[1-9]. The carbonation reaction equation is shown in Equation (1-5).

$$Ca(OH)_2 + CO_2 \rightarrow CaCO_3 + H_2O \qquad (1-5)$$

(5) Influential factors of steel corrosion in concrete

(a) Influence of water-cement ratio

Water-cement ratio in the original mix plays a decisive role in determining the pore structure of the hardened cement past. The excess water which can not be consumed in the hydration process is the direct cause of the high degree of porosity in ordinary cement[1-10]. This high degree of porosity causes to increase the penetration rate of the aggressive ions inside concrete and subsequently the depassivation of reinforcing steels. The influence of water-cement ratio on the oxygen permeability is as shown in **Fig.1.2.3**[1-11]. It is seen that as the water-cement ratio increases oxygen permeability also increases. The influence of carbonation depth with water-cement ratio is as showed in **Fig.1.2.4**[1-12]. It shows that the water-cement ratio increases the carbonation depth increases that can be explained due to the increase in permeability. Ohno[1-13] reported that rust area increases as the water-cement ratio increases. The narrower and more twisted the pores of the hardened cement pastes the more the transport is obstructed and this reduces the corrosion rate. Miyazato[1-14] reported that in case of Cl⁻ induced corrosion, the decrease of the water-cement ratio made the macrocell corrosion activated. On the other hand, increasing the water-cement ratio made the microcell corrosion activated.
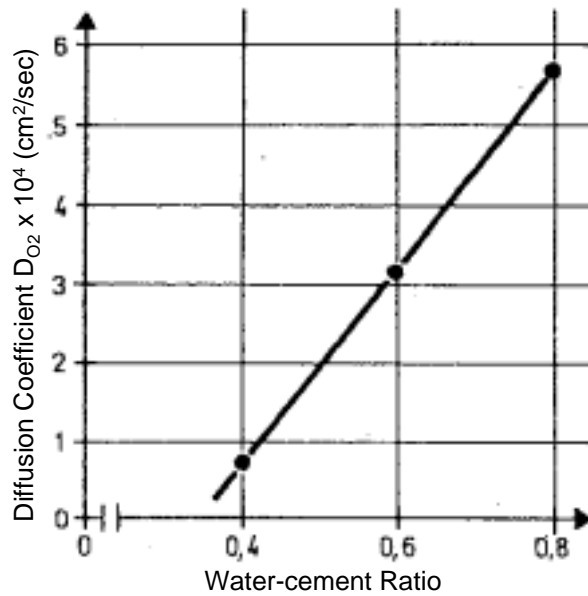
Fig. 1.2.3 Influence of Water-cement Ratio on Oxygen Permeability
Portland Cement, Curing 7days, 65 %R.H[1-11].
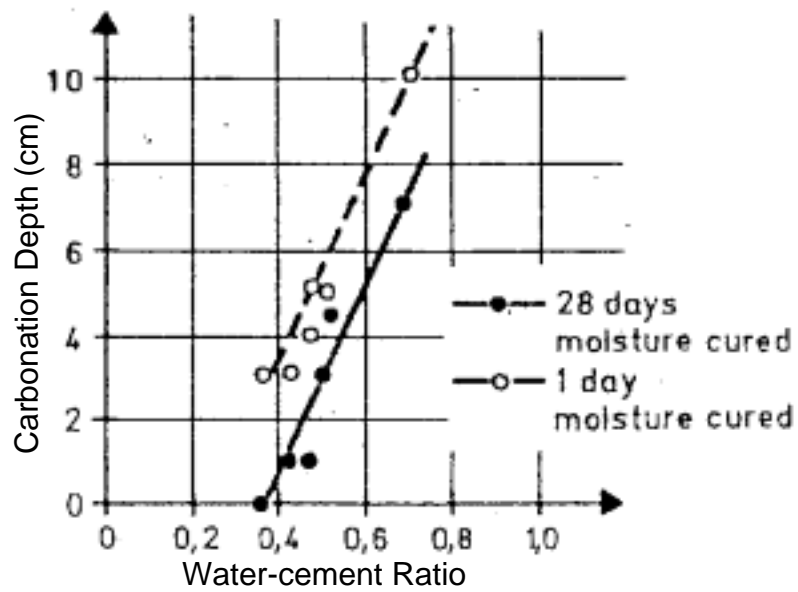
Fig.1.2.4 Influence of Water-cement Ratio and Curing on Carbonation Depth
Exposure Time: 9 months, Place: Bahrein, Middle East[1-12]

(b) Influence of pH of concrete

The progress of steel corrosion in concrete is easily influenced by pH in pore solution surrounding steel. Evans[1-9] reported that the corrosion rate increased as the pH of concrete decreased in the condition of pH lower than 10 as shown in **Fig.1.2.5**

Pourbaix proposed the practical potential-pH relation of iron in the solution with/without Cl[1-2] as shown in **Fig1.2.6** and **Fig.1.2.7** respectively. From these relations, it was confirmed that the corrosion of the iron in concrete was difficult to be generated under the environment without Cl⁻ or with high pH. On the other hand, it was confirmed that the corrosion of the iron in concrete was easy to be generated under the environment with Cl⁻ or with low pH.
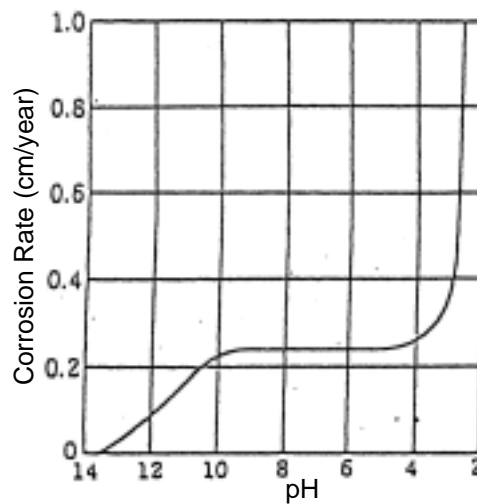
Fig.1.2.5 Relationship between Corrosion Rate and pH[1-9]
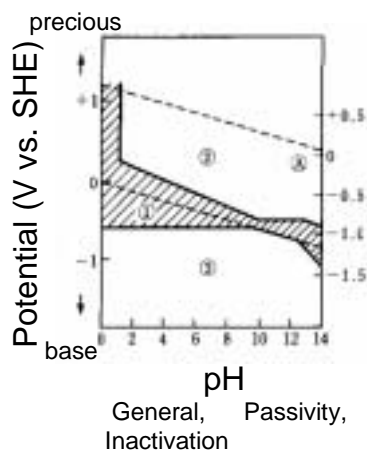
Fig.1.2.6 Potential-pH Diagram (Without Cl⁻)[1-2]
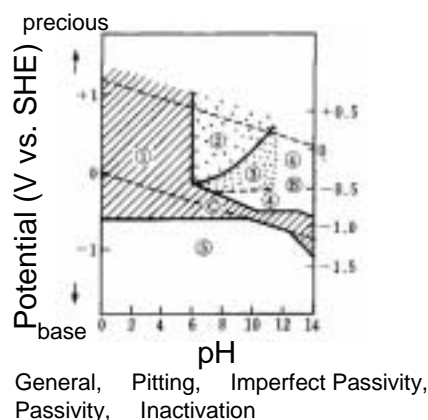
Fig.1.2.7 Potential-pH Diagram (With Cl⁻)[1-2]

(c) Influence of O_2 diffusivity

The O_2 diffusivity largely influences on the corrosion rate because it is used in cathodic reaction on the steel surface as mentioned in Equation (1-2). Regarding the influence of O_2 permeability on corrosion rate of steel bar, the following researches were reported.

Gjørv et al.[1-15] obtained the relation as shown in **Fig.1.2.8** by measuring the diffusion speed of O_2 in concrete which was submerged in the water. According to this relation, the diffusion quantity of the O_2 up to steel bar decreased, as the water-cement ratio decreased or as the concrete cover increased.
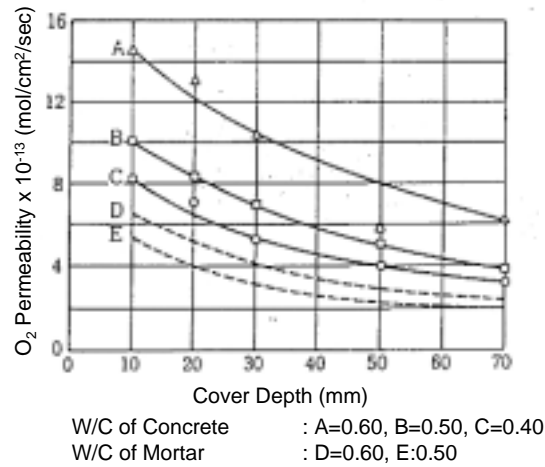
Fig.1.2.8 Influence Cover Depth and Water-cement Ratio on O_2 Permeability[1-15]

Moreover, Miyagawa et al.[1-16] investigated that the influence of concrete cover, water-cement ratio, curing condition and humidity on the O_2 permeability using reinforced concrete specimen. As a result of this investigation, in the young age concrete, the permeation of the O_2 was suppressed, as water-cement ratio decreased as shown in **Fig.1.2.9** Additionally according to **Fig.1.2.10**, which shows the effect of the relative humidity on the permeability of the O_2, O_2 permeation in concrete with 85%RH was larger than that with 60%RH.
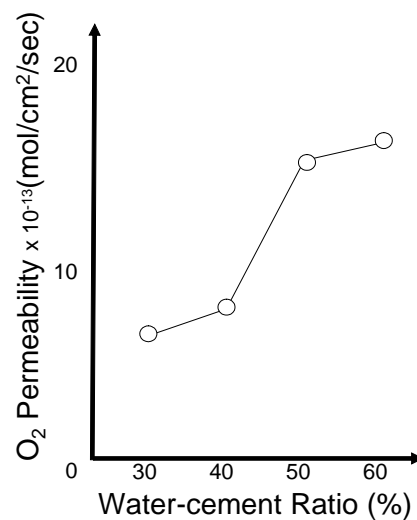
Fig.1.2.9 Influence of Water-cement Ratio on O_2 Permeability[1-16]
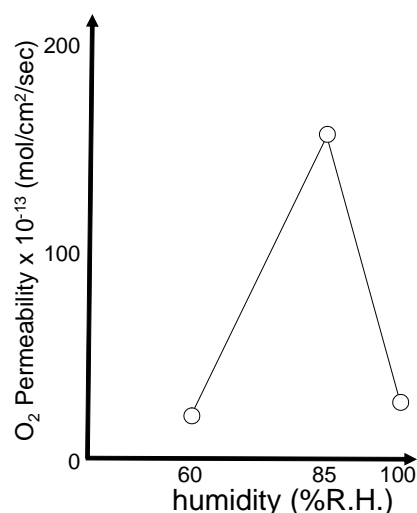
Fig.1.2.10 Influence of Humidity on O_2 Permeability[1-16]

(d) Influence of use of mineral admixtures

Fly ash, blast furnace slag, and silica fume are typical mineral admixtures for concrete[1-17]. Compared to OPC, blended cements those containing fly ash, blast furnace slag, silica fume, or natural pozzolans, are generally thought to have a finer pore structure[1-18] and they are more resistant to penetration of Cl^- from the environment[1-19]. Moreover, their sensitivity to high temperature curing is the opposite of that of OPC. Whereas OPC develops a coarse pore structure when hardened at high temperature, blended cements with slag or fly ash develop an even finer pore structure at high temperature than at room temperature[1-20]. The reason for the different chloride penetration is related to the fact that bleeding is reduced when a fine pozzolan is used thus preventing channeling at the paste aggregate interface. Related to the above, the rapid movement of Cl^- at the paste-aggregate interface in concrete was demonstrated in literature survey[1-21].

(e) Influence of casting direction, materials segregation etc.

It was observed that the horizontal steel has the higher rust area than the vertical bars depending on the casting direction[1-22]. The probable reason is explained as the poor structure between steel and cement matrix in the case of horizontal steels.

Kosmatka[1-23] reported that the bleeding water was the clear water that could gradually accumulate at the surface of freshly placed concrete, mortar, grout or paste. Bleeding water is caused by sedimentation or settlement of skid particles (cement or

aggregate). Eventually, the bleeding water is beneficial for reducing plastic shrinkage of concrete. However in the case of steel-concrete interface and aggregate-paste interface it may accumulate and create the weaker paths to infiltrate the aggressive ions and thereby acceleration corrosion. Bleeding water channels[1-23] also tend to migrate along the side of the coarse aggregates and also reduces the paste aggregate bond. This condition can partially be reduced by revibration the concrete after some bleeding has occurred[1-23].

1.2.2 Influence of Temperature on Deterioration of Reinforced Concrete

Most of the substance diffusion and the chemical reactions are speeded up with the increase of the temperature. Here the literature surveys related to the influence of temperature on deterioration of reinforced concrete were reviewed.

(1) Influence of temperature on Diffusion of substances

Fig.1.2.11 shows the influence of temperature on environmental aggressively reported in CEB code 84[1-24]. The scale is defined such that the aggressively is directly proportional to the cover required to produce a uniform risk of attack.
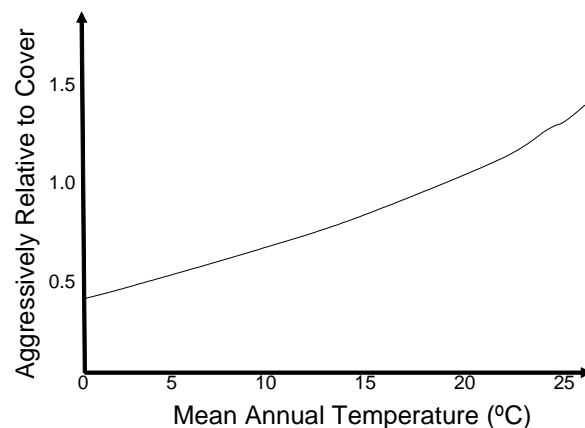
Fig.1.2.11 Influence of Temperature on Environmental Aggressively to Cover[1-24]
(CEB Code)

Maruya et. al. examined the situation of the diffusion of Cl^- in the concrete specimen which is exposed to the high-temperature and low humidity condition in order to simulate the deterioration of groundwater with high concentration of Cl^-[1-25]. As a result the following conclusions were obtained in high-temperature and low-humidity condition. (a) The diffusion of Cl^- in concrete is faster than the normal situation. (b) In the influence of crack in high temperature becomes larger than that in the normal situation.

Mori et. al. reported that the carbonation coefficient of concrete became large with temperature rising from the results of experiment under the condition with 10% of CO_2 gas and 80% of relative humidity. In this experiment the carbonation coefficient of concrete at 40℃ was twice of that at 20℃[1-26]. Ryu et. al. also conducted the same investigation and reported that the carbonation coefficient of concrete at 30℃ was 1.7 times of that at 10℃ under the condition with 5% of CO_2 gas and 60 % of relative humidity[1-27].

(2) Influence of temperature on steel corrosion

Detwiler et. al. [1-28] studied the influence of the curing temperature on the durability of reinforced concrete especially steel corrosion in concrete. By changing water-cement ratio, the Cl^- diffusivities were investigated on 5, 20, 50 degrees centigrade of curing temperature. In addition, the accelerated corrosion test was carried out, and corrosion situation of steel was observed. As a result, it was confirmed that resistance of Cl^- penetration of concrete decreased as curing temperature rises and that steel corrosion in concrete increases. Also it was confirmed that this tendency increased when the water-cement ratio was low.

Regardless of the significance of the influence of temperature on the corrosion rate of concrete reinforcement, the related data in the literature are very limited. For example, Tuutti[1-29] considers the ambient temperature with O_2 diffusion for significant controlling factor of the corrosion process. According to him, in the interval of -20 ℃ to +20 ℃, the dependence of corrosion rate is linear, and the corrosion rate increased 100 times. However, in the interval +10℃ to 20 ℃ the rate of increase was only 7 times[1-29]. Schiessel and Raupach reported that when the ambient temperature was increased from 15 ℃ to 20 ℃, corrosion current increased by about 50%[1-30), 1-31]. These

data show and confirm the significance of the ambient temperature as a factor of the corrosion rate of steel bar.

Also Zivica[1-32), 1-33)] reported that the increase of ambient temperature on the corrosion rate of steel bar induced by Cl^- in mortar with the size of 4 x 4 x 16 (cm) had two effect (a) acceleration of the rate when the ambient temperature was increased to about 40 ºC, and (b) inhibition of the rate when the ambient temperature was increased over the given value of the temperature. A thorough analysis of the corrosion process showed that the decrease of the content of O_2 and H_2O in the pore solution in the corroding system as a cause of the mentioned effects. The direct consequence of the decrease of the content in both vital reactants was the gradual inhibition of the cathodic reaction, and finally the inhibition of the corrosion process as a whole.

(3) Activation energy

It is generally said that the activation energy of diffusion phenomenon was from 2.4 to 10.8 kcal/mol[1-34)]. Related to this, C. L. Page et. al. investigated the activation energy of O_2 or Cl^- diffusion in saturated cement paste[1-35), 1-36)]. In the above investigations, it was reported that the activation energies of diffusion of O_2 and Cl^- in the cement paste with 0.4, 0.5 and 0.6 of water-cement ratio were 4.5, 5.3 and 3.6 kcal/mol and 10.0,10.7 and 7.7 kcal/mol respectively. Additionally they concluded that the activation energy decreases in high water-cement ratio because of the increase of the connected void.

Uomoto et. al. investigated the influential factors of carbonation coefficient. In this investigation, they reported that the activation energy of carbonation in concrete was 5.09 kcal/mol[1-37)].

Beverly J. Alexander et. al. studied the activation energy of corrosion reaction of iron and reported that the activation energy of iron was largely influenced by the anion in solution[1-38)]. Related to this study, J. J. Podesta' et. al. reported that the activation energy of corrosion of iron in the solution with Cl^- was 11.5 kcal/mol[1-39)], and C. De Waard C reported that the activation energy of corrosion of iron in the solution with CO_3^{2-} was 10.7 kcal/mol[1-40)].

(4) Acceleration Tests using Temperature as Driving Force for Investigating the Deterioration of Reinforced Concrete

The deterioration progress of reinforced concrete structure is relatively slow although it takes a few years or decades before the influence of deterioration observed from outside. Therefore some acceleration methods for the deterioration such as Cl⁻ induced corrosion or CO_2 induced corrosion were developed. The test method which exposes reinforced concrete in high temperature environment is one of the effective methods for accelerating the deterioration progress. This is based on the knowledge that the deterioration speed rises up with the increase of temperature as shown in previous section.

Uomoto et. al. studied the influence of temperature, concentration of CO_2 gas and water-cement ratio on rate of carbonation[1-37]. As a result, the following equation was constructed for calculating the carbonation depth in the acceleration test.

$$X = (2.804 - 0.847 \log C) \times e^{(8.748 - 2563/T)} \times (2.39 WC^2 + 44.6 WC - 3980) \times 10^{-4} \times \sqrt{C \cdot t} \qquad (1\text{-}6)$$

where,　X　　　: carbonation depth (mm)

　　　　C　　　: concentration of CO_2 gas

　　　　T　　　: temperature (K)

　　　　WC　　: water cement ratio (%)

　　　　t　　　: acceleration period

Sasabuchi et. al. [1-41] studied the difference of corrosion rate between acceleration test in laboratory and exposure test in outside for 9 years. And they reported that the corrosion rate of acceleration test in laboratory at 60 degrees centigrade was 7 times faster than that in the outdoor exposure test.

Masuda et. al. [1-42] also studied the influence of the temperature of acceleration test at 60 degree centigrade on the corrosion rate of steel bars in concrete and constructed an equation of corrosion rate as follows.

$$q = \sqrt{\frac{1}{C}} \left(0.007(W/C) - 0.459(NaCl) + 0.030(W/C)(NaCl) - 0.354 \right) \qquad (1\text{-}7)$$

where, q : corrosion rate of steel bar (%wt/month)

C : concrete cover (cm)

W / C : water- cement ratio

$NaCl$: concentration of Cl⁻ (%).

(5) Summary of this section

The common opinions in the literature survey related to the influence of temperature on deterioration of concrete are that the rate of diffusion of substance in concrete or corrosion of the steel bar rise with the increase of temperature.

However, the investigations related to following issues are still inadequate.

✓   Most of researches of temperature effect to deterioration of reinforced concrete are experimentally performed without considering macrocell and microcell corrosion separately, which seem to have different dependency against temperature.

✓   Theoretical investigation related to above phenomenon is insufficient.

✓   The activation energies obtained in literature surveys are considered as only one phenomenon for example diffusion phenomenon or corrosion phenomenon. The investigation for the significance of activation energy in deterioration in concrete should be done.

✓   There are some researches related to acceleration test which tried to convert the acceleration time to real time. However most of these studies used the experimental data without considering the theoretical background. Therefore it is not guaranteed whether it is able to apply to reinforced concrete exposed to another environment.

1.2.3 Deterioration Progress of Steel Corrosion in Concrete Induced by Cl⁻ or CO₂[1-43]

(1) Importance of prediction of deterioration progress

It is not always guaranteed that required performance of the structure is maintained in concrete structure during the scheduled service period. In the meantime, maintenance administrators of the concrete structure should check the performance of

the structure in during scheduled service period. Therefore the maintenance administrators must appropriately maintain it with based on the maintenance procedure such as inspection, degradation prediction, evaluation and judgment, countermeasure as shown in **Fig.1.2.12**[1-44].

Start * Numbers inside ( ) indicate chapters and sections

Standard Investigation

Causes of Cracking and Selection of Repair and Strengthening Methods based on the Standard Investigation — No → Detailed Investigation

Yes

Yes ← Causes of Cracking and Selection of Repair and Strengthening Methods based on Detailed Investigation

No

Advanced Judgment of Qualified Engineer

Cause of Cracking

Structural Member or Non Structural Member — Structural Member → Judgment for Necessity of Strengthening — Unclear →

Unnecessary

Necessary

Decision based on Advanced Judgment of Qualified Engineer

Necessary

Strengthening

Unnecessary

Non Structural Member

Unnecessary

Judgment for Necessity of Repair — Unclear →

Necessary

Necessary

Decision based on Advanced Judgment of Qualified Engineer

Repair

Unnecessary

End

Fig.1.2.12 Concept of Investigation, Repair and Strengthening of Cracks[1-44]

The information that how the performance deterioration of the structure changes under the environment and where the structure is used must be grasped in order to carry out the appropriate and systematic maintenance for the concrete structure. In this case, it is necessary to do the degradation prediction of the structure based on the

result of inspection. Appropriate prediction needs the evaluation and judgment of performance based on the following matters; (a) the evaluation and judgment of whether it has satisfied a demand level of concrete structure during the scheduled service period, (b) the estimation in the persistence in-service period of the structure and (c) the evaluation and judgment of necessity of detailed inspection and the repair.

(2) The method for the prediction

The deterioration progress due to steel corrosion in concrete such as Cl^- induced corrosion or CO_2 induced corrosion progress through 4 deterioration stages as follows; incubation stage, propagation stage, acceleration stage and deterioration stage as shown in **Fig.1.2.13**. Still, the factor which decides the each deterioration period is defined as shown in **Table 1.2.1**.
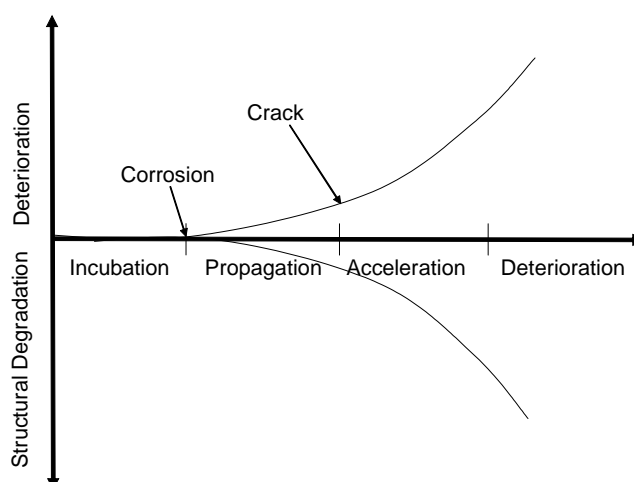
Fig.1.2.13 Deterioration Progress in Reinforced Concrete[1-43)]

Table1.2.1 Factor Which Decides Each Deterioration Period[1-43]

Deterioration Period	Definition	Factors
Incubation	The period before the steel bars in concrete starts to corrode	Cl⁻ diffusivity, Carbonation coefficient
Propagation	The period before cracking	
Acceleration	The period the corrosion rate of steel bar rises up	Corrosion rate of steel bar
Deterioration	The period the loading capacity of reinforced concrete decreases significantly	

(3) Summary of this section

It can be said that the prediction of deterioration period is very important factor in the discussion of service life of reinforced concrete structures. In this case it is considered that the temperature gives large influence of service life. Therefore in the region where the temperature is relatively high, especially tropical countries should take care about temperature effect.

1.2.4 Summary

In the above review of literature it can be seen that the deterioration of reinforced concrete due to steel corrosion such as Cl⁻ induced corrosion or CO_2 induced corrosion is easily influenced by temperature. However it can be realized that the investigations of temperature effect on deterioration progress of reinforced concrete are inadequate. Especially following points should be solved as soon as possible.

✓ Most of researches related to the influence of temperature on deterioration progress of reinforced concrete are experimentally performed without considering macrocell and microcell corrosion separately, which seem to have different dependency against temperature.

✓ Theoretical investigation related to above phenomenon is insufficient.

✓ The activation energies obtained in literature surveys are considering only one phenomenon for example diffusion phenomenon or corrosion phenomenon.

✓ The investigation for the significance of activation energy of deterioration in concrete due to steel corrosion based on Arrhenius theory should be done.

✓ In the most of studies on the conversion of acceleration time to real time used the experimental data without considering the theoretical background. Therefore it is not guaranteed whether it is able to apply to reinforced concrete exposed to another environment.

✓ It can be said that the deterioration period is very important factor in the discussion of service life of reinforced concrete structures. In this case it is considered that the temperature gives large influence on service life. Therefore in the region where the temperature is relatively high, especially tropical countries should take care about temperature effect.

1.3 Objectives

From above backgrounds and literature reviews, the main objectives of this study are decided as follows;

1. To investigate the influence of temperature on the rate of diffusion of substance and corrosion of steel bars in concrete induced by Cl^- or CO_2.

2. To study the influence of temperature on deterioration of reinforced concretes due to steel corrosion using the activation energy calculated by Arrhenius theory using the result of the objective 1.

3. To predict the deterioration progress of reinforced concrete due to steel corrosion considering temperature effect.

1.4 Significance and Originality

The rates of diffusion of substance, especially diffusion coefficient of the Cl^- or carbonation coefficient, and steel corrosion are very important factors in case of discussion of the deterioration progress of reinforced concrete structure. Moreover, it is generally said that the rates of material diffusion and steel corrosion rise up with temperature rising. Therefore there is high possibility that the deterioration progress of reinforced concrete structure becomes faster with the rise of the temperature. However, the research related to above matter is inadequate. Especially, there are few researches which explain the deterioration progress of reinforced concrete structure using Arrhenius theory, although the influence of temperature on the material diffusion and the chemical reaction can be explained by this theory. This study discusses the influence of temperature on the deterioration progress of reinforced concrete structure from experimental and theoretical viewpoints. Therefore it is considered that this study has a very important meaning for maintenance of the reinforced concrete structures. In addition, it is considered that the results obtained from this study are also useful for a tropical country to use the Japanese or United States standards.

1.5 Flow of This Study

The flow of this study is shown in **Fig.1.5.1**.

In Chapter 1, the backgrounds, literature reviews, objectives and significance of this study were presented.

In Chapter 2 and Chapter 3, the influence of temperature on the steel corrosion induced by Cl^- or CO_2 was studied respectively. First influence of temperature on the rates of diffusion of aggressive substances, such as Cl^-, CO_2 or O_2, into concrete was discussed. Next, the influence of temperature on the steel corrosion in concrete was discussed using the rate of macrocell and microcell corrosion.

In Chapter 4, the Arrhenius theory was applied to the results of Chapter 2 and Chapter 3. First the calculation method of activation energy of deterioration of reinforced concrete due to steel corrosion was arranged. Secondly the significances of activation energy of reinforced concrete were discussed. Finally the influential factors

on activation energy of diffusion of substances and steel corrosion in concrete were investigated using activation energy calculated by above method.

In Chapter 5, deterioration progress of reinforced concretes due to steel corrosion was predicted considering with temperature effect. First the influence of temperature on deterioration progress of reinforced concrete was discussed based on the Arrhenius theory. Secondly the deterioration progresses of reinforced concrete considering the regional and seasonal temperature were predicted using numerical analysis and Arrhenius equation.

In Chapter 6, the conclusions derived from this study are shown.

Chapter1
Introduction

Chapter2
Influence of Temperature on Cl^- Induced Corrosion in Concrete.

Chapter3
Influence of Temperature on CO_2 Induced Corrosion in Concrete.

Chapter4
Discussions for Temperature Influence on Deterioration of Reinforced Concrete Based on Arrhenius Theory.

$$k = a \exp\left(-\frac{\Delta E}{RT}\right)$$

Diffusion $< Cl^-, CO_2, O_2 >$

Corrosion $<$ Macro-cell and Micro-cell Corrosion. $>$

Chapter5
Prediction of Deterioration Progress of Reinforced Concrete Due to Steel Corrosion Considering Temperature Effect.

Chapter6
Conclusions

Fig.1.5.1 Flow of This Study

References of Chapter 1

1-1)   Hausmann, D.A., Electrochemical Behavior of Steel in Concrete, Journal of American Concrete Institute, Vol. 61, No.2, pp. 171-188, (1964).

1-2)   Pourbaix, M., Corrosion Science, Vol.14, (1975).

1-3)   Fontana and Greene, Corrosion Engineering, McGraw-Hill, (1978).

1-4)   Miyazato, S., Otsuki, N., Kimura, H., Estimation Method of Macrocell Corrosion Rate of Rebar in Existing Concrete Structures Using Non-destructive Test. East Asia-Pacific Conference (EASEC 8), Vol.2, pp.531-542, (2001).

1-5)   Ariva, A.J., Active-passive transition in metals, proceedings of the 8th International Congress on Metallic Corrosion, Vol.111 Mainz., pp.2065-2080, (1981).

1-6)   Glasser, F.P. and Sagoe-Crentsil, K.K., Steel in concrete. Part II. Electron microscopy analysis, Magazine of Concrete Research, Vol.41, No.149, pp.213-220, (1989).

1-7)   Hausmann, D.A., Steel Corrosion in Concrete, Materials Protection, 6, pp.19-23, (1967).

1-8)   Sagoe-Crentsil, K.K., and Glasser, P.P., Analysis of the Steel, Concrete interface, Third international Symposium on "Corrosion of Reinforcement in Concrete Construction", pp.74-86, (1990).

1-9)   Evans, U.R., The Corrosion and Oxidation, Journal of Chemistry, pp.1773, (1930).

1-10)   Rosenberg, A., Grace, W.R., Hansson M.C., Mechanisms of Corrosion of Steel in Concrete, Materials Science of Concrete, Vol.1, Skalny Jp. Ed. MRS, pp.285-316, (1989).

1-11)   Hurling, H., Oxygen Permeability of Concrete, RILEM-seminar "Durability of Concrete Structures under Normal Outdoor Conditions" Hanover, 03, (1984).

1-12)   Treadaway, et. al., The Influence of Concrete Quality on Carbonation in Middle Eastern Countries, Seminar on Corrosion of Steel in Concrete, London, (1983).

1-13)   Ohno, Y., Suzuki, K., Araparnatorn, S., Macrocell Corrosion of Steel in Uncracked Concrete, Proceedings of the International Conference on Corrosion and Corrosion Protection of Steel in Concrete, pp.224-235, (1994).

1-14)   Miyazato, S., Study on Macrocell Corrosion Induced by Chloride attack or Carbonation at Defect in Reinforced Concrete, Doctoral Thesis of Tokyo Institute of Technology, (2001).

1-15)   Gjørv, O.E., Vannesland and A.H.S.El-Busaidy, NACE Corrosion/76,Paper No.17, (1997).

1-16)   Miyagawa, T., Matsumura, T., Kobayasi, K., Fujii, M., Oxygen transmission through concrete related to reinforcement corrosion, Journal of Materials, Concrete Structures and Pavements, No.408/V-11,pp.111　120 (in Japanese), (1989).

1-17)   Nagataki, S., Mineral Admixtures in Concrete; State of Art and Trends, Special Publication of American Concrete Institute, No.SP-144, pp.447-482, (1994).

1-18)   Li, S., and Roy, D.M. Investigation of Relations between Porosity, Pore Structure and Cl- Diffusion of Fly Ash and Blended Cement Pastes, Cement and Concrete Research, Vol.16, No.5, pp.749-759, (1986).

1-19)   Page, C.L., Short, N.R., Tarras, A.El, Diffusion of Chloride Ions in Hardened Cement Paste, Cement and Concrete Research, Vol.11, No.3, pp.395-406, (1981).

1-20)   Bakker, R.M., Permeability of Blended Cement Concretes, Proceedings of the First International Conference on the Use of Fly Ash, Silica, Slag and other mineral by-Products in Concrete, Edited by V.M. Malhorta, Special Publication of American Concrete Institute, No. SP-79, Vol.1, pp.589-606, (1983).

1-21)   Crumpton, C.F., Jayaprakach, J.P., 66th Annual TRB Meeting, Comm. A3C15 Washington, D.C., (1987).

1-22)   Ohno, Y., Suzuki, K., Araparnatorn, S., Macrocell Corrosion of Steel in Uncracked Concrete, Proceedings of the International Conference on Corrosion and Corrosion Protection of Steel in Concrete, pp.224-235, (1994).

1-23)   Kosmatka, S.H., Bleeding, ASTM Special Technique Publication (American

Society of Test for Materials), No.169C, pp.88-111, (1994).

1-24)   CEB Design Guide to Durable Concrete Structures, Bulletin D' Information No.182, Committee Euro-International De Beton, (1989).

1-25)   Maruya, T., Hsu, K., Takeda, K., Uomoto, T., Diffusion and Corrosion in Concrete Exposed to High Temperature and Low Humidity Environmen, Concrete Research and Technology, No.49, pp. 315-322 (in Japanese), (1999).

1-26)   Mori, T., Shiroyama, K., Kamimura, K., Yoda, A., Carbonation of Blast Finest Slag Concrete, Annual Report of Cement Technology t Vol. 26, pp. 326-329 (in Japanese), (1972).

1-27)   Ryu, K., Tomozawa, F., Masuda, Y., Abe, M., Izumi, T., Experiment for Prediction of Carbonation of Concrete(part 2), Proceedings of Japan Architecture,No.1124,pp.247-248 (in Japanese), (1987).

1-28)   Detwiler, R.J., Detwiler, R.J., Kjellsen, K.O., GJorv, O.E., Resistance to chloride intrusion of concrete cured at different temperatures, ACI Mater Journal, Vol.88, No.1, pp. 19-24, (1991).

1-29)   Tuutti K, Service Life of Structures with Regard to Corrosion of Embedded Steel, Special Publication of American Concrete Institute, No.SP-65, pp.223-236, (1980).

1-30)   Schiessel P and Raupach M Beton-Informationen pp.28-33, (1988).

1-31)   Schiessel P and Raupach M Beton-Informationen pp.30-43, (1990).

1-32)   Zivica, V., Significance and Influence of the Ambient Temperature as a Rate Factor of Steel Reinforcement Corrosion, Bulletin material science, Vol.25, No.5 pp.375-379, (2002).

1-33)   Zivica, V., Influence of W/C Ratio on Rate of Chloride Induced Corrosion of Steel Reinforcement And Its Dependence on Ambient Temperature, Bulletin material science, Vol.26, No. 5, pp.471-475, (2003).

1-34)   West, J. M., Basic corrosion and oxidation, p.33, Ellis Horwood, (1983).

1-35)   Page, C. L., Lambert, P., Kinetics of Oxygen Diffusion in Hardened Cement Pastes, Journal of Materials Science, 22, pp.942-946, (1987).

1-36)   Page, C.L., Short, N.R., Tarras, El., Diffusion of Chloride Ions in Hardened Cement Pastes, Chemical and Concrete Research, Vol. 11, pp.395-406, (1981).

1-37)   Uomoto, T., Takada Y., Factors affecting concrete carbonation ratio, Journal of

Materials, Concrete Structures and Pavements, No.451/V-17, pp.119-128 (in Japanese), (1992).

1-38) Alexander, B.J.,Foley,R.T.,Anion Dependence of the Activation Energy for Iron Corrosion, Corrosion,31,No.4,pp.148-149, (1975).

1-39) Podesta., J. J., et. al. "Kinetics of the anodic dissolution of iron in concentrated ionic media", Electrochimica Acta,10,pp.171-182, (1965).

1-40) Waard, C.D., Milliams D.E., Carbonic Acid Corrosion of Steel, Corrosion, Vol.31, No.5, pp.177-181, (1975).

1-41) Sasabuchi, Y., Masuda, Y., Nakamura, N., Exposure Test on the Rate of Corrosion of Reinforcing Bar in Concrete Containing Chloride Ion, Proceedings of the Japan Concrete Institute, Vol.20, No.1, pp.317-322, (1998).

1-42) Masuda, Y., Kakegawa, M., Hanae, H., Experiment on the Influence of Various Factors on the Rate of Corrosion Loss of Reinforcing Bar in Concrete, Proceedings of the Japan Concrete Institute, Vol.14, No.1, Page781-786, (1992).

1-43) Japan Society of Civil Engineering Concrete Committee, Standard Specification for Concrete [Maintenance Edition], (2001).

1-44) Japan Concrete Institute, Practical Guideline for Investigation, Repair and Strengthening of Cracked Concrete Structures, (2003).

Chapter 2

Influence of Temperature on

Cl⁻ Induced Corrosion in Concrete.

2.1 Cl⁻ Induced Corrosion in Concrete

2.2 Experimental Procedures

2.3 Influence of Temperature on Cl⁻ Diffusivity in Concrete

2.4 Influence of Temperature on Cl⁻ Induced Corrosion in Concrete

2.5 Summary of Chapter 2

References of Chapter 2

2.1 Cl⁻ Induced Corrosion in Concrete

The steel bar in concrete has passive film and it is protected from severe corrosion. However, the steel bar easily starts to corrode due to the existence of Cl⁻ [2-1]. This phenomenon is called as Cl⁻ induced corrosion. The rate of Cl⁻ induced corrosion is comparatively faster than other steel corrosion phenomenon in concrete. Especially Cl⁻ induced corrosion should be considered in the structures constructed near coastal environment, which are always exposed to the environment with high concentration of Cl⁻.

In the deterioration process of Cl⁻ induced corrosion, rates of Cl⁻ diffusion and steel corrosion are one of the most important factors in case of the discussion about the deterioration period of concrete structures. Moreover, these rates are easily influenced by temperature. Consequently, it is important to know the influence of temperature on Cl⁻ diffusivity and/or rate of Cl⁻ induced corrosion quantitatively in order to maintain concrete structures.

For the reasons outlined above, the purposes of this chapter were chosen as follows;

(a) To study the influence of temperature on Cl⁻ diffusivity

(b) To study the influence of temperature on Cl⁻ induced corrosion

Especially in case of objective 1 Cl⁻ diffusivity in micro region in concrete was examined, while in case of objective 2 Cl⁻ induced corrosion in concrete affected by bleeding was examined.

2.2 Experimental Procedures

In this section the experimental methodology and experimental procedure used in this chapter were explained. In this chapter, two types of specimen were used. One was the cylindrical concrete specimens (TYPE A (C2)) with the size of φ10cm x 20cm for investigating the influence of temperature on Cl⁻ diffusivity. The other one was the rectangle concrete specimens (TYPE B (C2)) with the size of 150 cm x 30 cm x 10cm. Three levels of water-cement ratio and water contents were also investigated in both types of specimens because it was considered that these factors were largely influenced on the progress of the deterioration caused by Cl⁻ induced corrosion.

2.2.1 Materials Used

(1) Cement

Ordinary Portland cement (Taiheiyo Co.) was used as cement. The physical properties and chemical components are shown in **Table 2.2.1**.

Table 2.2.1 Physical Properties and Chemical Components of Cement.

(a) Physical Properties.

Density (g/cm^3)	Specific surface area (cm^2/g)	Compressive strength (MPa)		
		3d	7d	28d
3.16	3270	28.4	43.0	60.2

(b) Chemical Components.

MgO (%)	SO$_3$ (%)	Loss on ignition (%)	Total alkali (%)	Cl$^-$(%)
1.6	1.9	1.4	0.62	0.006

(2) Aggregates

River sand (Obitsu, Chiba-prefecture) was used as fine aggregate. Also Crash stone (Ome, Tokyo) was used as course aggregate. The physical properties of fine and course aggregate are shown in **Table 2.2.2**.

Table 2.2.2 Physical Properties of Fine and Course Aggregates.

Kinds of aggregate	Density (g/cm^3)		F.M.^{2*}	W.A.R.^{3*}	WV^{4*}
	SSD^{1*}	DRY		(%)	(kg/l)
Fine aggregate	2.60	2.54	2.59	2.20	1.74
Course aggregate	2.64	2.62	7.00	0.93	1.54

1*: Surface saturated dry condition, 2*: Fine modulus, 3*: Water adsorption ratio,
4*: Weight per volume.

(3) Mixing water

Tap water was used as mixing water. Before mixing the tap water was put in the experimental room in order to make the temperature of water same with temperature of room (20±2 ℃).

(4) Chemical admixture

Water-reducing agent and air-entrained agent (FLOWRIC Co., Ltd.) were used as chemical admixtures.

(5) Steel

In TYPE B (C2) specimen, the steel of SD295A (D13, deformed bar) was embedded (detail of steel bar will be explained later). The chemical compositions and physical property of steel is shown in **Table 2.2.3**.

Table 2.2.3 Chemical Compositions and Physical Property of Steel.

	Fe (%)	C (%)	Si (%)	Mn (%)	P (%)	S (%)	Yield strength (N/mm^2)
JIS standard	—	—	—	—	<0.050	<0.05	295<
Mesured	98.78	0.21	0.18	0.78	0.023	0.029	358

2.2.2 Manufacturing Procedure of Specimen

(1) Outline of specimen

In this chapter, two types of specimens, cylindrical concrete specimen (TYPE A (C2)) and rectangle reinforced concrete specimen (TYPE B (C2)), were used for the investigation of influence of temperature on Cl⁻ diffusion and steel corrosion in concrete. The details of each specimen are shown below.

The outline of TYPE A (C2) specimen for the investigation of influence of temperature on Cl⁻ diffusivity in minute region of concrete is shown in **Fig.2.2.1**. The size of specimen was φ10 cm x 20 cm. The test pieces for the diffusion test were taken from the 4 locations of concrete specimen in terms of top surface, middle surface, bottom surface and inner layers. Especially in this investigation, the detailed investigation using the minute diffusion test was conducted (the detail of minute diffusion test will be explained later).
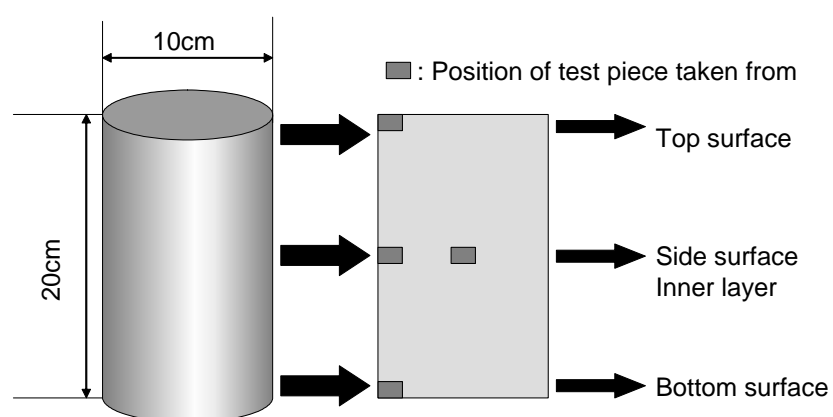

Fig. 2.2.1 Outline of TYPE A (C2) Specimen.

The outline of TYPE B (C2) specimen for the investigation of influence of temperature on steel corrosion induced by Cl^- is shown in **Fig. 2.2.2.** The size of specimen was 150 cm (height) x 30 cm (width) x 10 cm (depth). This specimen had steel bar with which were composed of divided steel elements as shown in **Fig. 2.2.3** (the reason will be explained later). The divided steel bars were electrically connected as one because each steel element had lead wires soldered on it. In this study, divided steel bars were classified into two types namely: vertical divided steel bar and horizontal divided steel bar. This is because it is believed that there are two types of corrosion cell formation in reinforced concrete affected by bleeding. The first type is concentration corrosion cell formed on the vertical steel bar, which occurs due to the concentration difference between the upper part and lower part of concrete. The other is crevice corrosion cell formed on the horizontal steel bars, which is caused by gaps generated under the horizontal steel bar [2-2), 2-3)].
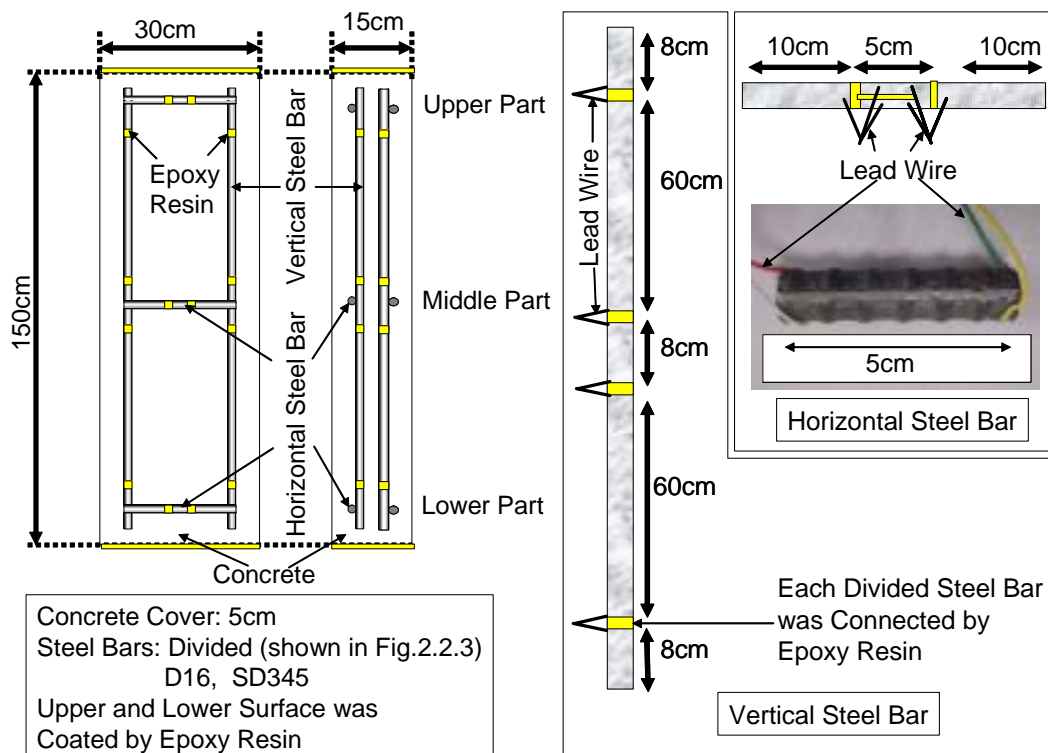

Fig. 2.2.2 Outline of TYPE B (C2) Specimen.   **Fig. 2.2.3** Divided Steel Elements.

(2) Mixture proportion

The mixture proportions of TYPE A (C2) and TYPE B (C2) specimens are shown in **Table 2.2.4**.

Table 2.2.4 Mixture Proportion of Specimens.

(a) TYPE A (C2) Specimen

W/C	kg/m³				g/m³		%
	W	C	S	G	AD1[1*]	AD2[2*]	BR[3*]
	140	255	862	1042	561.0	17.85	0.18
0.55	210	382	733	855	840.4	26.74	0.51
	280	509	596	734	1120.0	35.64	4.58

(b) TYPE B (C2) Specimen

W/C	kg/m³				g/m³		%
	W	C	S	G	AD[1*]	AD2[2*]	BR[3*]
0.30	175	583	755	458	4083	5833	0.05
	225	750	634	384	5250	7500	0.02
0.55	175	318	854	518	2226	3180	0.62
	225	409	760	462	2863	4090	1.08
	275	500	668	405	3500	5000	6.67
0.80	175	219	1098	540	1533	2190	0.00
	225	281	809	491	1967	2810	1.39

1*: Water-Reducing Agent, 2*: Air-Entrained Agent, 3*: Bleeding ratio

(3) Mixing and placing

Cement was sandwiched between two layers of fine aggregate in the mixer, and then those were mixed for 30 seconds. Water was added as the mixer was continuously rotating for 30 seconds. As soon as all the water was poured, the mixer was stopped for 60 seconds, and the mortar adhered to the sides and paddle of the mixer was scraped off. Finally, the coarse aggregate was added and the concrete was mixed for 120 seconds. The concrete specimens were cast as soon as the mixing finishes. The casting was done

in approximate lifts. Each lift was vibrated for 6 seconds prior to the placing of the next lift.

(4) Curing

In case of TYPE A (C2) specimen, they were demoulded after 24 hours of moist curing (20±2ºC, 90%R.H.) and cured in water at 20±2ºC for 28 days.

In case of TYPE B (C2) specimen, they were demoulded after 24 hours of moist curing (20ºC, 90%R.H.) and cured in the environmental control room (20ºC, 60%R.H.) for 56 days.

After curing, both of concrete specimens, TYPE A (C2) and TYPE B (C2), were placed in environmental control room. The temperature was varied from 20ºC, 30ºC, and 40ºC at constant relative humidity set at 60%R.H. when the corrosion rate of steel bars were measured.

2.2.3 Parameters

The parameters of the investigation are shown in **Table 2.2.5**. Exposure temperature is the primary factor considered in Cl⁻ induced corrosion. Therefore three exposure temperatures (20ºC, 30ºC and 40ºC) were considered.

Secondary parameters were bleeding ratio. Concrete is easily affected by bleeding because concrete consist of several materials such as cement, water, fine aggregate, coarse aggregate. Therefore all concrete is affected by bleeding even if concrete is carefully cast. In this investigation the influence of bleeding on the progress of Cl⁻ induced corrosion were also investigated. The locations taken from the test peace in TYPE A (C2) specimen were top surface, middle surface, bottom surface and inner layers as shown in **Fig. 2.2.1**. While, the location of the investigation conducted in TYPE B (C2) specimen were as shown in **Fig. 2.2.2**. Especially it is considered that the influence of temperature on the corrosion rate induced by Cl⁻ in the vertical steel bars and horizontal steel bars are quite different because the generation of corrosion cell in these steel bars are different. Therefore in this investigation the steel corrosions induced by Cl⁻ in vertical steel bars and horizontal steel bars were separately discussed.

Table 2.2.5 Experimental Parameters

(a) For TYPE A (C2) Specimen

		Bleeding Ratio (%)		
		0.18	0.51	4.58
Temp.	20ºC	O	O	O
	30ºC	O	O	O
	40ºC	O	O	O

The test pieces were taken from top surface, middle surface, bottom surface and inner layers as shown in F**ig 2.2.1.**

(b) For TYPE B (C2) Specimen

|		Bleeding Ratio (%)		
		0.62	1.68	6.67
Temp.	20ºC	O	O	O
	30ºC	O	O	O
	40ºC	O	O	O

The corrosion rate is measured in upper (145cm), middle (70cm) and lower (5cm) part of steel bars as shown in **Fig. 2.2.2**.

2.2.4 Items of Investigation

(1) Minute diffusion test[2-4)]

In this investigation, the diffusivity of mortar part in concrete measured by minute diffusivity test was used as item of investigation. Outline of the preparation technique of test piece is shown in **Fig. 2.2.4**. First, a bar of 15 x 15 x 50 mm was cut using a diamond cutter. This bar was then cut crosswise by means of low rate saw (ISOMET[TM]) into a size of 15 x 15 x 3 mm piece. Next, the 15 x 15 x 3 mm piece was adhered to the glass plate by electron wax. Then 5 x 5 x 4 mm test piece was cut from the 15 x 15 x 4 mm test piece by selecting the proper position containing only mortar matrix phase. The 5 x 5 x 4 mm test piece was set in the plastic mould in order to set-in the hard epoxy. After setting the hard epoxy, both sides of the test piece was polished using the grinder and polisher (METASERVE®2000) until the thickness of the test

piece became 0.5 mm. The final test piece set in the hard epoxy is shown in **Fig. 2.2.5**.
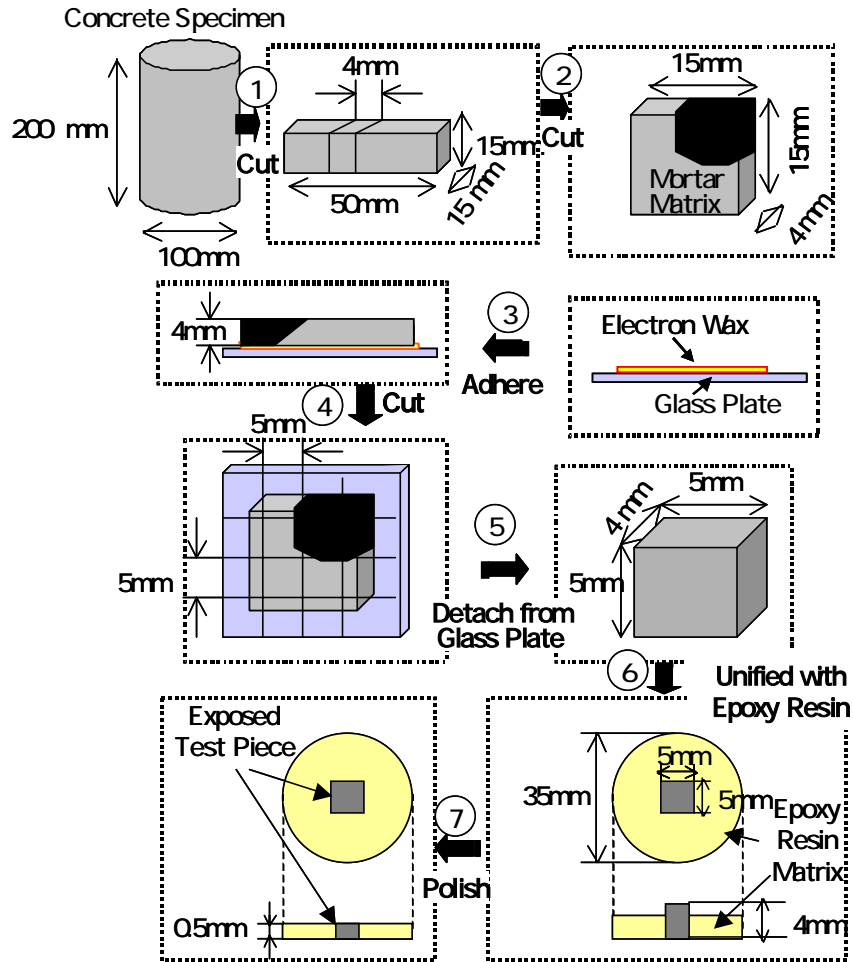
Fig. 2.2.4 Outline of Preparation Technique of Test Piece.

Fig. 2.2.5 Final Test Piece Set in Hard Epoxy.

The procedure for testing is explained as follows;

1. The test piece was set inside an acrylic cylinder cell as shown in **Fig. 2.2.6**. A thin rubber sheet was used to serve as a waterproof.

2. 3.0 % NaCl solution was filled into one side of the cell, while a saturated $Ca(OH)_2$ solution was filled into the other side.

3. To measure the time-dependent changes of Cl^- concentrations in saturated $Ca(OH)_2$ solution side, the sample solution was gathered every day.

4. The concentration of chloride ions was measured using ion chromatography.

The concentration changes of chloride ions at saturated $Ca(OH)_2$ solution side is schematically shown in **Fig. 2.2.7**. In this figure, the inclination where the concentration change becomes constant is called the penetration rate, ΔQ in mol/l/sec. The flux, J can be calculated from the concentration change, because the penetration rate and the flux have the following equation;

$$J = \Delta Q \cdot \frac{V_{cell}}{A} \qquad\qquad (2\text{-}1)$$

where, ΔQ : penetration rate of ion (mol/l/sec)

     J : flux of ion (mol/cm^2/sec)

     V_{cell} : solution volume of saturated $Ca(OH)_2$ solution side (cm^3)

     A : cross sectional area of test piece (cm^2).
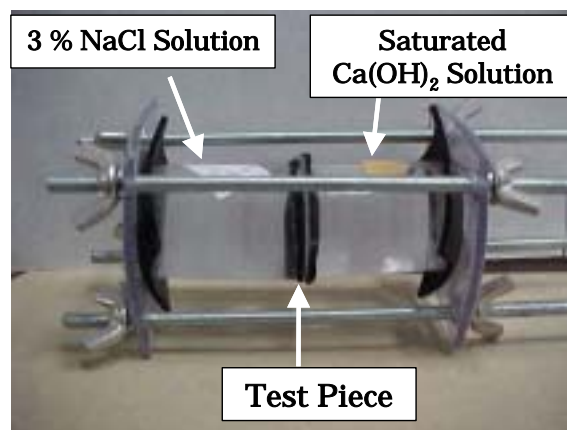

**Fig. 2.2.6** Cell Filled with NaCl and $Ca(OH)_2$ Solutions
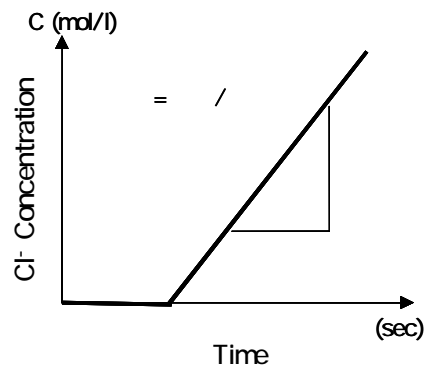
Fig. 2.2.7 Variation of Concentration of Chloride Ion in Saturated Ca(OH)$_2$ Solution Side

The diffusion coefficient was calculated form the Fick's first law of diffusion. The concentration gradient Cl$^-$ is known, and the flux of Cl$^-$ can be estimated. Therefore, the diffusion coefficient of Cl$^-$ can e calculated from the equation given below.

$$D_{Cl} = \frac{J_{Cl}}{\partial C_{Cl} / \partial x} \tag{2-2}$$

(2) Specific resistance of concrete

The specific resistances of concrete were measured using corrosion monitor (Rikendinshi. CO., LTD). First the connection of steel elements was separated. In this condition, the electric current could not flow from one steel element to another steel element, and the voltage of steel element was uniformly distributed. The specific concrete resistance was measured at 10 kHz of frequency with 50 mV of voltage. The resistance given in this frequency was considered as the solution resistance in the evaluation of steel corrosion[2-5], and in this study this resistance was defined as concrete resistance. The specific resistance was calculated from this concrete resistance.

(3) Oxygen permeability[2-6]

The measurement set-up of the oxygen permeability test is shown in **Fig. 2.2.8.** As shown in the figure the electrochemical cell consisted of the reinforcing steel bar, a

stainless steel plate counter electrode and Ag/AgCl reference electrode. The limiting current density was measured using a potential stat. The rate of oxygen permeability was obtained from the limiting current using Equation (2-3).

$$\frac{dQ}{dt} = -\left(\frac{i_{\lim}}{nF}\right)$$

(2-3)

where, dQ/dt : oxygen permeability (mol/cm^2/sec)

       $l_{\lim}$: limiting cathodic current density (A/cm^2)

       F : Faradays constant (96,500 coulombs/mol)

 n : number of electron exchanged (=4).
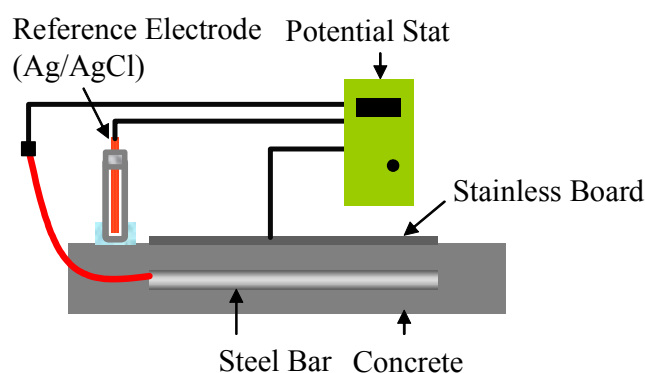
Fig. 2.2.8 Measurement Set-up of Oxygen Permeability Test.

(4) Gap area

      The area of gaps formed between the steel and concrete especially underneath the horizontal steel bars was measured using a digital microscope.

(5) Corrosion rate of steel bar in specimen

      Macrocell corrosion current and microcell corrosion current were measured in this chapter. In macrocell corrosion the anode and the cathode exist non-uniformly, while, in case of microcell corrosion the anode and the cathode exist uniformly.

      In order to measure the macrocell corrosion and microcell corrosion rate separately, divided steel bars were used in this study. The measuring method for the

macrocell corrosion rate was done as follows. The macrocell current was the total electric current flowing through all the adjacent steel elements. For example, the macrocell current density of the steel element No. i as shown in **Fig. 2.2.9** could be calculated using Equation (2-4). The anodic current density was denoted as positive, while the cathodic current was denoted as negative.

$$I_{macro} = \frac{I_{i-1,i} - I_{i,i+1}}{S_i}$$

(2-4)

where; I_{macro} : macrocell corrosion current density (A/cm^2)

       S_i : surface area of steel element i (cm^2)

 $I_{i-1,i}$: current flowing from component i-1 to i (A).
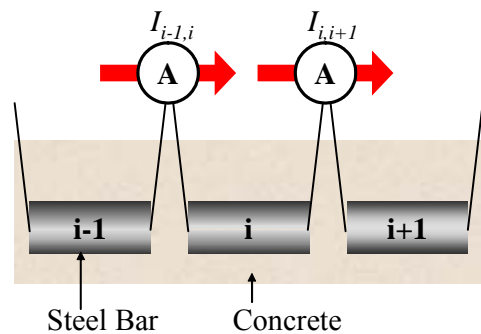
Fig. 2.2.9 Measurement Method of Macrocell Corrosion Rate.

On the other hand, the method of measuring the microcell corrosion rate was done as follows: First, the polarization resistance on the steel element was measured by AC impedance with FRA (Frequency Response Analyzer) as shown in **Fig. 2.2.10**[2-7]. The measurement was done by supplying a 50 mV voltage, with amplitude within 0.05Hz-5000Hz. And then, the microcell corrosion current density was calculated using Equation (2-5).

$$I_{micro} = \frac{K}{R_{pi} \times S_i}$$

(2-5)

where, I_{macro} : microcell corrosion current density (A/cm^2)

K : constant (= 0.0209V)[2-7)]

R_{pi} : polarization resistance (Ω)

S_i : surface area of component i (cm^2).
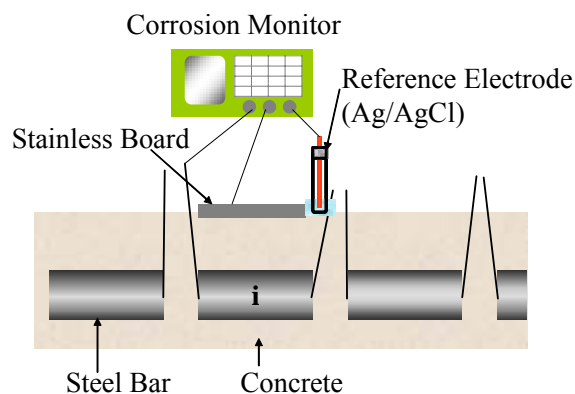
Fig. 2.2.10 Measurement Method of Microcell Corrosion Rate.

The total corrosion current density was simply the sum of the macrocell corrosion current density and the microcell corrosion current density. The corrosion rate can be calculated from the corrosion current density using the conversion factor 100 A/cm^2 of corrosion current equal to 1.16 mm/year of corrosion rate[2-9)].

2.3 Influence of Temperature on Cl⁻ Diffusivity in Concrete

2.3.1 Influence of Bleeding on Cl⁻ Diffusivity in Minute Region of Concrete at 20ºC

The distribution of Cl⁻ diffusivity in concrete is shown in **Fig. 2.3.1**. From this figure it can be seen that the Cl⁻ diffusivity in concrete increases with the higher position of concrete. This tendency becomes larger in case of concrete with high bleeding. This is because that the water content in upper part of concrete increases with higher bleeding ratio. **Fig 2.3.2** shows the influence of bleeding on Cl⁻ diffusivity in minute region of concrete. From this, it can be conclued that the high bleeding in concrete causes the high Cl⁻ diffusivity.
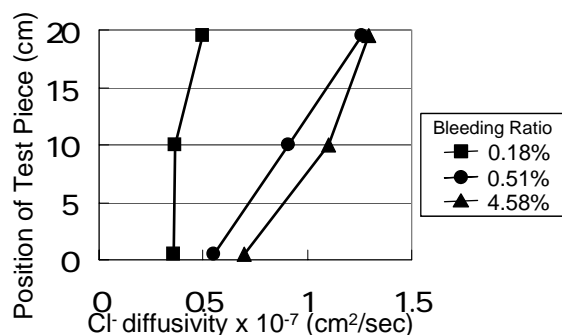
**Fig. 2.3.1** Distribution of Cl⁻ Diffusivity in Concrete
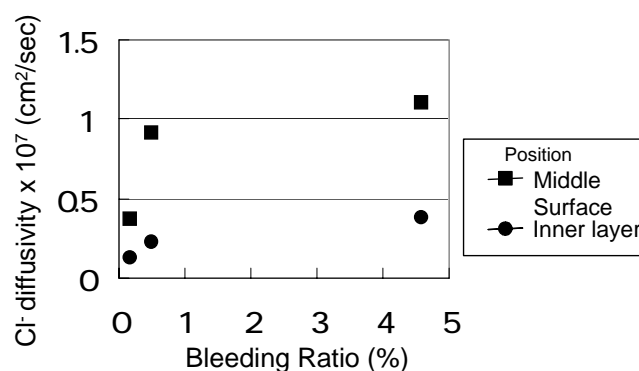
Fig. 2.3.2 Influence of Bleeding Ratio on Cl⁻ Diffusivity in Concrete

2.3.2 Influence of temperature on Cl⁻ diffusivity in minute region of concrete

Table 2.3.1 shows the average values of chloride ion diffusivity in the minute region of the three positions of outer layers and inner layer of mortar matrix taken from TYPE A (C2) specimen. The Cl⁻ diffusivity of the minute region in mortar matrix becomes high for higher exposure temperature in any position of test piece. And **Table 2.3.2** shows the magnification of Cl⁻ diffusivity of 10ºC difference of temperature. From this table it can be seen that the magnification of inner layer of concrete is relatively larger than that of outside. This is because the outside of concrete is porous compared to inside. So it is considered that the outside of concrete has much continuous porosity. The Cl⁻ diffusivity is largely related to the pore structure. As a result the influence of temperature became smaller in outside of concrete than inside.

Table 2.3.1 Chloride Ion Diffusivity (cm^2/sec)

Position \ Bleeding	Top surface			Middle surface		
	20ºC	30ºC	40ºC	20ºC	30ºC	40ºC
0.18%	4.95E-08	2.24E-07	8.82E-07	3.68E-08	1.45E-07	3.36E-07
0.51%	1.26E-07	3.25E-07	-	9.10E-08	2.17E-07	3.40E-07
4.58%	1.29E-07	7.47E-07	-	1.10E-07	4.59E-07	9.75E-07
Position \ Bleeding	Bottom surface			Inner layer		
	20ºC	30ºC	40ºC	20ºC	30ºC	40ºC
0.18%	3.56E-08	1.23E-07	5.81E-07	1.24E-08	6.43E-08	3.07E-07
0.51%	5.49E-08	1.99E-07	7.82E-07	2.22E-08	1.19E-07	7.82E-07
4.58%	6.95E-08	4.14E-07	-	3.78E-08	2.84E-07	1.28E-06

Table 2.3.2 Magnification of Chloride Ion Diffusivity

Position \ Bleeding	Top surface		Middle surface	
	30ºC/20ºC	40ºC/30ºC	30ºC/20ºC	40ºC/20ºC
0.18%	4.53	3.94	3.94	2.32
0.51%	2.58		2.38	1.57
4.58%	5.79		4.17	2.12
Position \ Bleeding	Bottom surface		Inner layer	
	30ºC/20ºC	40ºC/30ºC	30ºC/20ºC	40ºC/20ºC
0.18%	3.46	4.72	5.19	4.77
0.51%	3.62	3.93	5.36	6.57
4.58%	5.96		7.51	4.51

The influence of bleeding on Cl⁻ diffusivity in minute region of concrete with the temperature rising is shown in **Fig. 2.3.3**. From this figure, it can be confirmed that the Cl⁻ diffusivity increases with the temperature rising. Additionally this tendency becomes large with increase of the bleeding ratio. Therefore it can be concluded that the influence of temperature becomes high in the high bleeding concrete.
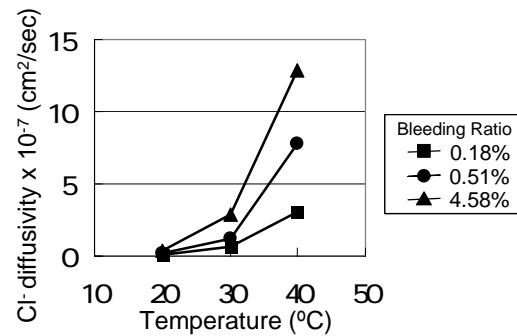
Fig. 2.3.3 Influence of Bleeding on Cl⁻ Diffusivity in Minute Region of Concrete with Elevated Temperature Environment (Position of Test Piece: Inner layer).

The influence of position taken from the test piece on Cl⁻ diffusivity in minute region of concrete with the temperature rising is shown in **Fig. 2.3.4**. From this figure, it can be confirmed that the Cl⁻ diffusivity increases with the temperature rising. Additionally this tendency becomes large with increase of the height of test piece. Therefore it can be concluded that the influence of temperature becomes large in the high bleeding part in concrete. Also it can be said that the influence of temperature on Cl⁻ diffusivity in bleeding ratio is larger than that in the height of test piece with comparison of the figures of **Fig. 2.3.3** and **Fig. 2.3.4**.
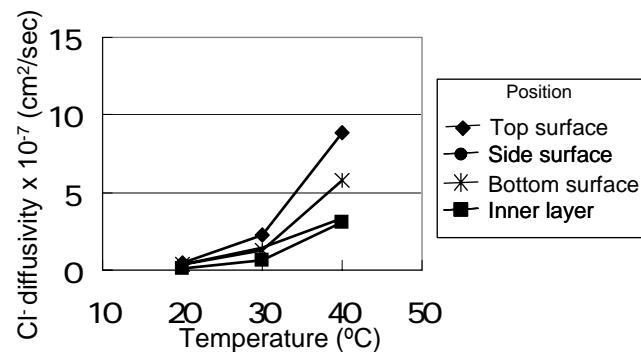

Fig. 2.3.4 Influence of Position of Test Piece on Cl⁻ Diffusivity in Minute Region of Concrete with Elevated Temperature Environment (Bleeding Ratio: 0.18)

2.3.3 Arrhenius Plot of Cl⁻ Diffusivity in Concrete

The Arrhenius plot of the results of **Fig.2.3.3** and **Fig.2.3.4** are shown **Fig.2.3.5** and **Fig.2.3.6** respectively. From these figures it can be said that the logarithm of Cl⁻ diffusivity is proportional to the reciprocal of absolute temperature. The slopes, slices and R are shown in **Table 2.3.3**. From this figure it can be said that the value of R^2 is more than 0.97. These facts indicate that the Cl⁻ diffusivity of minute region in concrete apparently agrees with the Arrhenius theory.
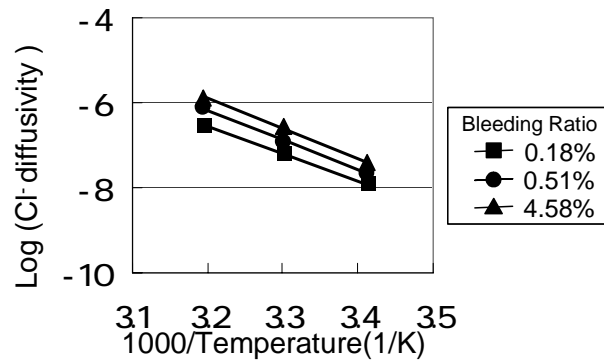
Fig. 2.3.5 Arrhenius Plot of Fig.2.3.3
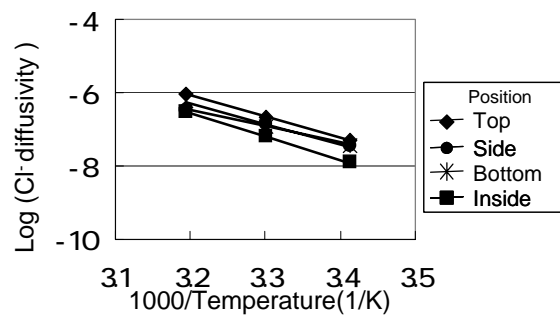
Fig. 2.3.6 Arrhenius Plot of Fig.2.3.4

Table 2.3.3 Slope, slice and R^2 of Cl⁻ Diffusivity of Minute Region in Concrete.

No. of test piece	Slope	Slice	R^2
0.18-Top surface	-5.74	12.28	0.9999
0.18-Side surface	-5.55	11.47	0.9929
0.18-Bottom surface	-4.41	7.65	0.9856
0.18-Inner layer	-6.39	13.89	1.0000
0.51-Top surface *	-3.66	5.59	-
0.51-Side surface	-5.28	10.76	0.9986
0.51-Bottom surface	-2.63	1.973	0.9732
0.51-Inner layer	-7.09	16.52	0.9973
4.58-Top surface *	-6.77	16.20	-
4.58-Side surface *	-6.88	16.34	-
4.58-Bottom surface	-4.36	7.95	0.9754
4.58-Inner layer	-7.03	16.60	0.9959

*: Calculated from only the data of 2 points

2.3.4 Summary

The Cl⁻ diffusivity of the minute region in concrete increases with the temperature rising. This tendency becomes large in high bleeding concrete. Additionally the logarithm of Cl⁻ diffusivity is proportional to the reciprocal of absolute temperature. This fact indicates that the Cl⁻ diffusivity of minute region in concrete apparently agrees with the Arrhenius theory.

2.4 Influence of Temperature on Cl⁻ Induced Corrosion in Concrete

2.4.1 Distribution of Cl⁻ Induced Corrosion in Concrete at 20ºC

(1) Distribution of corrosion rate in vertical steel bars

The distribution of macrocell, microcell and total corrosion rate on the vertical steel bars in reinforced concrete specimen affected by bleeding is shown in **Fig. 2.4.1**. From these figures, it is confirmed that the corrosion rate at the upper part of the vertical steel bar is higher compared to its lower part. The better condition of corrosion at the upper part of concrete is prevalent in concrete with high bleeding ratio. And this can be confirmed by the results obtained in the distribution of specific concrete resistance and oxygen permeability of concrete shown in **Table 2.4.1**. As shown on the table, specific concrete resistance at the upper part of concrete is smaller as compared to its lower part, contrary to the case of the oxygen permeability it is higher at the upper part and smaller at the lower part. Since corrosion reaction on the steel is influenced by specific concrete resistance and oxygen permeability of concrete, therefore, corrosion reaction may be accelerated due to the presence of water and the availability of oxygen near the steel. Low specific concrete resistance and high oxygen permeability in concrete implies greater risk of corrosion.

On the other hand, as mentioned on the result obtained from the electrochemical measurement, macrocell corrosion rate often prevailed over the microcell corrosion rate. Therefore, it can be said that the type of corrosion prevailed on the vertical steel bar in concrete affected by bleeding was macrocell corrosion type.
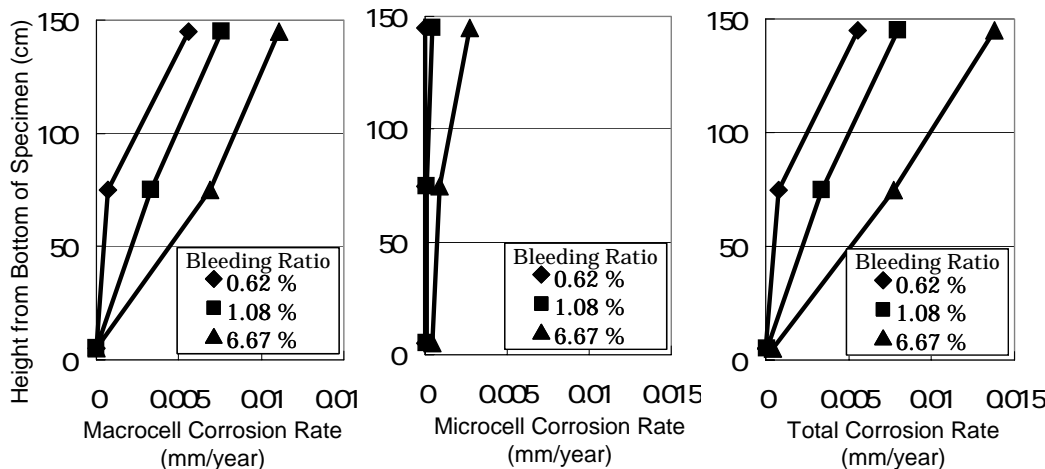
(a) Macrocell Corrosion Rate　　　(b) Microcell Corrosion Rate　　　(c) Total Corrosion Rate

**Fig. 2.4.1** Distribution of Corrosion Rate in Vertical Steel Bar in Concrete Affected by Bleeding (W/C = 0.55, Cl⁻ Content = 10kg/m³, Temp. = 20).

Table 2.4.1 Distribution of Specific Concrete Resistance and Oxygen Permeability of Concrete Affected by Bleeding.

Measurement items	Specific concrete resistance(kΩ cm)			Oxygen permeability $\times 10^{-11}$ (mol/cm²/sec)		
Bleeding ratio(%) ／ Position of concrete	0.62	1.68	6.67	0.62	1.68	6.67
Upper part (145cm)	8.16	3.87	2.82	3.2	3.7	5.0
Middle part (70cm)	1.04	4.60	3.44	2.7	3.5	4.1
Lower part (5cm)	1.44	6.49	6.01	1.6	2.3	3.1

(2) Distribution of corrosion rate in horizontal steel bars.

　　　The distribution of macrocell, microcell and total corrosion rate on the horizontal steel bars in reinforced concrete specimen affected by bleeding is shown in **Fig. 2.4.2**. As shown in this figure, the divided steel bar located in the center of the horizontal steel bar are composed of two steel element, upper steel and lower steel. And based on the result of the corrosion rate obtained here, it is proven that corrosion rate at the lower part of the horizontal steel bar is higher than that of upper part. And this condition is clearly shown when the bleeding ratio is high due to the formation of gaps

under the horizontal steel bars (Please refer to **Fig. 2.4.3**). The relationship between the total corrosion rate on the horizontal steel bar and the area of the gaps formed under steel bar is shown in **Fig. 2.4.4**.

By comparing the macrocell corrosion rate and the microcell corrosion rate obtained in the measurement, it is clear that macrocell corrosion rate prevailed over the microcell corrosion rate. Therefore it can be said that the type of corrosion prevailed on the horizontal steel bar in concrete affected by bleeding was macrocell corrosion type.

(a) Microcell Corrosion Rate   (b) Macrocell Corrosion Rate   (c) Total Corrosion Rate
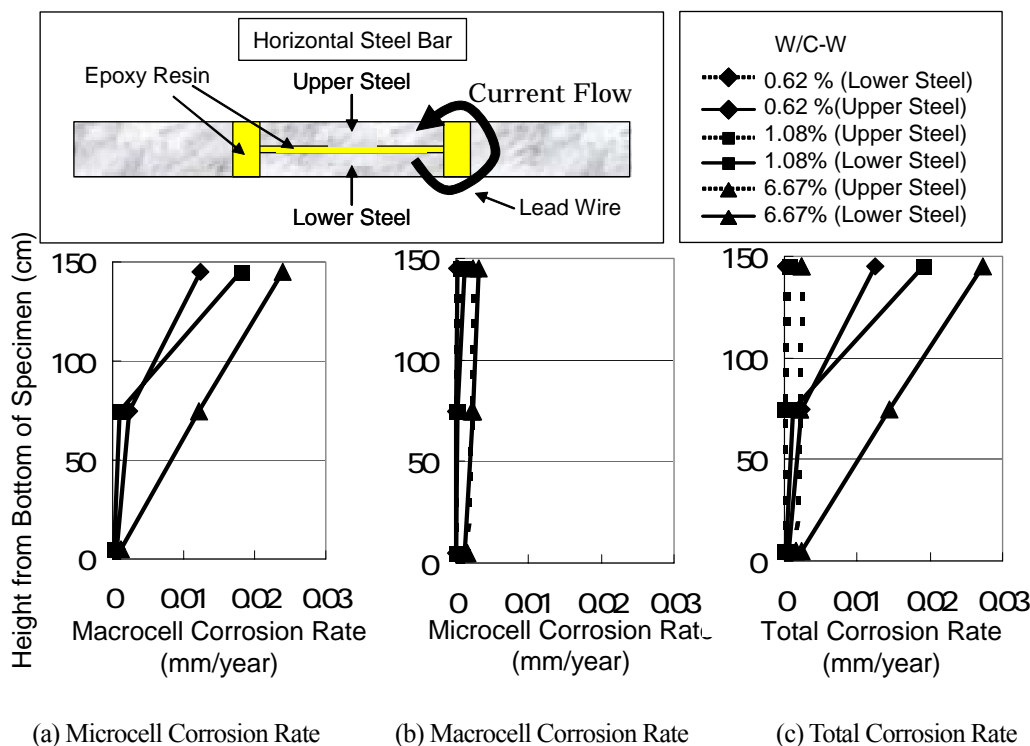
Fig. 2.4.2 Distribution of Corrosion Rate in Horizontal Steel Bar in Concrete Affected by Bleeding (W/C = 0.55, Temp. = 20ºC).
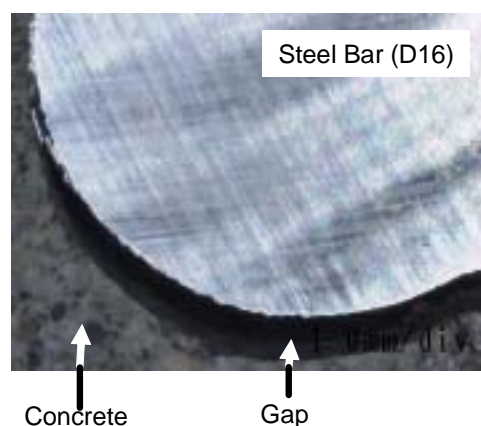
Fig. 2.4.3 Example of Gaps under Horizontal Steel Bar
(W/C =0.55, Bleeding ratio = 1.68).
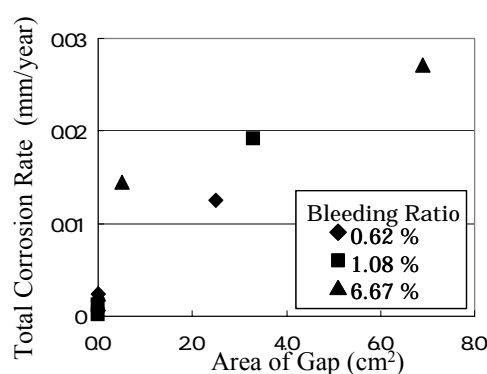
Fig. 2.4.4 Relationship between Total Corrosion Rate and Area of Gap
(W/C=0.55, Temp=20ºC).

2.4.2 Influence of Temperature on Cl⁻ Induced Corrosion in Concrete Affected by Bleeding

(1) Influence of temperature on corrosion rate in vertical steel bars

The influences of temperature on macrocell and microcell corrosion rate in vertical steel bars are shown in **Fig. 2.4.5** to **Fig 2.4.7** respectively. **Fig.2.4.5** shows the data of the different position of concrete, **Fig. 2.4.6** shows the data of different W/C, and **Fig. 2.4.7** shows the data of different bleeding ratio. From these figures it can be seen that the macrocell and microcell corrosion rate of vertical steel bars in concrete

increased with the temperature rising in any experimental parameter. Also it can be seen that the macrocell corrosion rate is almost 10 times higher than microcell corrosion rate in any temperature.
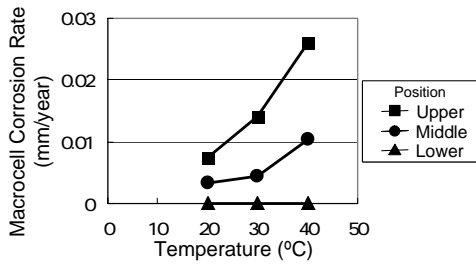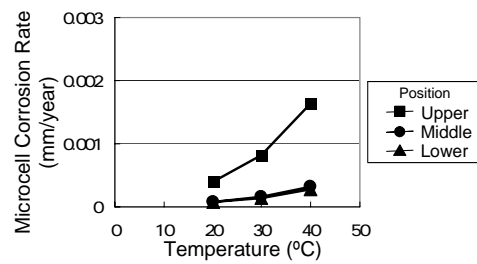
(a) Macrocell Corrosion Rate   (b) Microcell Corrosion Rate

Fig. 2.4.5 Influence of Temperature on Macrocell and Microcell Corrosion Rate
of Different Part of Concrete.
(Vertical Steel Bar, W/C = 0.55, Bleeding Ratio= 1.08%)
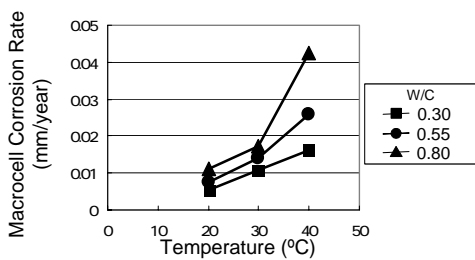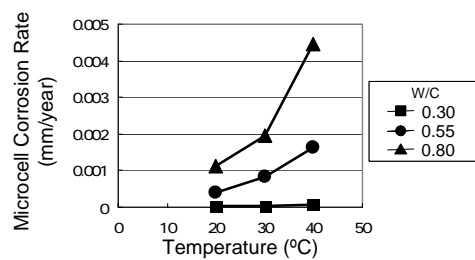
(a) Macrocell Corrosion Rate   (b) Microcell Corrosion Rate

Fig. 2.4.6 Influence of Temperature on Macrocell and Microcell Corrosion Rate
of Different W/C.
(Vertical Steel Bar, Position=Upper, Bleeding Ratio=1.08%)

(a) Macrocell Corrosion Rate   (b) Microcell Corrosion Rate
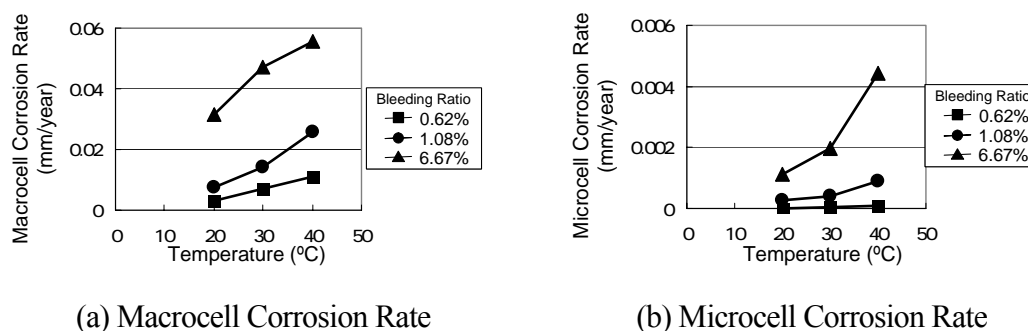
Fig. 2.4.7 Influence of Temperature on Macrocell and Microcell Corrosion Rate
of Different Bleeding Ratio.
(Vertical Steel Bar, Position=Upper, W/C=0.55)

The magnifications of macrocell and microcell corrosion rate in vertical steel bars are shown in **Table 2.4.2** to **Table 2.4.4** respectively. **Table 2.4.2** shows the data of the different position of concrete, **Table 2.4.3** shows the data of different W/C, and **Table 2.4.4** shows the data of different bleeding ratio. From these tables it can be seen that the magnification at 10 ℃ difference of temperature is almost 2.0. This indicates that the corrosion rate becomes 2 times with the 10 ℃ of temperature rising. Also it can be seen that the magnification of microcell corrosion rate is relatively larger than that of macrocell corrosion rate in vertical steel bars.

Table 2.4.2 Magnification of Macrocell and Microcell Corrosion Rate
of Different Part of Concrete.
(Vertical Steel Bar, W/C = 0.55, Bleeding Ratio= 1.08%)

Height of steel	Macrocell corrosion		Microcell corrosion	
	30℃/20℃	40℃/30℃	30℃/20℃	40℃/30℃
145	1.9	1.8	2.0	2.0
75	1.3	2.4	2.0	2.0
5	Cathode	Cathode	2.0	2.0

Table 2.4.3 Magnification of Macrocell and Microcell Corrosion Rate

of Different W/C.

(Vertical Steel Bar, Position=Upper, Bleeding Ratio=1.08%)

W/C	Macrocell Corrosion		Microcell Corrosion	
	30ºC /20ºC	40ºC /30ºC	30ºC /20ºC	40ºC /30ºC
0.30	2.2	1.6	2.2	1.8
0.55	1.9	1.8	2.0	2.0
0.80	1.5	1.2	1.8	2.3

Table 2.4.4 Magnification of Macrocell and Microcell Corrosion Rate

of Different Bleeding Ratio.

(Vertical Steel Bar, Position=Upper, W/C=0.55)

Bleeding (%)	Macrocell Corrosion		Microcell Corrosion	
	30ºC /20ºC	40ºC /30ºC	30ºC /20ºC	40ºC /30ºC
0.62	2.0	1.5	1.5	2.2
1.08	1.9	1.8	2.0	2.0
6.68	1.6	2.5	1.6	2.0

(2) Influence of temperature on corrosion rate in horizontal steel bars

The influences of temperature on macrocell and microcell corrosion rate in horizontal steel bars are shown in **Fig. 2.4.8** to **Fig. 2.4.10** respectively. **Fig. 2.4.8** shows the data of the different position of concrete, **Fig. 2.4.9** shows the data of different W/C, and **Fig. 2.4.10** shows the data of different bleeding ratio. From these figures it can be seen that the macrocell and microcell corrosion rate of horizontal steel bars in concrete increased with the temperature rising in any experimental parameter.

(a) Macrocell Corrosion Rate   (b) Microcell Corrosion Rate
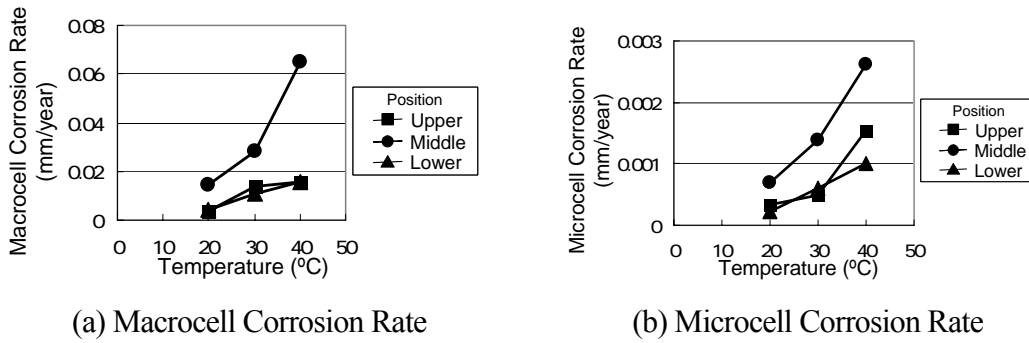
Fig. 2.4.8 Influence of Temperature on Macrocell and Microcell Corrosion Rate

of Different Position in Concrete.

(Horizontal Steel Bar, W/C = 0.55, Bleeding Ratio= 1.08%)

(a) Macrocell Corrosion Rate   (b) Microcell Corrosion Rate
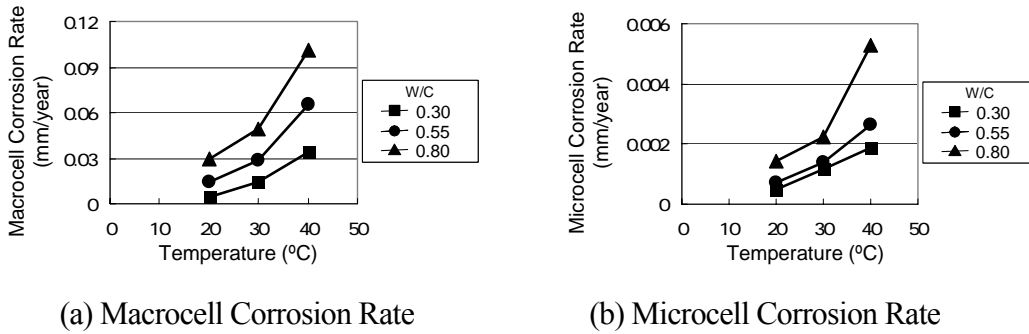
Fig. 2.4.9 Influence of Temperature on Macrocell and Microcell Corrosion Rate

of Different W/C

(Horizontal Steel Bar, Position=Upper, Bleeding Ratio= 1.08%)

(a) macrocell corrosion rate   (b) microcell corrosion rate
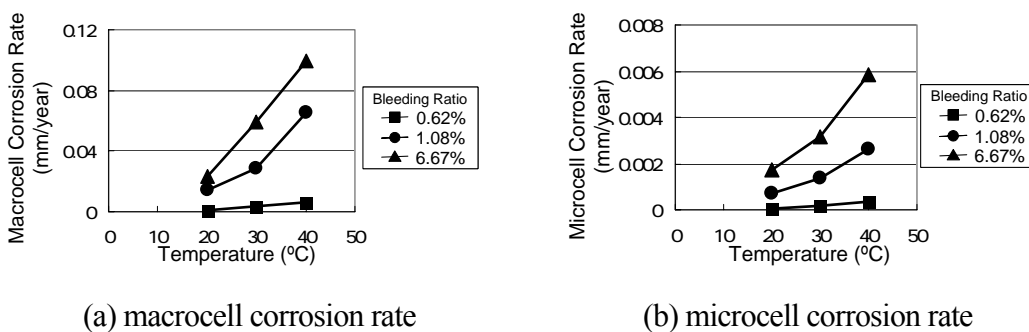
Fig. 2.4.10 Influence of Temperature on Macrocell and Microcell Corrosion Rate

of Different Bleeding Ratio

(Horizontal Steel Bar, Position= Upper, W/C = 0.55)

The magnifications of macrocell and microcell corrosion rate in horizontal steel bars are shown in **Table 2.4.5** to **Table 2.4.7** respectively. **Table 2.4.5** shows the data of the different position of concrete, **Table 2.4.6** shows the data of different W/C, and **Table 2.4.7** shows the data of different bleeding ratio. From these tables it can be seen that the magnification at 10 ℃ difference of temperature is almost 2.0. This indicates that the corrosion rate becomes 2 times with the 10 ℃ of temperature rising. Also it can be seen that the magnification of macrocell corrosion rate is relatively larger than that of microcell corrosion rate in horizontal steel bars.

Table 2.4.5 Magnification of Macrocell and Microcell Corrosion Rate
of Different Position in Concrete.

(Horizontal Steel Bar, W/C = 0.55, Bleeding Ratio= 1.08%)

Corrosion type / Height	Macrocell corrosion		Microcell corrosion	
	30℃ /20℃	40℃ /30℃	30℃ /20℃	40℃ /30℃
145	2.0	2.3	2.0	1.9
75	3.9	1.1	1.5	3.1
5	Cathode	Cathode	2.6	1.7

Table 2.4.6 Magnification of Macrocell and Microcell Corrosion Rate
of Different W/C

(Horizontal Steel Bar, Position= Upper, Bleeding Ratio= 1.08%)

Corrosion type / W/C	Macrocell corrosion		Microcell corrosion	
	30℃ /20℃	40℃ /30℃	30℃ /20℃	40℃ /30℃
0.3	3.5	1.6	2.5	1.9
0.55	2.0	2.3	2.0	1.9
0.8	2.5	1.7	1.8	1.9

Table 2.4.7 Magnification of Macrocell and Microcell Corrosion Rate
of Different Bleeding Ratio.

(Horizontal Steel Bar, Position= Upper, W/C = 0.55)

Corrosion type Bleeding Ratio	Macrocell corrosion		Microcell corrosion	
	30ºC /20ºC	40ºC /30ºC	30ºC /20ºC	40ºC /30ºC
0.62 %	2.8	2.4	2.4	1.6
1.08 %	2.0	2.3	2.0	1.9
6.67 %	1.7	2.1	1.5	2.4

2.4.3 Arrhenius plot of Cl⁻ Induced Corrosion

(1) Arrhenius plot in vertical steel bars

Arrhenius plot of experimental results in vertical steel bar shown in **Fig. 2.4.5**
to **Fig. 2.4.7** are shown in **Fig. 2.4.11** to **Fig. 2.4.13** respectively. From these figures it
can be seen that the logarithm of macrocell and microcell corrosion rate is proportional
to the reciprocal of the absolute temperature. The values of slope, the slopes, slices and
R^2 of approximate line in Arrhenius plot in vertical steel bar are shown in **Table 2.4.8**.
From this table it can be seen that R^2 of the approximate lines are more than 0.95 and
the macrocell and microcell corrosion rate of vertical steel bar in concrete apparently
agrees with the Arrhenius theory.

(a) Macrocell Corrosion Rate   (b) Microcell Corrosion Rate
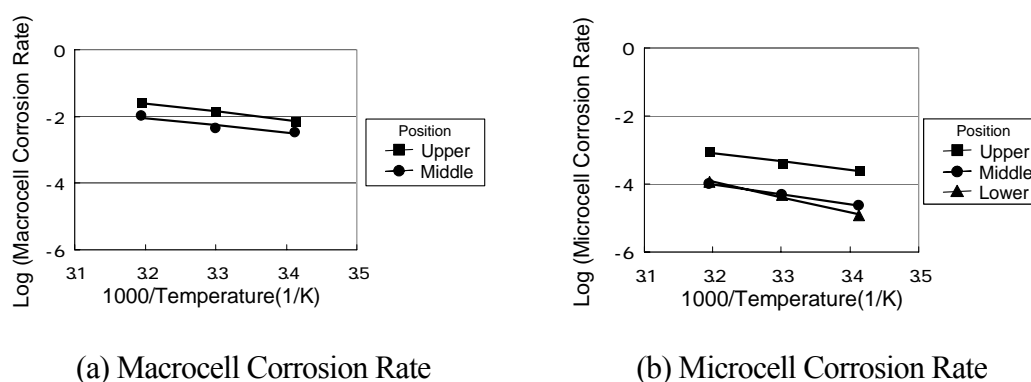
Fig. 2.4.11 Arrhenius Plot of Macrocell and Microcell Corrosion Rate
of Different Position in Concrete.

(Vertical Steel Bar, W/C = 0.55, Bleeding Ratio= 1.08%)

(a) Macrocell Corrosion Rate   (b) Microcell Corrosion Rate
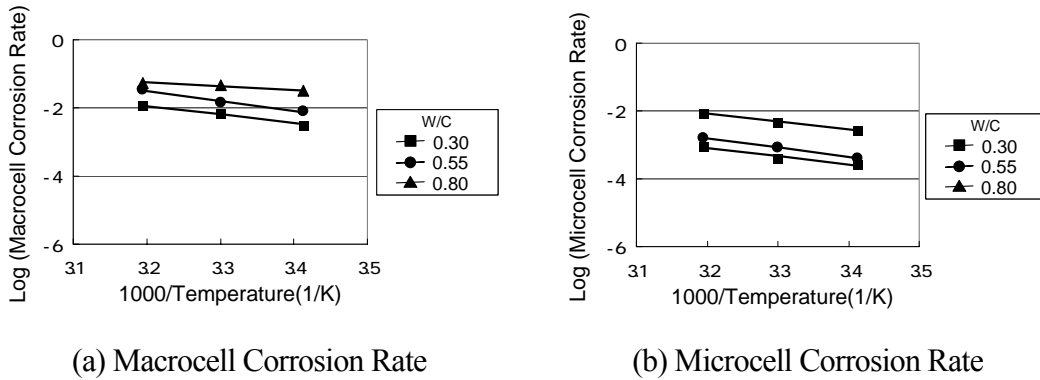
Fig. 2.4.12 Arrhenius Plot of Macrocell and Microcell Corrosion Rate

of Different W/C.

(Vertical Steel Bar, Position=Upper, Bleeding Ratio= 1.08%)

(a) Macrocell Corrosion Rate   (b) Microcell Corrosion Rate
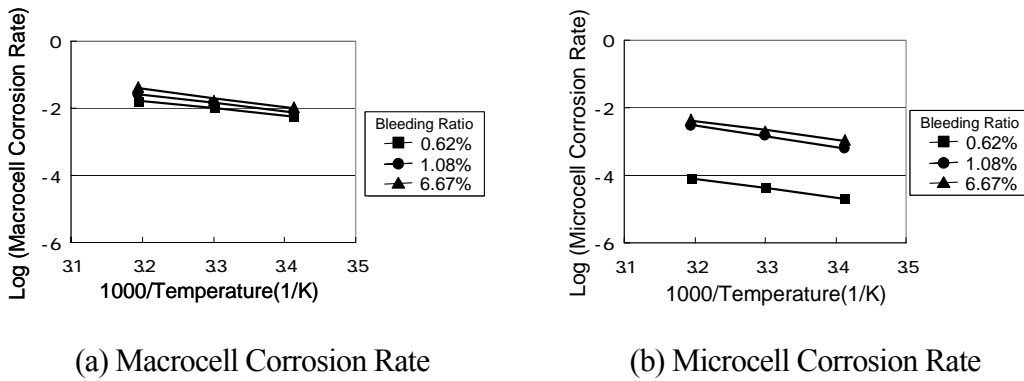
Fig. 2.4.13 Arrhenius Plot of Macrocell and Microcell Corrosion Rate

of Different Bleeding Ratio.

(Vertical Steel Bar, Position=Upper, W/C=0.55)

Table 2.4.8 Slopes, Slices and R^2 of Approximate Line in Arrhenius Plot of Vertical Steel Bar.

Corrosion type / No. of test piece*	Macrocell			Microcell		
	Slope	Slice	R^2	Slope	Slice	R^2
Upper-0.55-1.08	-2.46	6.2782	1.00	-2.76	6.02	0.96
Middle-0.55-1.08	-2.29	5.274	0.92	-2.76	5.34	1.00
Lower-0.55-1.08				-2.76	5.28	0.97
Upper-0.30-1.08	-2.55	6.2211	0.98	-2.78	4.78	0.99
Upper-0.55-1.08	-2.46	6.2782	1.00	-2.76	6.02	0.96
Upper-0.80-1.08	-1.14	2.3933	0.95	-2.75	6.41	0.99
Upper-0. 55-0.62	-2.12	5.0134	0.98	-2.48	10.40	0.99
Upper-0.55-1.08	-2.46	6.2782	1.00	-2.76	6.02	1.00
Upper-0. 55-6.67	-2.66	7.0944	0.96	-2.34	5.41	0.99

* No. of test piece expresses position (Upper, Middle or Lower) - water-cement ratio (0.30, 0.55 or 0.80) - bleeding ratio (0.62, 1.08 or 6.67)

(2) Arrhenius plot in horizontal steel bars

Arrhenius plot of experimental results in horizontal steel bar shown in **Fig. 2.4.8** to **Fig2.4.10** are shown in **Fig. 2.4.14** to **Fig. 2.4.16** respectively. From these figures it can be seen that the logarithm of macrocell and microcell corrosion rate in horizontal steel bar is proportional to the reciprocal of the absolute temperature.

The values of slope, slice and R^2 of a proximate line in Arrhenius plot in horizontal steel bar are shown in **Table 4.4.9**. From this table it can be seen that R^2 of the approximate lines are more than 0.95 and the macrocell and microcell corrosion rate of vertical steel bar in concrete apparently agrees with the Arrhenius equation.
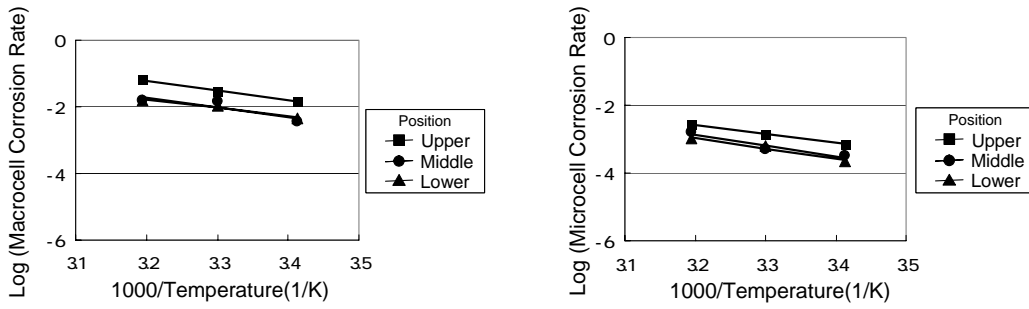
(a) Macrocell Corrosion Rate　　　(b) Microcell Corrosion Rate

Fig. 2.4.14 Arrhenius Plot of Macrocell and Microcell Corrosion Rate

of Different Position in Concrete.

(Horizontal Steel Bar, W/C = 0.55, Bleeding Ratio= 1.08%)
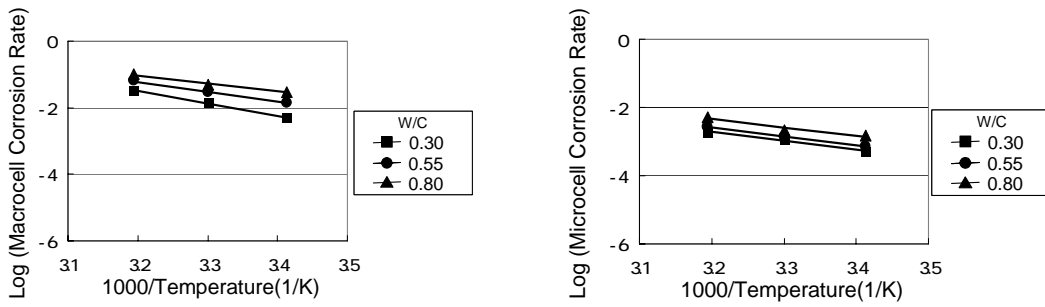
(a) Macrocell Corrosion Rate　　　(b) Microcell Corrosion Rate

Fig. 2.4.15 Arrhenius Plot of Macrocell and Microcell Corrosion Rate

of Different W/C.

(Horizontal Steel Bar, Position=Upper, Bleeding Ratio= 1.08%)

(a) Macrocell Corrosion Rate   (b) Microcell Corrosion Rate
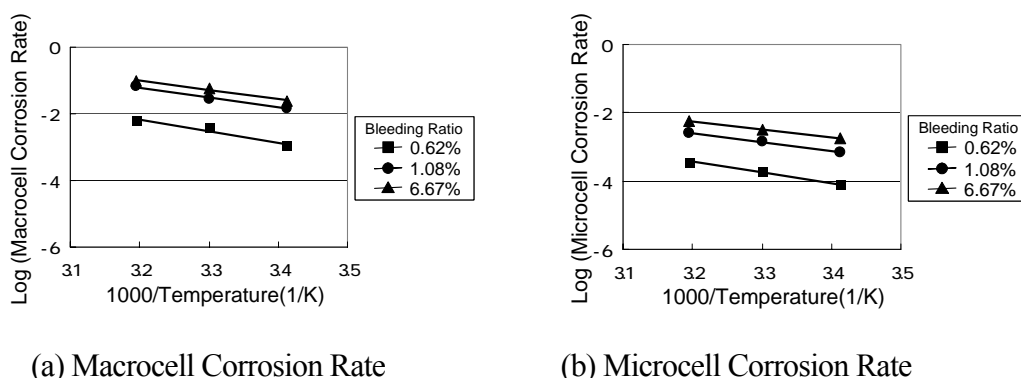
Fig. 2.4.16 Arrhenius Plot of Macrocell and Microcell Corrosion Rate
of Different Bleeding Ratio.

(Horizontal Steel Bar, Position=Upper, W/C=0.55)

Table 2.4.9 Slopes, Slices and R^2 of Approximate Line in Arrhenius Plot in
Horizontal Steel Bar.

Corrosion type / No. of test piece*	Macrocell			Microcell		
	Slope	Slice	R^2	Slope	Slice	R^2
Upper-0.55-1.08	-2.99	8.33	0.99	-2.63	5.84	1.00
Middle-0.55-1.08	-2.95	7.70	0.82	-3.09	7.01	0.93
Lower-0.55-1.08	-2.57	3.91	0.96	-2.98	6.54	0.98
Upper-0.30-1.08	-3.49	9.00	0.95	-3.13	6.59	0.99
Upper-0.55-1.08	-2.99	8.33	1.00	-2.63	5.84	1.00
Upper-0.80-1.08	-2.87	8.19	0.98	-2.04	5.46	1.00
Upper-0. 55-0.62	-3.86	10.88	1.00	-2.66	5.79	0.98
Upper-0.55-1.08	-2.99	8.33	0.99	-2.63	5.84	1.00
Upper-0. 55-6.67	-2.44	6.78	0.99	-2.56	5.87	0.96

* No. of test piece expresses corrosion form (macrocell or microcell) - position (Upper,
Middle or Lower) - water-cement ratio (0.30, 0.55 or 0.80) - bleeding ratio (0.62, 1.08
or 6.67)

2.4.4 Summary

The macrocell and microcell corrosion rate of Cl⁻ induced corrosion in concrete increased with the temperature rising. Additionally the logarithm of the corrosion rate is proportional to the reciprocal of absolute temperature. This fact indicates that the corrosion rate of steel bars in concrete induced by Cl⁻ apparently agrees with the Arrhenius theory.

2.5 Summary

The conclusions derived from this chapter can be summarized as follows:

1   It was confirmed that the Cl⁻ diffusivity of concrete increased with the temperature rising. Also the rate of macrocell and microcell corrosion of steel bar in concrete induced by Cl⁻ increased with the temperature rising. Especially the Cl⁻ diffusivity became almost 1.6 ~7.5 times, while the corrosion rate of steel bar in concrete induced by Cl- became almost 1.2 ~3.5 times with 10 oC of temperature rising.

2   The logarithms of these phenomena, diffusion of substance or corrosion of steel bar in concrete, were proportional to the reciprocal of absolute temperature. This fact indicated that the deterioration of reinforced concrete due to the steel corrosion induced by Cl⁻ apparently agreed with the Arrhenius theory.

3   The Cl⁻ diffusivity in concrete increased with the higher position of concrete. This tendency became larger in case of concrete with high bleeding.

4   Macrocell and microcell corrosion rate in concrete affected by bleeding became high with the bleeding ratio increasing. Moreover, higher macrocell corrosion rate generally prevailed in concrete affected by bleeding.

References of Chapter 2

2-1)   Fontana and Greene, Corrosion Engineering, McGraw-Hill, (1978).

2-2)   Otsuki, N., Hisada, M., Diola, N.B., Kobayashi, N., Experimental Study on

the effects of Rebar and Matrix Properties on the Gaps at the Interfacial Transition Zones in Reinforced Concrete,6th South East Asia-Pacific Conference on Structural Engineering & Construction,pp.1271-1276 (1998).

2-3)   Mohammed, T.U., Otsuki, N., Hamada, H., Chloride-Induced Corrosion of Steel Bars in Concrete with Presence of Gap at Steel-Concrete Interface,ACI Materials Journal,99/No.2,pp149-156 (2002).

2-4)   Otsuki, N., Yodsudjai, W., Nishida, T., Yamane, H., New Test Methods for Measuring Strength and Chloride Ion Diffusion Coefficient of Minute Region in Concrete, ACI Materials Journal, VOL.101, NO.2/A (2004).

2-5)   Moshiduki, N., Corrosion Monitoring of Roinforcing Steel Bars in Concrete using A-C Impedance Spectroscopy, Zairyo to Kankyo, 48,pp.693-696 (1999).

2-6)   Miyagawa, T., Matsumura, T., Kobayashi, K., Fujii, M., Oxygen transmission through concrete related to reinforcement corrosion, Journal of Materials, Concrete Structures and Pavements, No.408/V-11,pp.111-120 (1989).

2-7)   Tsuru, T., Maeda, R., Haruyama, S., Applying of A.C. method monitor to local corrosion, Technique of corrosion prevention 28, pp. 638-644 (1979).

2-8)   Miyazato, S., Otsuki N., Kimura, H., Steel Corrosion Induced by Chloride Ions and Carbonation in Mortar with Bending Cracks and Joints", Second Int. Conf. on Eng. Materials, Vol.2, pp.531-542 (2001).

Chapter 3

Influence of Temperature on

CO_2 Induced Corrosion in Concrete.

3.1 CO_2 Induced Corrosion in Concrete

One of the most common forms of deterioration of reinforced concrete observed today was caused by carbonation. Carbonation is a phenomenon that occurs when CO_2 gas in the air penetrates concrete and reacts with hydroxides to form calcium carbonates. The ensuing carbonation of the calcium hydroxide in the hydrated cement paste leads to the reduction in the alkalinity of the pore solution in concrete and consequently the corrosion of the embedded steel. While carbonation does not adversely affect the concrete itself, the durability of steel may be compromised because the passive ferrous oxide layer on the surface of the steel breaks down when the surrounding pH falls below 9.[3-1] "Thus, it could be argued that the potential service life of most steel in concrete is governed by the rates of carbonation and steel corrosion.

In the deterioration process of CO_2 induced corrosion, rate of carbonation of concrete and steel corrosion are one of the most important factors in case of the discussion about the deterioration period of concrete structures[3-2]. Moreover, these

rates are easily influenced by temperature. Consequently, it is necessary to know the influence of temperature on rate of carbonation of concrete and/or rate of CO_2 induced corrosion in order to maintain concrete structures efficiently.

For the reasons outlined above, the purposes of this chapter were chosen as follows;

(a) To study the influence of temperature on carbonation in concrete,

(b) To study the influence of temperature on the rate of steel CO_2 induced corrosion in concrete.

Especially in case of objective 1 influence of type of cement was examined, while in case of objective 2 CO_2 induced corrosion in concrete with cold-joint was examined.

3.2 Experimental Procedures

In this section the experimental methodology and experimental procedure used in this chapter were explained. Especially in this chapter, laboratory tests and field survey were conducted using three types of specimen and an existing reinforced concrete. Three types of specimen were named as TYPE A (C3), TYPE B (C3), TYPE C (C3) respectively. TYPE A (C3) was the cylindrical concrete specimens with the size of φ10cm x 20cm for investigating the influence of temperature on carbonation in concrete. TYPE B (C3) with the size of 10 cm x 10 cm x 40cm and TYPE C (C3) with the size of 180 cm x 20 cm x 10cm were the rectangle concrete specimens for investigating the influence of temperature on CO_2 induced corrosion. Additionally in case of TYPE A (C3) and TYPE B (C3) specimen, the influences of cement type on the rate of carbonation and steel corrosion in concrete were examined. On the other hand in case of TYPE C (C3) specimen influence of construction joint (cold-joint) on rate of steel corrosion was examined.

3.2.1 Materials Used

(1) Cement

In TYPE A (C3) and TYPE B (C3) specimens, three types of cements were used namely, Ordinary Portland Cement (OPC), High Early Strength Portland Cement (HESC) and Blast Furnace Slag Cement (BFSC). On the other hand in TYPE C (C3) specimens, OPC was used. The physical properties and chemical compositions of the said cements are shown in **Table 3.2.1** and **Table 3.2.2**.

Table 3.2.1 Physical Properties of Cement

Types of Cement	Density (g/cm^3)	Relative Surface Area (cm^2/g)	Setting			Compressive Strength (MPa)		
			Water Content (%)	Start (h-m)	Finish (h-m)	3d	7d	28d
OPC	3.16	3270	28.1	2-25	3-49	28.4	43.0	60.2
HESC	3.14	4510	30.1	1-50	2-55	46.9	56.8	67.3
BFSC	3.04	3860	28.9	3-00	4-15	21.2	35.2	61.3

Table 3.2.2 Chemical Composition of Cement.

Type of cement	MgO (%)	SO$_3$ (%)	Loss on Ignition (%)	Total alkali content (%)	Cl$^-$ (%)
OPC	1.49	2.06	1.96	0.58	0.008
HESC	1.33	2.95	1.09	0.49	0.005
BFSC	3.16	1.98	1.68	0.48	0.006

(2) Aggregates

River sand (Obitsu, Chiba-prefecture) was used as fine aggregate. Also Crash stone (Ome, Tokyo) was used as course aggregate. The physical properties of fine and course aggregate are shown in **Table 3.2.3**.

Table 3.2.3 Physical Properties of Fine and Course Aggregates.

Kinds of aggregate	Density (g/cm^3)		F.M.[2*]	W.A.R.[3*] (%)	WB[4*] (kg/l)
	SSD[1*]	DRY			
Fine aggregate	2.63	2.59	2.51	1.54	1.73
Course aggregate	2.65	2.63	6.71	1.09	1.54

1*: Surface saturated dry condition, 2*: Fine modulus, 3*: Water adsorption ratio, 4*: Weight per volume.

(3) Mixing water

Tap water was used as mixing water. Before mixing the tap water was put in the experimental room in order to make the temperature of water same with temperature of room (20±2 ℃).

(4) Chemical admixture

Water-reducing agent and air-entrained agent (FLOWRIC Co., Ltd.) were used as chemical admixtures.

(5) Steel

Inside of TYPE B (C3) specimen, the steel of SD345 (D13, deformed bar) was embedded. The chemical compositions and physical property of steel is shown in **Table 3.2.4**.

Table 3.2.4 Chemical Compositions and Physical Property of Steel (TYPE B (C3)).

	Fe (%)	C (%)	Si (%)	Mn (%)	P (%)	S (%)	Yield strength (N/mm^2)
JIS standard	—	—	—	—	<0.050	<0.05	345<
Measured	98.25	0.22	0.3	1.21	0.012	0.009	358

On the other hand, inside of TYPE C (C3) specimen, the steel of SD345 (D19, deformed bar) was embedded. The chemical compositions and physical property of steel is shown in **Table 3.2.5**.

Table 3.2.5 Chemical Compositions and Physical Property of Steel (TYPE C (C3)).

	Fe (%)	C (%)	Si (%)	Mn (%)	P (%)	S (%)	Yield strength (N/mm^2)
JIS standard	—	—	—	—	<0.050	<0.05	345<
Measured	98.26	0.22	0.3	1.21	0.012	0.009	358

3.2.2 Manufacturing Procedure of Specimen

(1) Outline of specimen

In this chapter, three types of specimen were used. The details of specimen are shown in below.

TYPE A (C3) specimens were un-reinforced concrete specimen. These specimens were made of concrete cylinders having a diameter of 10 cm and a height of 20 cm. These specimens were used in the tests for depth of carbonation and void ratio of concrete.

TYPE B (C3) specimens were reinforced concrete specimens. **Fig. 3.2.1** shows the detailed layout of TYPE B (C3) specimen (10 cm x 10 cm x 40 cm) used. To compare the rate of corrosion, two-13 mm diameter deformed steel bars having a length of 30 cm were embedded in the concrete specimen. The steel bar with 10 mm cover was positioned at the front side, while the other steel bar with 25 mm concrete cover was positioned at the rear side parallel to the first bar. In order to measure the current density in the steel bars, electrical wires were soldered on it serving as contact points for the electrical connection. To ensure that the diffusion of CO_2 will be concentrated only along the surfaces adjacent to the location of the steel bars with 10 mm and 25 mm cover, except for the two exposed surfaces all the other sides of the concrete specimens were covered with epoxy resin.
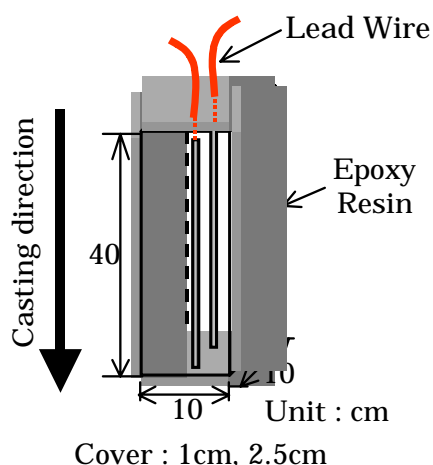
Fig.3.2.1 Outline of TYPE B (C3) Specimen.

TYPE C (C3) specimens were also reinforced concrete specimen. **Fig. 3.2.2** shows the detailed layout of the TYPE C (C3) specimen (180cm x 20 cm x 10 cm) used. The steel bar in concrete was divided into elements with 20 cm or 25 cm length, and the divided steel bars were regarded as one electrically because each steel element was connected by lead wire. To ensure that the diffusion of CO_2 was concentrated only from the side surfaces, top and bottom of the concrete specimens were covered with epoxy resin.
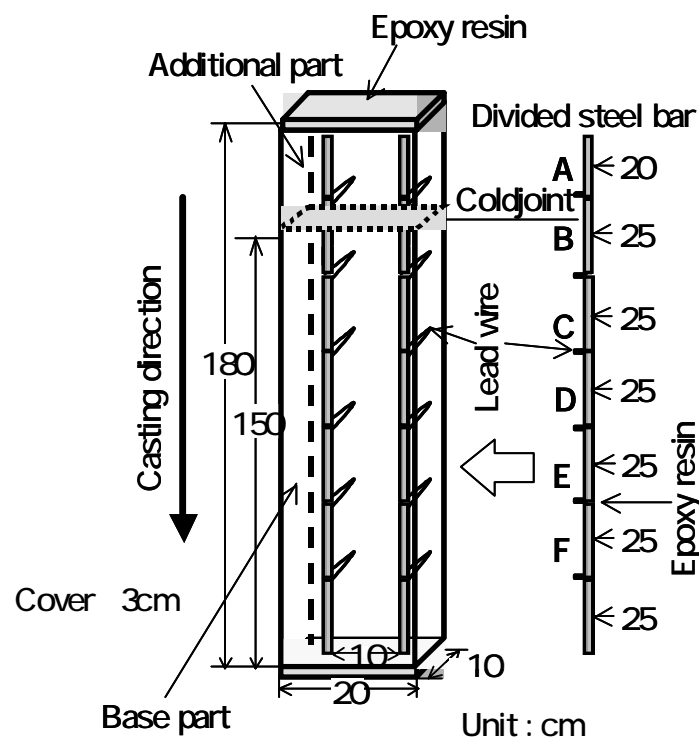
Fig.3.2.2 Outline of TYPE C (C3) Specimen

(2) Mixture proportion of specimen

In case of TYPE A (C3) and TYPE B (C3) specimens, the water cement (W/C) ratio used in the investigation was 0.55. The details of the amount of cement, sand, gravel, air-entraining agent (AE) and air-entraining water reducing agent (AEWRA) used in the concrete mix preparations are shown in **Table 3.2.6**. **Table 3.2.7** shows the summary of the slump, air content and the bleeding rate of concrete that were mixed and cast at 20ºC, 30ºC and 40ºC temperatures, respectively. As shown in the table,

specimens containing BFSC have shown higher slump as compared with the specimens with OPC and HESC. The air content in OPC concrete at 20ºC was quite higher as compared with the concrete specimens with HESC and OPC. Generally, the percentage of bleeding in the concrete specimens was low.

Table 3.2.6 Mixture Proportion of TYPE A (C3) and TYPE B (C3) Specimens.

Cement type	W/B (%)	Unit (kg/m^3)				Unit (g/m^3)	
		W	C	S	G	AD1[1*]	AD2[2*]
OPC	55	165.0	300.0	774.4	1018.0	660.0	21.0
	45	152.6	339.1			746.0	24.0
HESC	55	165.0	300.0	773.8	1017.1	660.0	21.0
	45	152.6	339.0			746.0	24.0
BFSC	55	165.0	300.0	770.2	1012.4	660.0	21.0
	45	152.3	338.5			745.0	24.0

1*: Water-Reducing Agent, 2*: Air-Entrained Agent

Table 3.2.7 Slump, Air Content and Bleeding in Concrete.

Temperature (℃)	Type of Cement	W/C	Slump (cm)	Air Content (%)	Bleeding Rate (%)*
20	OPC	0.55	9.0	3.3	0.44
	HESC	0.55	9.0	2.8	0.32
	BFSC	0.55	13.0	2.5	0.76
30	OPC	0.55	8.0	2.5	0.14
	HESC	0.55	9.5	2.5	0.10
	BFSC	0.55	11.0	2.1	0.44
40	OPC	0.55	6.5	2.1	
	HESC	0.55	7.0	2.0	
	BFSC	0.55	10.0	1.8	

*JIS A 1123

On the other hand, in case of TYPE C (C3) specimens, three levels of water cement (W/C) ratio was used. The details of the amount of cement, sand, gravel, air-entraining agent (AE) and air-entraining water reducing agent (AEWRA) used in the concrete mix preparations are shown in **Table 3.2.8**.

Table 3.2.8 Mixture Proportion of TYPE C (C3) Specimens.

W/C	kg/m^3				g/m^3		%
	W	C	S	G	AD1^{1*}	AD2^{2*}	BR^{3*}
30	165	550	621	958	3437	—	0.10
	165	550	621	958	6875	—	1.00
55	173	315	771	1037	—	—	0.27
	216	392	682	922	—	—	1.90
80	206	258	826	912	—	3000	0.42
	375	469	587	636	—	2600	5.00

1*: Water-Reducing Agent, 2*: Air-Entrained Agent, 3*: Bleeding ratio

(3) Mixing and placing of specimen

Cement was sandwiched between two layers of fine aggregate in the mixer, and then those were mixed for 30 seconds. Water was added as the mixer was continuously rotating for 30 seconds. As soon as all the water was poured, the mixer was stopped for 60 seconds, and the mortar adhered to the sides and paddle of the mixer was scraped off. Finally, the coarse aggregate was added and the concrete was mixed for 120 seconds. The concrete specimens were cast as soon as the mixing finishes. The casting was done in approximate lifts. Each lift was vibrated for 6 seconds prior to the placing of the next lift.

In case of TYPE A (C3) and C3-B specimens, mixing and placing of the specimens for each case were done inside a controlled environmental chamber set at 20ºC, 30ºC and 40ºC temperatures, respectively and at 90% constant relative humidity. On the other hand TYPE C (C3) specimens, mixing and placing of the specimens for each case were done inside a controlled environmental chamber set at 20ºC temperatures, and at 60% constant relative humidity.

(4) Curing

In case of TYPE A (C3) and TYPE B (C3) specimens, they were demoulded after 24 hours of moist curing (20ºC, 30ºC and 40ºC, 90% R.H.). Demoulded specimens were cured in the same moist condition for 7 days. After that, specimens

exposed to carbonation condition (CO_2 concentration: 15%, temperature: 20ºC, 30ºC and 40, relative humidity: 75 %) for fixed days.

In case of TYPE C (C3) specimens, they were demoulded after 24 hours of moist curing and these concrete specimens were cured in the laboratory (temperature : 20ºC, relative humidity: 60%) for 28 days. After that, they were cured in the carbonation condition (Concentration of CO_2: 10%, temperature: 40ºC, relative humidity: 90%) for 56 days in order to accelerate the carbonation process in concrete. Moreover, they were exposed outdoors for 24 months (Mean temperature: 17ºC, Mean rainfall: 130 mm/month).

3.2.4 Outline of Existing Reinforced Concrete

The existing concrete member used in the field test is shown in **Fig. 3.2.3.** It was the wall located at 20 m above ground and about 36 years old. There were three cold-joints in the upper part of the measuring area. Cover concrete, 75mm thickness originally, came off in some degree. Compressive strength was about 35 MPa and carbonation depth was 43 mm. Also, it was assumed that the steel in concrete was imaginarily divided into 7 elements with 15 cm length, and they were named "A" to "G". The field tests were performed in three seasons. They were winter (10.4ºC, 35 %R.H.), spring (22.2ºC, 55 %R.H.) and summer (31.4ºC, 34 %R.H.).
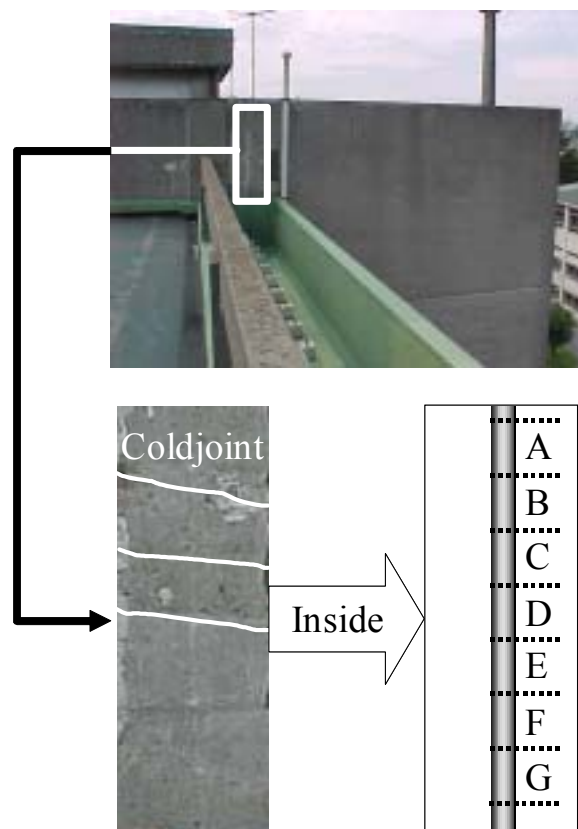
Fig. 3.2.3 Outline of Existing Reinforced Concrete

3.2.5 Parameters

TYPE A (C3) and C3-B specimens after curing were placed in environment control room where temperature and relative humidity could be controlled arbitrarily. The range of temperature was set at 20ºC, 30ºC and 40ºC, and that of relative humidity was set at 75%. The experimental cases are shown in **Table 3.2.9**.

Table 3.2.9 Experimental Cases for TYPE A (C3) and C3-B Specimens.

Cement type	W/B(%)	Temperature (ºC)		
		20	30	40
OPC	45	○	○	
	55	○	○	○
HESC	45	○	○	
	55	○	○	○
BFSC	45	○	○	
	55	○	○	○

TYPE C (C3) specimens after curing were placed in environment control room where temperature and relative humidity could be controlled arbitrarily. The range of temperature was set at 10ºC, 20ºC, 30ºC and 40ºC, and that of relative humidity was set at 60%, 75% and 90 %. The experimental cases are shown in **Table 3.2.10**.

Table 3.2.10 Experimental Cases for TYPE C (C3) Specimens.

Humidity(%)	Temperature (ºC)			
	10	20	30	40
60	○	○	○	○
75		○	○	
90		○	○	

3.2.6 Items of Investigation

(1) Carbonation depth

Determination of the carbonation depth in the concrete specimens at 7, 14, 21 and 35 days was made using the phenolphthalein test method. The indicator solution was prepared using 1.0% of phenolphthalein powder and 99% ethyl alcohol by weight. This test was performed by spraying the indicator solution on the surfaces of freshly

broken concrete cylinder specimens free from dust. If the concrete was carbonated, its' color remained the same. However, if it was not carbonated the color of the concrete specimens will changed into purple color. The depths of carbonation in the concrete specimens were measured by tracking the edges of the color changes whose mean were recorded.

(2) Void ratio of concrete

Determination of the void ratio in the concrete specimens was done by cutting sample test pieces (about 10 mm thick) from the un-reinforced cylindrical concrete specimens. Air present in the pores of the test pieces was removed by immersing it in water for 24 hours inside a vacuum dessicator with low pump pressure. The test pieces were then removed from the vacuum dessicator and the excess water from the specimens was shaken off and wiped with a clean piece of cloth. At this stage, the specimens were considered to be water saturated and surface dry (SSD). Their weights in air (W1) and in water (W2) at SSD condition were then measured and recorded. Subsequently, the sample test pieces were oven-dried at 65ºC for 48 hours. The weight of the specimens after oven dried (W3) were measured and recorded. Calculation of the void ratio was done by using the equation shown below

$$\varepsilon = \left(\frac{W_1 - W_3}{W_1 - W_2} \right)$$

(3-1)

where, ε : void ratio

W_1 : weight in air at saturated surface dry condition (g)

W_2 : weight of the sample in water at saturated surface dry condition (g)

W_3 : weight of the sample after oven dried (g)

(3) Oxygen permeability test

Oxygen permeability was measured by the same method with Chapter 2.

(4) Corrosion rate

Macrocell, microcell and total corrosion rate of steel bar in concrete specimens were measured by the same method with Chapter 2.

On the other hand measurement method in field survey was shown in below[3-3]. First the model of the steel corrosion in existing reinforced concrete is explained. The corrosion reaction is occurred by electrochemical reaction as mentioned in Chapter 1. And, the electric double layer with several Å of thickness has formed in the interface of steel and concrete. It can be considered as the electric circuit with resistance and condenser. However, the condenser be not seem to the factor which controls corrosion current of the steel bar in the concrete, since it flows only in the unidirection.

Considering above, the electro circuit model were constructed as shown in **Fig. 3.2.4**. In this model, Rc and Rp express the concrete resistance and polarization resistance respectively. And these values can be measured by non-destructive test. Vs means half-cell potential on steel surface and it also can be measured by non-destructive test. Consequently Vc means potential in concrete and can not measured by non-destructive test. Therefore concrete potential is calculated as follows.

The sum of current of one point in concrete equal to 0. Considering above, the sum of the current at No. 4 equal to 0 and Equation (3-2) can be obtained.
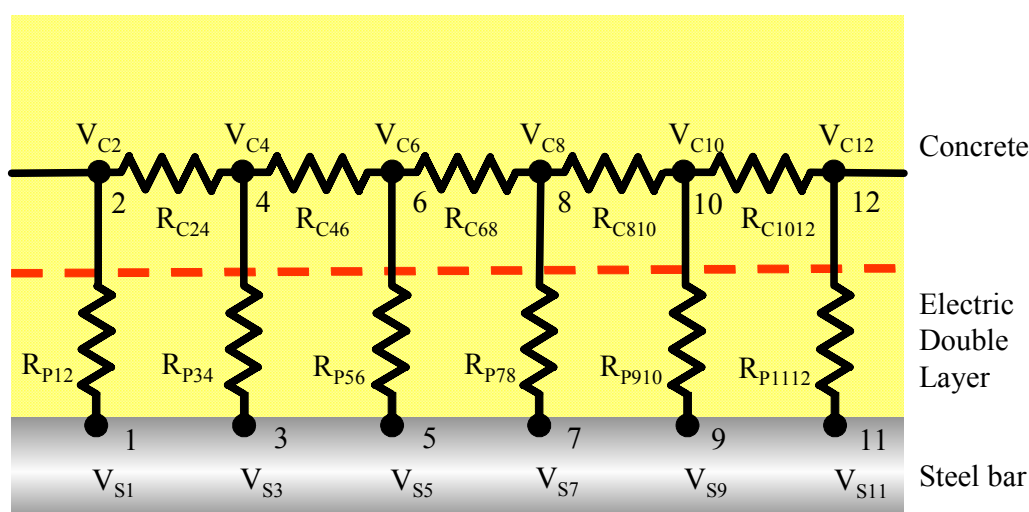
Fig.3.2.4 Electro Circuit Model of Steel Corrosion in Concrete.

$$\sum_n I_i = I_{24} + I_{64} + I_{34} = 0 \qquad\qquad\qquad\qquad (3\text{-}2)$$

where, I_{ij} : current flowing from point i to point j

And the current can be expressed as shown in Equation (3-3) from Ohm's low.

$$I = \frac{V}{R} \qquad\qquad\qquad\qquad (3\text{-}3)$$

where, I_{ij} : current (A)

        V : potential difference (V)

        R : means resistance (Ω)

From Equation (3-2) and Equation (3-3), Equation (3-4) can be obtained.

$$\frac{V_{C4} - V_{C2}}{R_{C24}} + \frac{V_{C4} - V_{C6}}{R_{C46}} + \frac{V_{C4} - V_{S3}}{R_{P34}} = 0 \qquad (No.4) \qquad\qquad (3\text{-}4)$$

Same equations can be obtained as follows

$$\frac{V_{C2} - V_{C4}}{R_{C24}} + \frac{V_{C4} - V_{S1}}{R_{S12}} = 0 \qquad\qquad (No.2) \qquad\qquad (3\text{-}5)$$

$$\frac{V_{C6} - V_{C4}}{R_{C46}} + \frac{V_{C6} - V_{C8}}{R_{C68}} + \frac{V_{C6} - V_{S5}}{R_{P56}} = 0 \qquad (No.6) \qquad\qquad (3\text{-}6)$$

$$\frac{V_{C8} - V_{C6}}{R_{C68}} + \frac{V_{C8} - V_{C10}}{R_{C810}} + \frac{V_{C8} - V_{S7}}{R_{P78}} = 0 \qquad (No.8) \qquad\qquad (3\text{-}7)$$

$$\frac{V_{C10} - V_{C8}}{R_{C810}} + \frac{V_{C10} - V_{C12}}{R_{C1012}} + \frac{V_{C10} - V_{S9}}{R_{P910}} = 0 \qquad (No.10) \qquad\qquad (3\text{-}8)$$

$$\frac{V_{C12} - V_{C10}}{R_{C1012}} + \frac{V_{C12} - V_{S11}}{R_{P1112}} = 0 \qquad \text{(No.12)} \qquad \text{(3-9)}$$

From above equations, the current flow from steel surface to concrete can be expressed as follows.

$$I_{12} = \frac{V_{S1} - V_{C2}}{R_{P12}} \quad 、 \quad I_{34} = \frac{V_{S3} - V_{C4}}{R_{P34}} \quad 、 \quad I_{56} = \frac{V_{S5} - V_{C6}}{R_{P56}}$$

$$\text{(3-10)}$$

$$I_{78} = \frac{V_{S7} - V_{C8}}{R_{P78}} \quad 、 \quad I_{910} = \frac{V_{S9} - V_{C10}}{R_{P910}} \quad 、 \quad I_{1112} = \frac{V_{S11} - V_{C12}}{R_{P1112}}$$

These current shows the macrocell current from steel bar to concrete. The macrocell current density in existing reinforced concrete can be calculated using this macrocell current.

On the other hand microcell current in existing reinforced concrete measured by the same method with Chapter 2.

3.3 Influence of Temperature on Carbonation of Concrete

In this section, the influence of temperature on carbonation in concrete was investigated using TYPE A (C3) specimen.

3.3.1 Influence of Cement Type on Carbonation of Concrete

The influence of cement type on carbonation depth in the concrete specimens is shown in **Fig.3.3.1** to **Fig.3.3.3**. This figures show relatively high variation in the carbonation depth of the three types of concrete used, OPC, HESC and BFSC. The specimens containing BFSC showed the greatest rate of carbonation followed by OPC and HESC, respectively. The possible reason for this was due to the less free $Ca(OH)_2$ in BFSC. On the other hand, in the case of HESC concrete specimens it can be

observed that its resistance to carbonation was relatively higher as compared with the other two types of cement used.
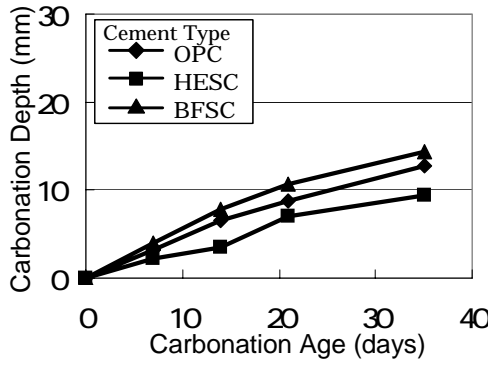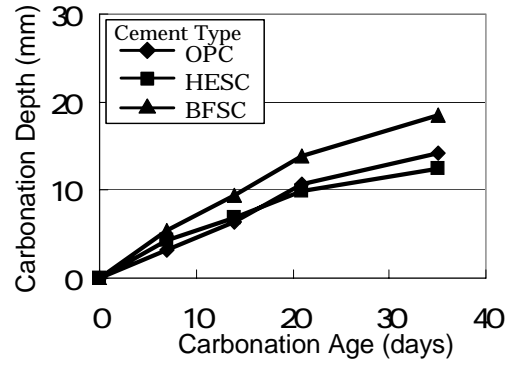
(a) Water-Cement Ratio=0.45   (b) Water-Cement Ratio=0.55

Fig. 3.3.1 Influence of Cement Type on Rate of Carbonation (20ºC).
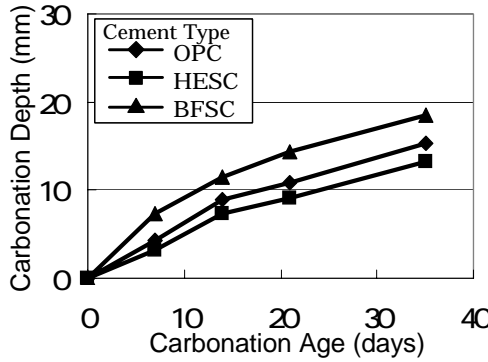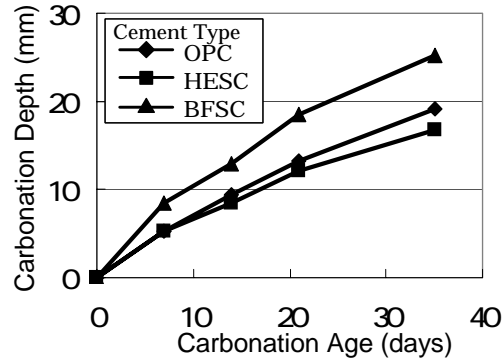
(a) Water-Cement Ratio=0.45   (b) Water-Cement Ratio=0.55

Fig. 3.3.2 Influence of Cement Type on Rate of Carbonation (30ºC).
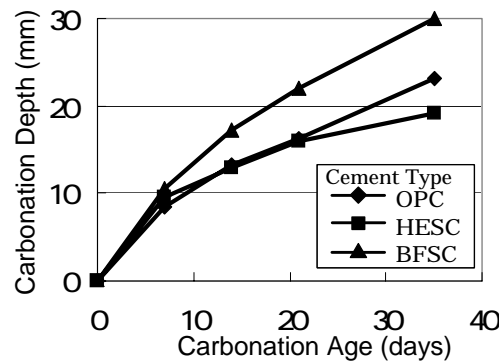
Water-Cement Ratio=0.55

Fig. 3.3.3 Influence of Cement Type on Rate of Carbonation (40ºC).

3.3.2 Influence of Temperature on Carbonation of Concrete

Generally it is said that the progress of carbonation follows the root t rules as shown Equation (3-11).

$$C = A\sqrt{t} \tag{3-11}$$

where, C : carbonation depth (mm)

         A : carbonation coefficient (mm/$t^{0.5}$)

         t : Carbonation age (days)

So the carbonation progress using the carbonation coefficient shown above can be evaluated. **Table 3.3.1** shows the average values of the carbonation coefficient. The carbonation coefficient is large in case of higher exposure temperature. **Table 3.3.2** shows the magnification of carbonation coefficient. From this table it can be seen that the carbonation coefficient becomes 1.2~1.9 times as the temperature rises with 10 °C.

Table 3.3.1 Carbonation Coefficient.

Cement type	W/C	Temperature (ºC)		
		20	30	40
OPC	0.55	2.57	3.22	3.87
	0.45	2.16	2.61	
HESC	0.55	2.27	2.81	3.30
	0.45	1.88	2.24	
BFSC	0.55	3.33	4.25	5.10
	0.45	2.61	3.16	

Table 3.3.2 Magnification of Carbonation Coefficient.

Cement type	W/C	Temperature (ºC)	
		30ºC /20ºC	40ºC/30ºC
OPC	0.55	1.25	1.20
	0.45	1.21	
HESC	0.55	1.24	1.17
	0.45	1.91	
BFSC	0.55	1.28	1.20
	0.45	1.21	

The influence of cement type on carbonation coefficient is shown in **Fig.3.3.4**. From this figure, it can be confirmed that the carbonation coefficient increases with the temperature rising.
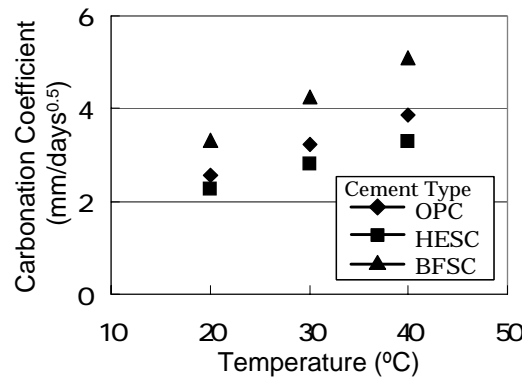
Fig. 3.3.4 Influence of Cement Type on Carbonation Coefficient with Elevated Temperature Environment (W/C=0.55).

3.3.3 Arrhenius Plot of Carbonation of Concrete

The Arrhenius plot of the result of **Fig.3.3.4** is shown **Fig.3.3.5**. From these figures it can be concluded that the logarithm of carbonation coefficient is proportional to the reciprocal of absolute temperature. This fact indicates that the carbonation of concrete apparently agrees with the Arrhenius theory. The slopes, slices and R are shown in **Table 3.3.3**.
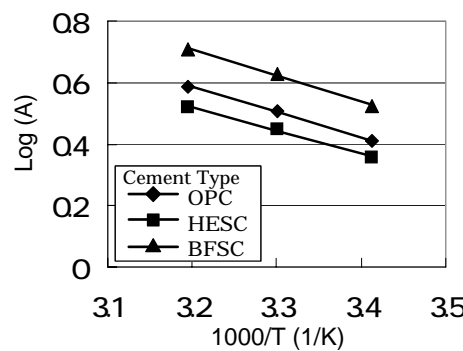
Fig. 3.3.5 Arrhenius Plot of Fig. 3.3.4**.**

Table 3.3.3 Slopes, Slices and R^2 of Approximate Line in Arrhenius Plot of Carbonation of Concrete.

Cement type	W/C	Slop	Slice	R^2
OPC	0.55	-0.82	3.20	0.9984
	0.45*	-0.73	2.82	-
HESC	0.55	-0.75	2.90	0.9962
	0.45*	-0.68	2.58	-
BFSC	0.55	-0.85	3.43	0.9959
	0.45*	-0.74	2.93	-

*: Calculated from only the data of 2 points

3.3.4 Summary

Concrete specimens containing Ordinary Portland cement have shown better performance against carbonation at lower temperature (20°C) as compared with Blast Furnace Slag Cement. On the other hand, Blast Furnace Slag Cement concrete performs better (higher corrosion resistance) at higher temperature (30°C and 40°C) as compared with Ordinary Portland Cement concrete and High Early Strength Cement concrete especially when exposed at longer period of time.

The carbonation coefficient in concrete increases with the temperature rising. Additionally the logarithm of the carbonation coefficient is proportional to the reciprocal of absolute temperature. This fact indicates that the carbonation coefficient in concrete apparently agrees with the Arrhenius theory.

3.4 Influence of Temperature on CO_2 Induced Corrosion in Concrete

In this section, the influence of temperature on CO_2 induced corrosion in concrete was investigated using TYPE B (C3) and TYPE C (C3)specimen. TYPE B (C3) was used for the investigation on the influence of temperature on CO_2 induced

corrosion of steel bar in concrete containing different cement. Additionally in case of TYPE B (C3) specimen there are 2 ways of casting, curing and testing. In one case the reinforced concrete specimen exposed to same temperature during casting, curing and testing. And in the other case the reinforced concrete specimen exposed to 30 ℃ during casting and curing, and exposed to 20 ℃, 30 ℃ or 40℃ during testing. First one can evaluate the influence of temperature and cement type, while second one can evaluate the influence of temperature. On the other hand TYPE C (C3) specimen was used for the investigation on the influence of temperature on CO_2 induced corrosion of steel bar in concrete with cold-joint.

3.4.1 Influence of Temperature on CO_2 Induced Corrosion in Concrete with Different Cement

(1) Influence of cement type in different temperature

In this investigation TYPE B (C3) specimen exposed to same temperature during casting, curing and testing was used.

The result of the half-cell potential test using Ag/AgCl as a reference electrode is shown in **Fig. 3.4.1** to **Fig. 3.4.3**. A more negative reading in the specimens generally indicates higher probability of corrosion. However, this general rule may not always be applicable due to various factors that influence the result of the half-cell potential measurements such as the oxygen concentration or the carbonation in the concrete. The result only provides information on the probability of corrosion occurring at a given location and time but not the actual rate of corrosion. For the specimens having 10 mm cover depth, it was very clear that BFSC containing specimens have more negative potential after 7 and 14 days as compared with the specimens containing OPC and HESC. The reason for this was due to the greater carbonation rate in BFSC concrete specimens, causing earlier initiation of corrosion in the steel bars as a result of the breaking down of the protective film which are protecting the steel bars. However, as the specimens were exposed over a longer period of time (21-35 days) variation in their half-cell potentials were very minimal. Perhaps this may be due to the simultaneous corrosion taking place in the steel bars as a result of the depasivation of the protective film protecting the steel bars in the specimens containing OPC and HESC. As for the

specimens with 25 mm cover depth, BFSC concrete specimens generally exhibited greater corrosion potential than in the specimens with OPC and HESC. The same reason can be said and this was due to the effect of carbonation in BFSC containing specimens causing a lower concrete resistance in the said specimens.
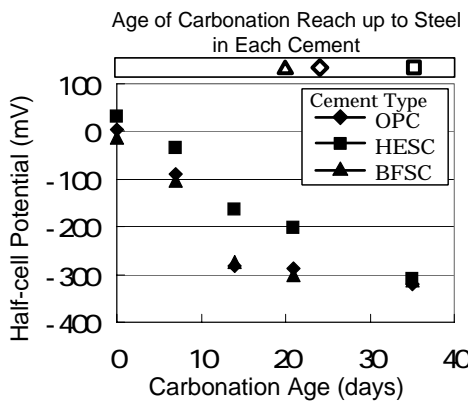
(a) Cover = 10 mm, W/C=0.45   (b) Cover = 10 mm, W/C=0.55
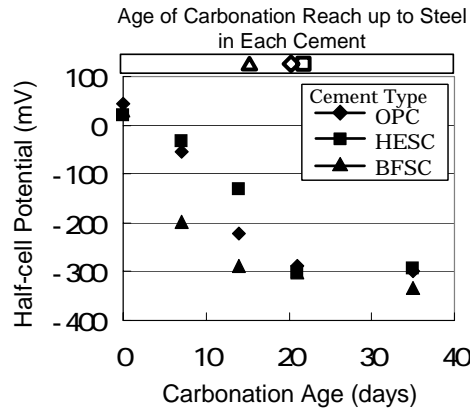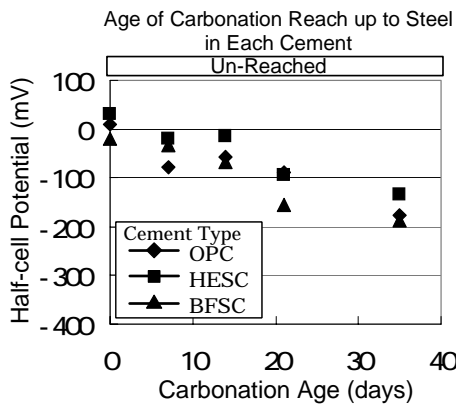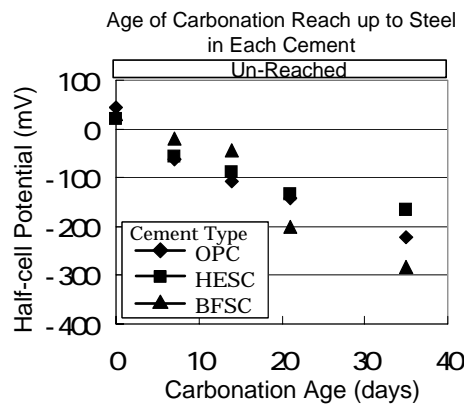
(c) Cover = 25 mm, W/C=0.45   (d) Cover = 25 mm, W/C=0.55

Fig. 3.4.1 Influence of Cement Type on Half-cell Potential (20ºC).
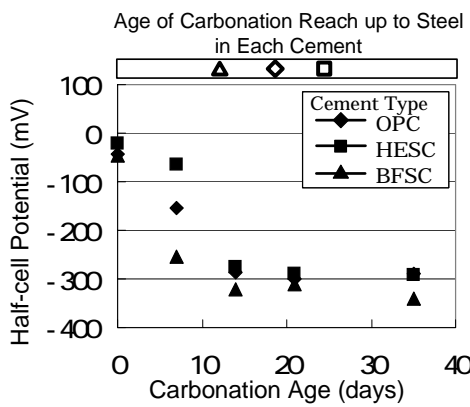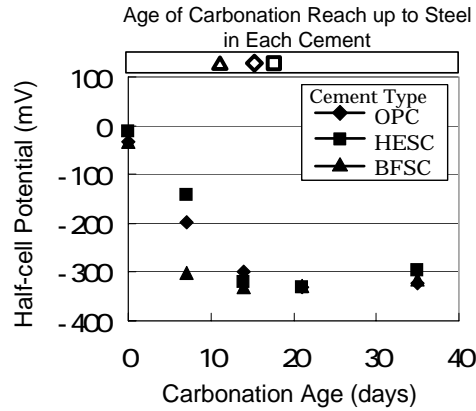
(a) Cover = 10 mm, W/C=0.45
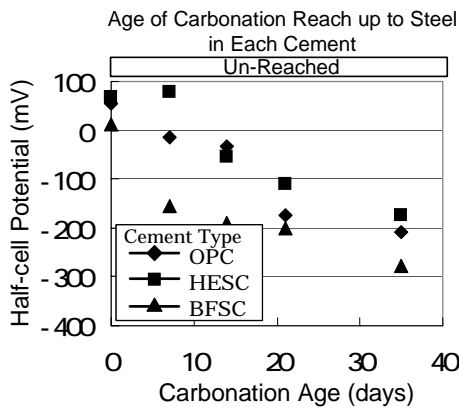
(b) Cover = 10 mm, W/C=0.55
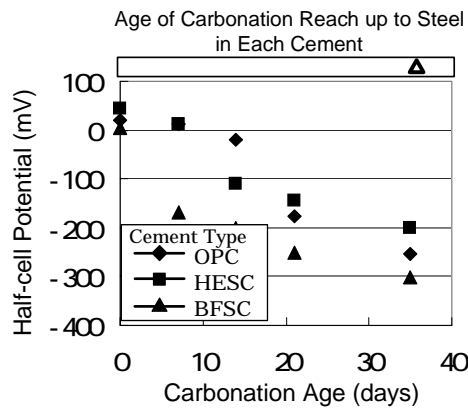
(c) Cover = 25 mm, W/C=0.45

(d) Cover = 25 mm, W/C=0.55

Fig. 3.4.2 Influence of Cement Type on Half-cell Potential (30ºC).
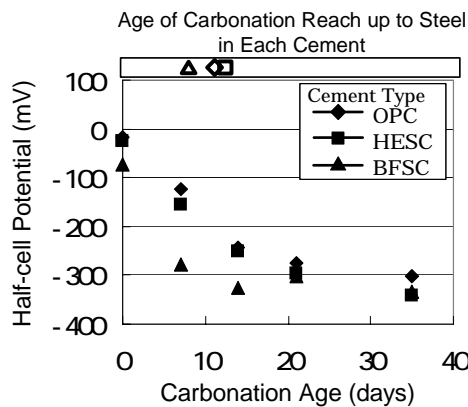
(a) Cover = 10 mm, W/C=0.55
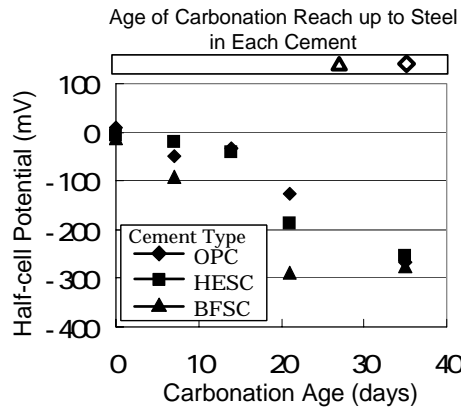
(b) Cover = 25 mm, W/C=0.55

Fig. 3.4.3 Influence of Cement Type on Half-cell Potential (40ºC).

Above phenomenon can be explained by **Fig. 3.4.4** to **Fig. 3.4.6**. These figures show the relationship between half-cell potential and the depth of uncarbonated region at each temperature. From these figures it can be seen that the half-cell potential decreases with the depth of uncarbonated region decreasing. Although the half-cell potential does not directly indicate the corrosion speed on steel surface, it is considered that the CO_2 induced corrosion in concrete follows the depth of uncarbonated region regardless of cement type.
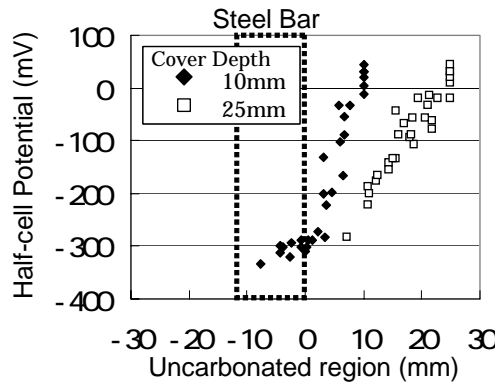
Fig. 3.4.4 Relationship between Half-cell Potential and Depth of Uncarbotated Region (20ºC).
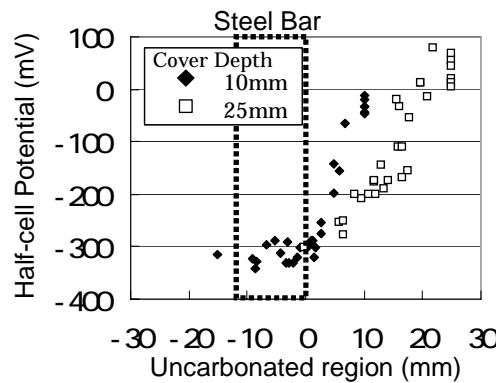
Fig. 3.4.5 Relationship between Half-cell Potential and Depth of Uncarbonated Region (30ºC).
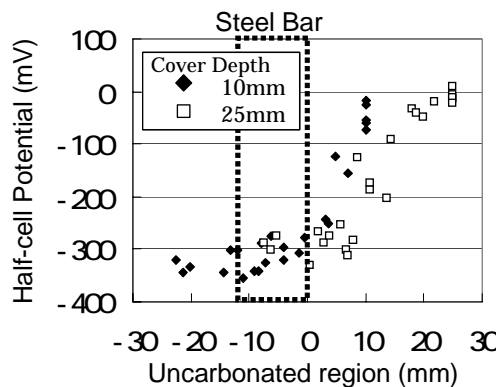
Fig. 3.4.6 Relationship between Half-cell Potential and Depth of Uncarbonated Region (40ºC).

Fig. 3.4.7 to **Fig. 3.4.9** show the results of the corrosion test. Specimens with BFSC gave a high rate of corrosion than in specimens containing either HESC or OPC at 20 ºC (see **Fig. 3.4.7**). This is due to the effect of temperature, which will be discussed in the next section. The corrosion rate of the specimen with a 10 mm cover showed what looks like a parabolic dependence with depth. As the carbonation progresses, the pH is bound to be lowered in the vicinity of the steel bar, resulting in increased rate of corrosion. For steel bars with 25 mm concrete cover (BFSC) the corrosion rate increased with temperature rising as shown in **Fig. 3.4.7**, **Fig. 3.4.8** and **Fig. 3.4.9**. The rate of corrosion of the steel in all of the concrete specimens showed increasing trend with time.
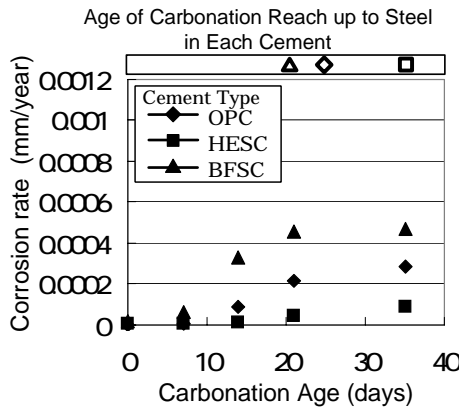
(a) Cover = 10 mm, W/C=0.45
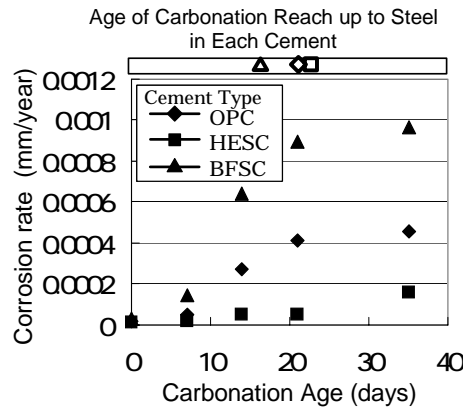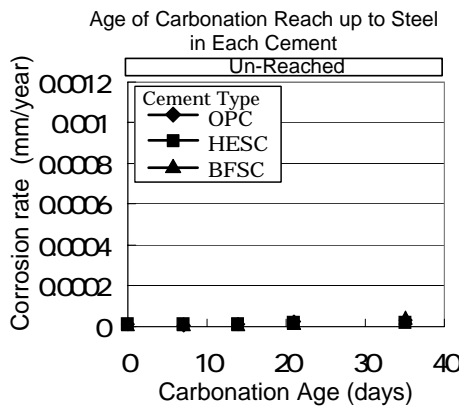
(b) Cover = 10 mm, W/C=0.55
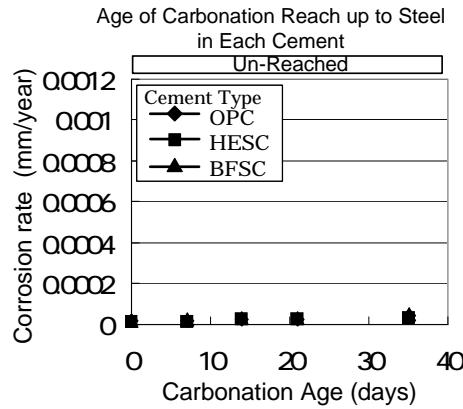
(c) Cover = 25 mm, W/C=0.45

(d) Cover = 25 mm, W/C=0.55

Fig. 3.4.7 Influence of Cement type on Corrosion Rate (20ºC).
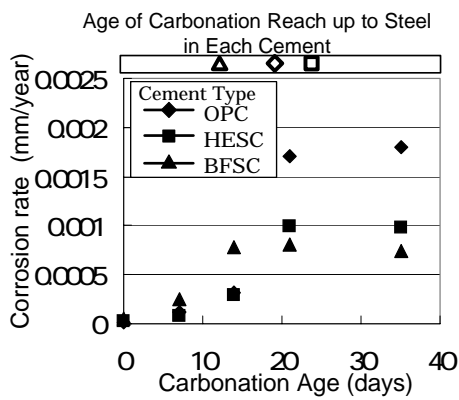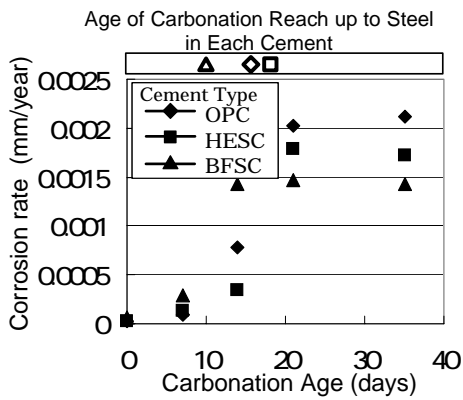
(a) Cover = 10 mm, W/C=0.45
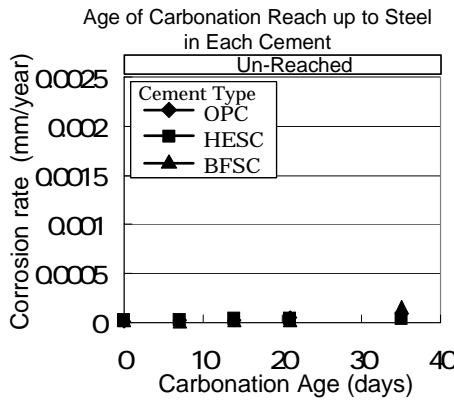
(b) Cover = 10 mm, W/C=0.55
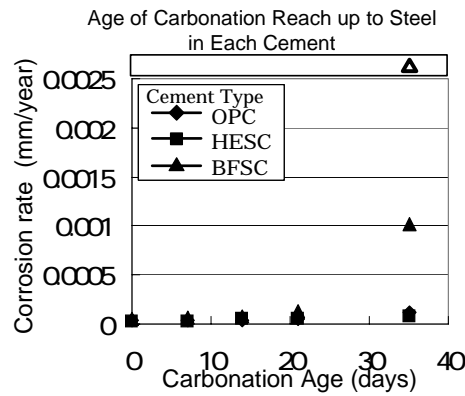
(c) Cover = 25 mm, W/C=0.45 (d) Cover = 25 mm, W/C=0.55

Fig. 3.4.8 Influence of Cement Type on Corrosion Rate (30ºC).
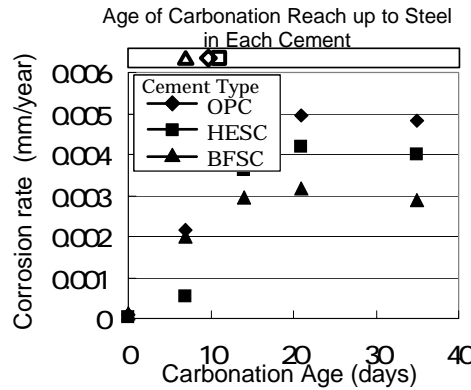
(a) Cover = 10 mm, W/C=0.55
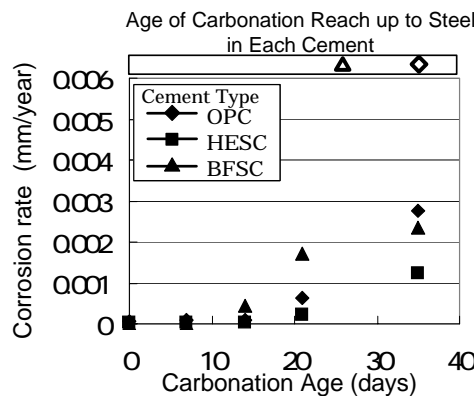
(b) Cover = 25 mm, W/C=0.55

Fig. 3.4.9 Influence of Cement Type on Corrosion Rate (40ºC).

Above phenomenon can be explained by carbonation progress and oxygen permeability. **Fig. 3.4.10**, **Fig.3.4.11** and **Fig. 3.4.12** show the relationship between corrosion rate and depth of uncarbonated region. And **Fig. 3.4.13** shows the relationship between corrosion rate and oxygen permeability after the carbonation depth reaches up to steel bar. From these figures, it can be seen that the corrosion rate of steel bar in concrete is controlled by depth of uncarbonated region before the carbonation depth reaches up to steel bar, and after that the corrosion rate in concrete is controlled by oxygen permeability.
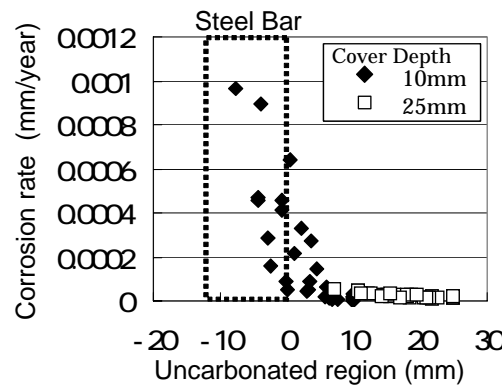
Fig. 3.3.10 Relationship between Corrosion Rate and Depth of Uncarbonated Region (20ºC).
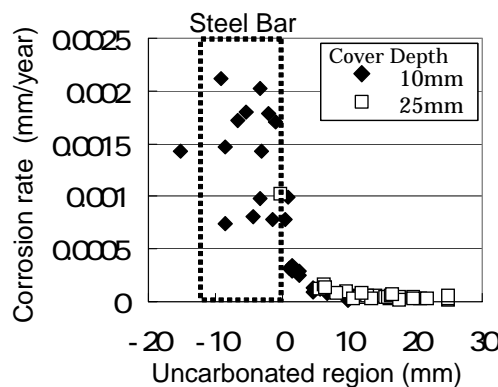
Fig. 3.3.11 Relationship between Corrosion Rate and Depth of Uncarbonated Region (30ºC).
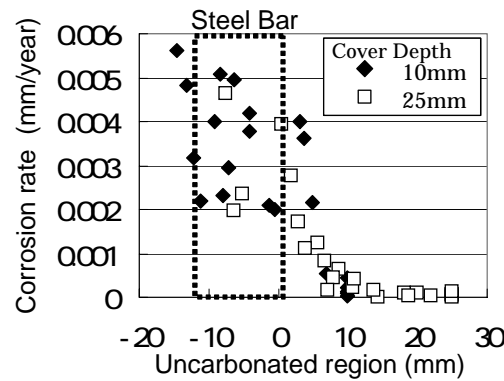
Fig. 3.3.12 Relationship between Corrosion Rate and Depth of Uncarbonated Region (40℃).
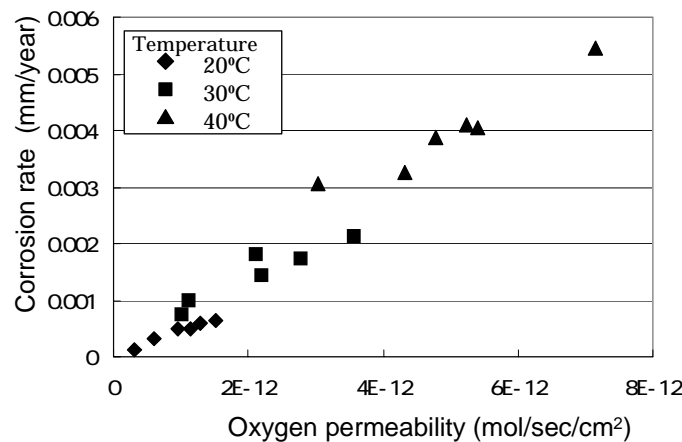
Fig. 3.3.13 Relationship between Corrosion Rate and Oxygen Permeability after Carbonation Depth Reaches up to Steel Bar.

(2) Influence of temperature on CO_2 induced corrosion

In this investigation TYPE B (C3) specimen exposed to 30 ℃ during casting and curing, and exposed to 20 ℃, 30 ℃ or 40℃ during testing.

The influences of temperature on corrosion rate of steel bars are shown in **Fig. 3.4.14**. Also influences of temperature on oxygen permeability are shown in **Fig. 3.4.15**. From these figures it can be seen that the corrosion rate of steel bars induced by CO_2 and oxygen permeability in concrete increases with the temperature rising in any experimental parameter.
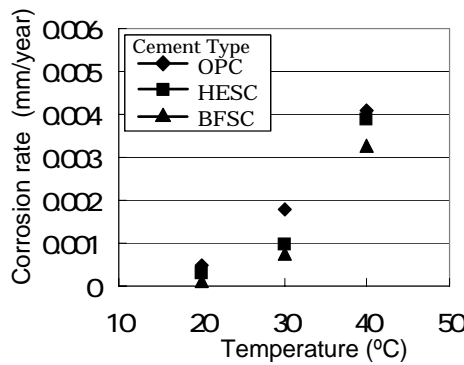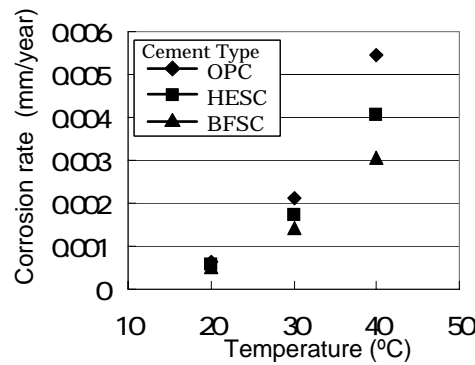
(a) Cover = 10 mm, W/C=0.45   (b) Cover = 10 mm, W/C=0.55

Fig. 3.4.14 Influence of Temperature on Corrosion Rate.
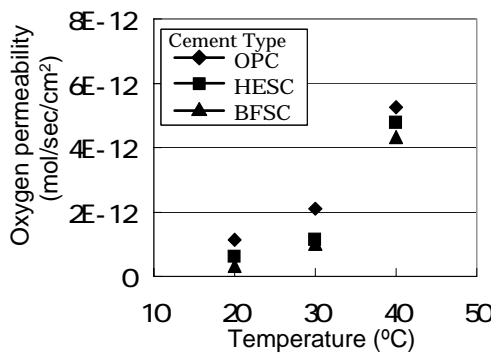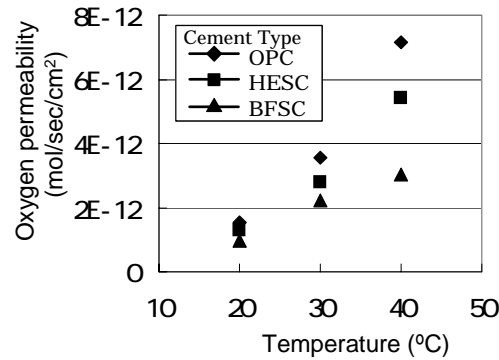
(a) Cover = 10 mm, W/C=0.45   (b) Cover = 10 mm, W/C=0.55

Fig. 3.4.15 Influence of Temperature on Oxygen Permeability.

The magnifications of corrosion rate and oxygen permeability in concrete are shown in **Table 3.4.1**. From this table it can be seen that the magnification at 10 ºC difference of temperature is almost 2.0. This indicate that the corrosion rate and the oxygen permeability become 2.0 times with the 10 ºC of temperature rising.

Table 3.4.1 Magnification of Corrosion Rate and Oxygen Permeability.

Evaluation Item / Cement type	Corrosion rate		Oxygen permeability	
	30ºC/20ºC	40ºC /30ºC	30ºC /20ºC	40ºC /30ºC
OPC-0.45	3.60	2.28	1.85	2.49
HESC-0.45	3.15	3.96	1.84	4.23
BFSC-0.45	6.04	4.40	3.17	4.28
OPC-0.55	3.25	2.58	2.35	2.00
HESC-0.55	2.92	2.35	2.16	1.95
BFSC-0.55	2.86	2.13	2.29	1.38

(3) Arrhenius plot of corrosion rate in concrete induced by CO2 (different cement type)

Arrhenius plot of experimental results of corrosion rate are shown in **Fig. 3.4.16**. Also Arrhenius plot of experimental results of oxygen permeability are shown in **Fig. 3.4.17**. From these figures it can be seen that the logarithm of corrosion rate is proportional to the reciprocal of the absolute temperature.

The values of slope, slice and R^2 of approximate line in Arrhenius plot of corrosion rate and oxygen permeability are shown in **Table 3.4.2**. From this table it can be seen that R^2 of the approximate lines are more than 0.95 and the macrocell and microcell corrosion rate of vertical steel bar in concrete apparently agrees with the Arrhenius equation.

(a) Cover = 10mm (b) Cover = 25mm
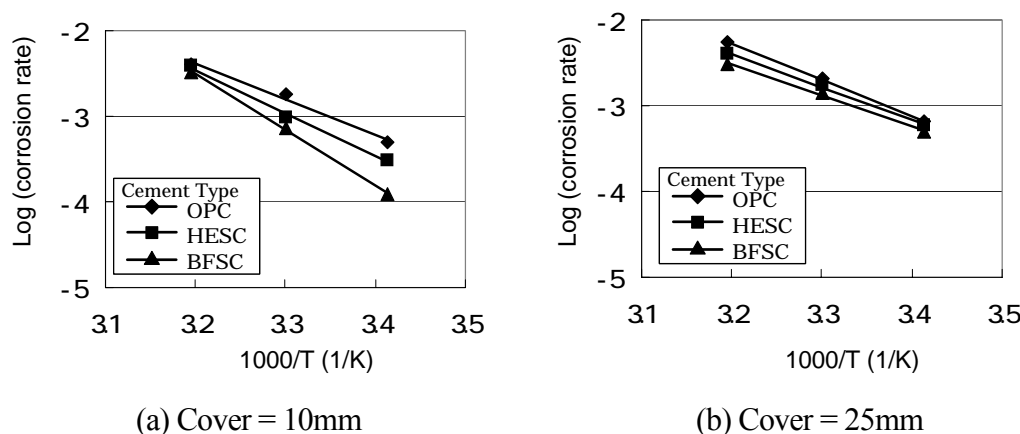
Fig. 3.4.16 Arrhenius Plot of Corrosion Rate.

(a) Cover = 10mm   (b) Cover = 25mm
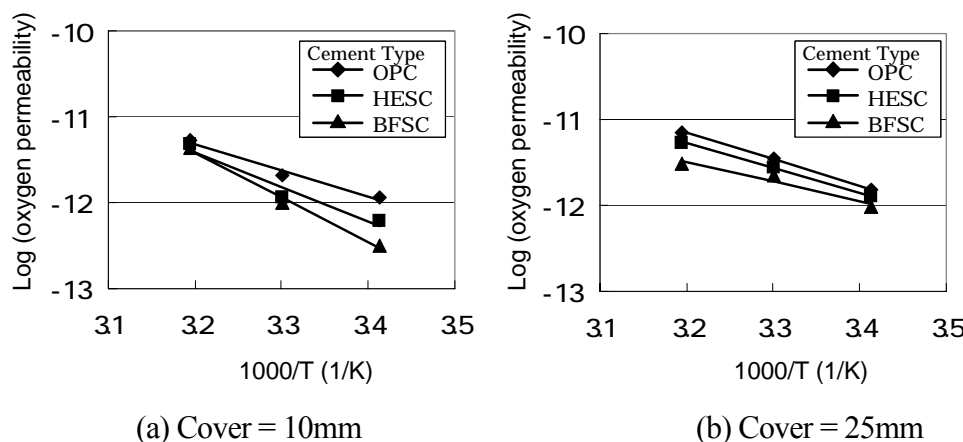
Fig. 3.4.17 Arrhenius Plot of Oxygen Permeability.

Table 3.4.2 Slopes, Slices and R^2 of Approximate Line in Arrhenius Plot of Corrosion Rate and Oxygen Permeability.

Evaluation Item / Cement type	Corrosion rate			Oxygen permeability		
	Slope	Slice	R^2	Slope	Slice	R^2
OPC-0.45	-4.20	11.06	0.99	-3.03	-1.63	0.98
HESC-0.45	-5.02	13.60	0.99	-4.07	1.62	0.94
BFSC-0.45	-6.53	18.40	1.00	-5.19	5.17	0.99
OPC-0.55	-4.24	11.29	1.00	-3.09	-1.27	1.00
HESC-0.55	-3.84	9.89	1.00	-2.87	-2.11	1.00
BFSC-0.55	-3.60	9.00	0.99	-2.30	-4.14	0.95

3.4.2 Influence of Temperature on CO_2 Induced Corrosion in Concrete with Cold-joint

(1) Distribution of corrosion rate of steel bars in specimen

The distribution of macrocell, microcell and total corrosion rate on the steel bars in reinforced concrete specimen with cold-joint is shown in **Fig. 3.4.18** to **Fig.3.4.19**. From these figures, it is confirmed that the corrosion rate near cold-joint is higher compared to its lower part. The better condition of corrosion at the upper part of cold-joint is prevalent in concrete with high bleeding ratio. Since corrosion reaction on

the steel is influenced by concrete resistance and oxygen permeability, therefore, corrosion reaction on the steel may be accelerated due to the presence of water and the availability of oxygen near the steel. Low concrete resistance and high oxygen permeability in concrete implies greater risk of corrosion.

On the other hand, as manifested on the result obtained from the electrochemical measurement, macrocell corrosion rate dominantly prevailed over the microcell corrosion rate. Therefore, it can be concluded that the type of corrosion prevailed on the vertical steel bar in concrete with cold-joint is macrocell corrosion type.

(a) Macrocell Corrosion Rate   (b) Microcell Corrosion Rate
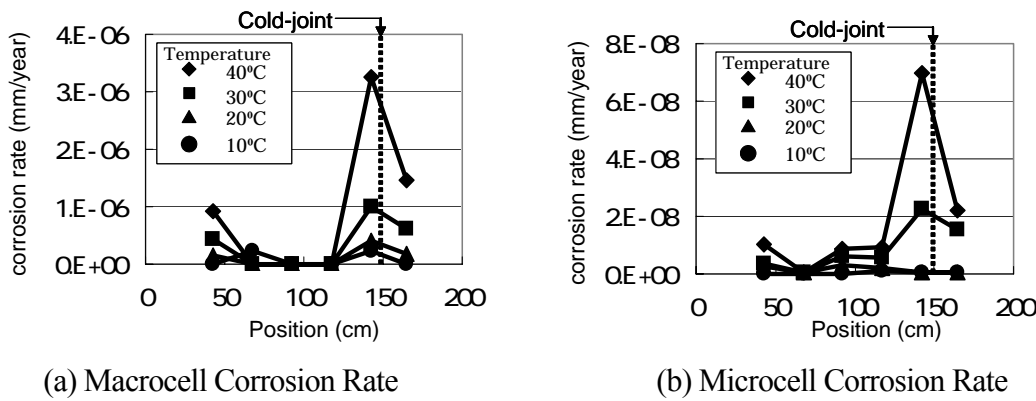
Fig. 3.4.18 Distribution of Corrosion Rate of Steel Bar in Concrete with Cold-joint.
(W/C=0.30)

(a) Macrocell Corrosion Rate   (b) Microcell Corrosion Rate
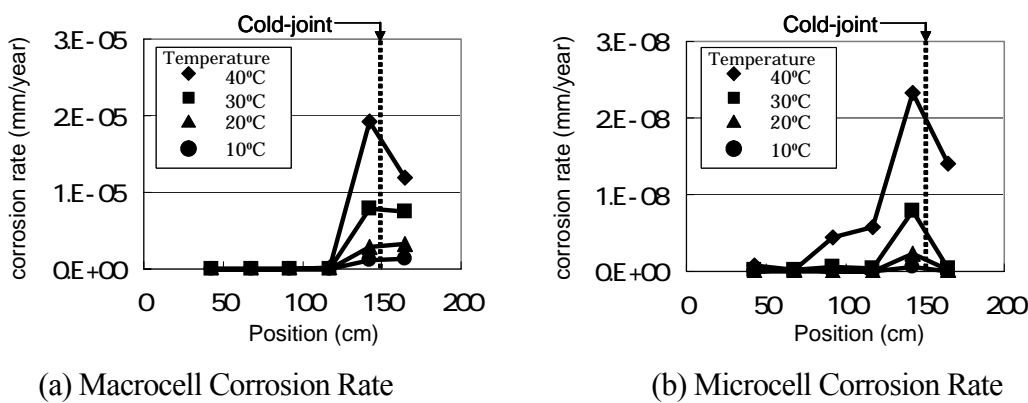
Fig.3.4.19 Distribution of Corrosion Rate of Steel Bar in Concrete with Cold-joint.
(W/C=0.55)

(a) Macrocell Corrosion Rate (b) Microcell Corrosion Rate
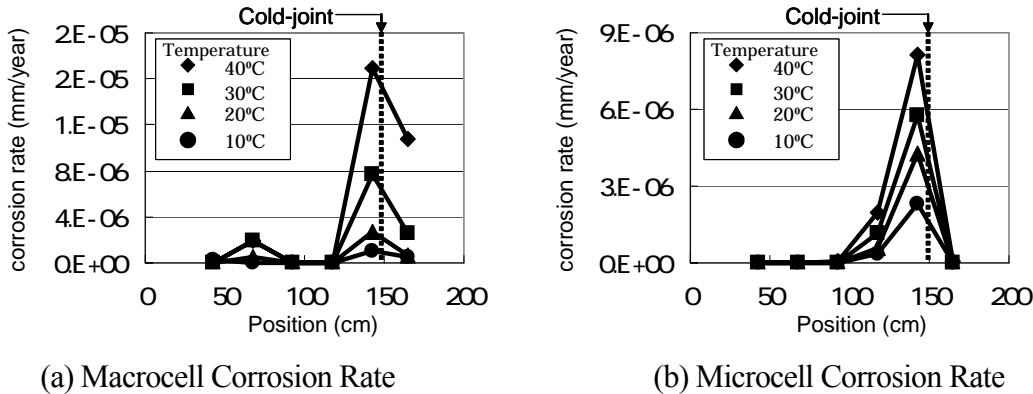
Fig. 3.4.20 Distribution of Corrosion Rate of Steel Bar in Concrete with Cold-joint.
(W/C=0.80)

(2) Influence of temperature on corrosion rate of steel bar at cold-joint

The influences of temperature on macrocell and microcell corrosion rate of steel bars in concrete specimen with cold-joint are shown in **Fig. 3.4.21** to **Fig. 3.4.22**. From these figures it can be seen that the macrocell and microcell corrosion rate of steel bars in concrete increases with the temperature rising.

(a) Macrocell Corrosion rate (b) Microcell Corrosion Rate
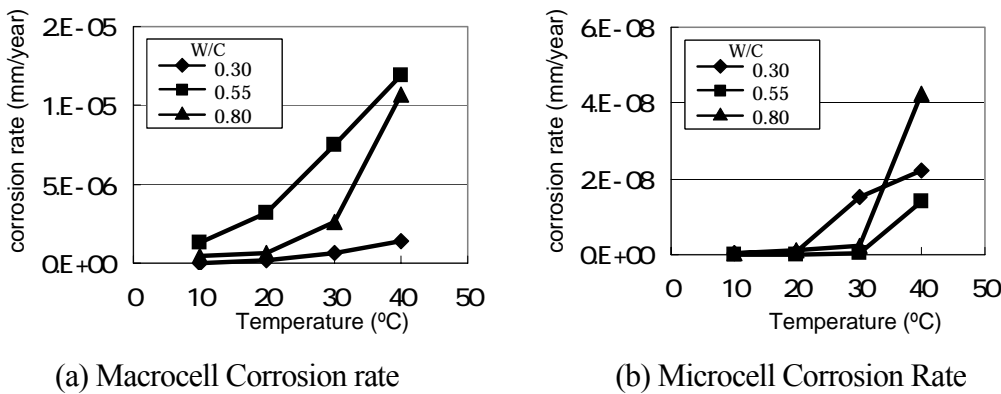
Fig. 3.4.21 Influence of Temperature on Macrocell and Microcell Corrosion Rate in Concrete with Cold-joint. (Upper Part of Cold-joint)

(a) Macrocell Corrosion Rate (b) Microcell Corrosion Rate
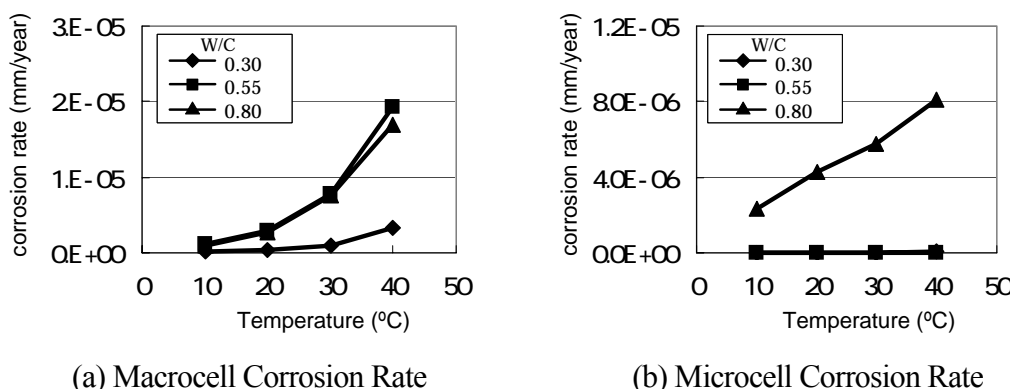
Fig. 3.4.22 Influence of Temperature on Macrocell and Microcell Corrosion Rate in Concrete with Cold-joint. (Lower Part of Cold-joint)

The magnifications of macrocell and microcell corrosion rate of steel bars are shown in **Table 3.4.3**. From this table it can be seen that the magnification at 10 ℃ difference of temperature is almost 2.0~3.0. This indicate that the corrosion rate becomes 2.0~3.0 times with the 10 ℃ of temperature rising.

Table 3.4.3 Magnification of Macrocell and Microcell Corrosion Rate of Steel Bar in Concrete with Cold-joint.

W/C	Macrocell corrosion rate					
	Upper part of cold-joint			Lower part of cold-joint		
	20℃/10℃	30℃ /20℃	40℃ /30℃	20℃ /10℃	30℃ /20℃	40℃ /30℃
0.30	18.00	3.56	2.34	1.86	2.39	3.26
0.55	2.53	2.35	1.58	2.54	2.66	2.47
0.80	1.40	3.86	4.11	2.69	2.83	2.21
W/C	Microcell corrosion rate					
	Upper part of cold-joint			Lower part of cold-joint		
	20℃/10℃	30℃ /20℃	40℃ /30℃	20℃ /10℃	30℃ /20℃	40℃ /30℃
0.30	1.37	25.16	1.46	2.24	37.66	3.12
0.55	6.09	3.22	34.49	3.51	3.50	2.96
0.80	3.52	1.78	19.68	1.85	1.35	1.41

(3) Arrhenius plot of corrosion rate in concrete induced by CO_2 (with cold-joint)

Arrhenius plot of experimental results are shown in **Fig. 3.4.23** to **Fig3.4.28** respectively. From these figures it can be seen that the logarithm of macrocell and microcell corrosion rate is proportional to the reciprocal of the absolute temperature.

The values of slope, slice and R^2 of approximate line in Arrhenius plot of CO_2 induced corrosion in concrete with cold-joint are shown in **Table 3.4.4**. From this table it can be seen that R^2 of the approximate lines are more than 0.95 and the macrocell and microcell corrosion rate of vertical steel bar in concrete apparently agrees with the Arrhenius equation.

(a) Macrocell Corrosion Rate   (b) Microcell Corrosion Rate
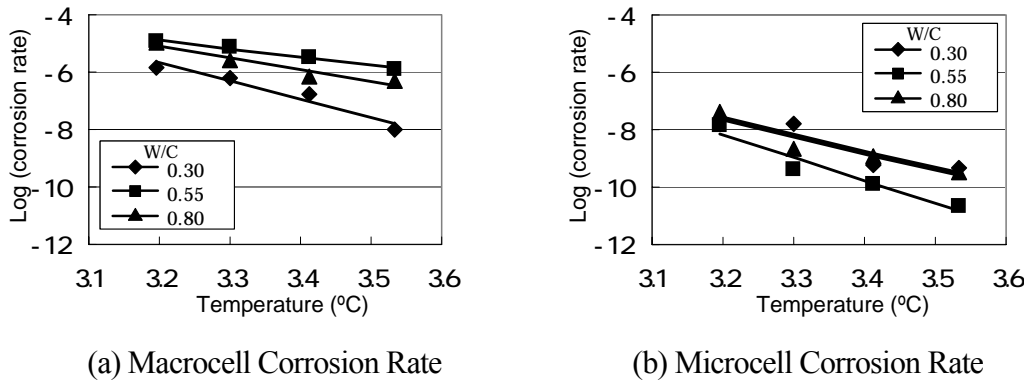
Fig. 3.4.23 Arrhenius Plot of Macrocell and Microcell Corrosion Rate.

(Height: 165 cm)

(a) Macrocell Corrosion Rate   (b) Microcell Corrosion Rate
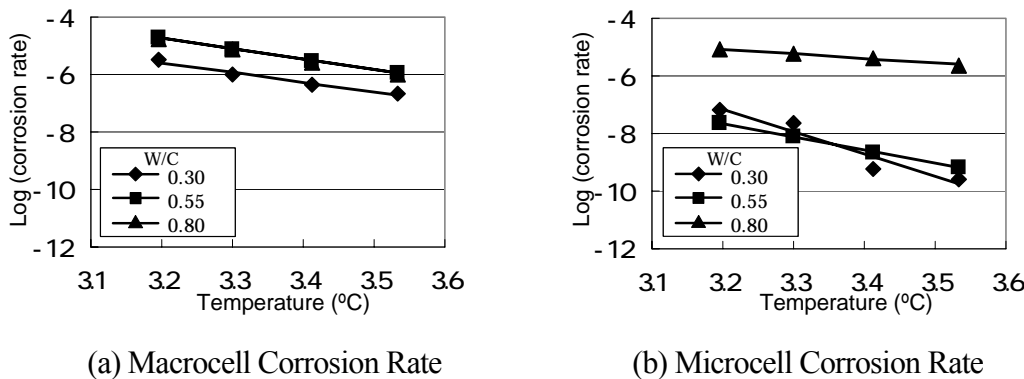
Fig. 3.4.24 Arrhenius Plot of Macrocell and Microcell Corrosion Rate.

(Height: 142 cm)
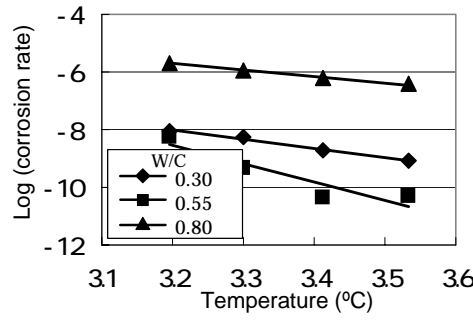
Fig. 3.4.25 Arrhenius Plot of Microcell Corrosion Rate. (Height: 117cm)
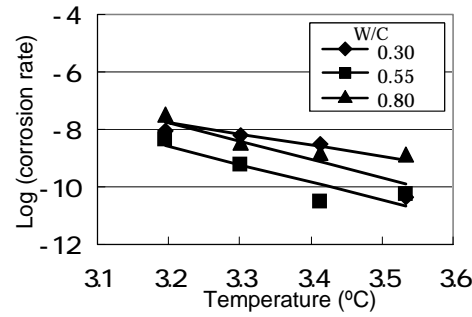
Fig. 3.4.26 Arrhenius Plot of Microcell Corrosion Rate. (Height: 92.5cm)
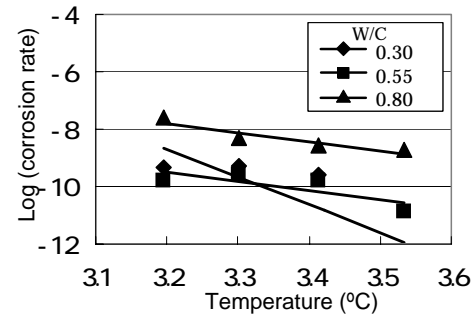
Fig. 3.4.27 Arrhenius Plot of Microcell Corrosion Rate. (Height: 67.5cm)
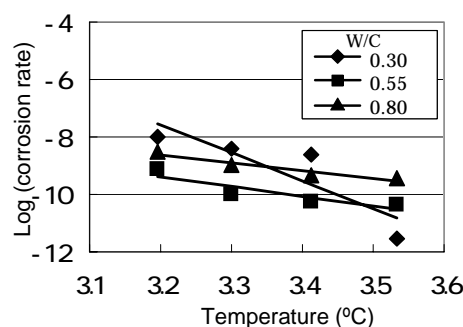
Fig. 3.4.28 Arrhenius Plot of Microcell Corrosion Rate. (Height: 42.5cm)

Table 3.4.4 Slopes, Slices and R^2 of Approximate Line in Arrhenius Plot.

Height	W/C	Macrocell corrosion			Microcell corrosion		
		Slope	Slice	R2	Slope	Slice	R2
	0.3	-6.3194	14.531	0.9376	-5.7584	10.837	0.8697
165	0.55	-2.9234	4.4644	0.9863	-7.9238	17.174	0.9357
	0.8	-4.0662	7.9048	0.9305	-5.7312	10.653	0.8883
	0.3	-3.4031	5.3064	0.9715	-7.8114	17.847	0.9318
142.5	0.55	-3.6254	6.8593	0.9993	-4.6295	7.1607	0.9998
	0.8	-3.6618	6.9421	0.9987	-1.5776	-0.0326	0.9785
	0.3	-	-	-	-3.1332	2.0188	0.9858
117.5	0.55	-	-	-	-6.3224	11.683	0.8498
	0.8	-	-	-	-2.1871	1.2724	0.9934
	0.3	-	-	-	-6.4035	12.736	0.7853
92.5	0.55	-	-	-	-6.0997	10.909	0.8007
	0.8	-	-	-	-3.952	4.8788	0.8052
	0.3	-	-	-	-9.6954	22.319	0.6766
67.5	0.55	-	-	-	-3.1062	0.4195	0.6051
	0.8	-	-	-	-3.1796	2.3888	0.8627
	0.3	-	-	-	-9.7268	23.551	0.7717
42.5	0.55	-	-	-	-3.4482	1.6563	0.8182
	0.8	-	-	-	-2.7896	0.3104	0.9328

3.4.3 Verification in Existing Reinforced Concrete

In this study the steel bar embedded in existing reinforced concrete was imaginary divided into 6 elements as shown in **Fig. 3.2.3**. The length of one steel element was 15 cm. And the macrocell corrosion rate and microcell corrosion rate were calculated using the measured values of half-cell potential, polarization resistance and concrete resistance as mentioned in 3.3.

The distribution of macrocell and microcell corrosion rate of steel bar embedded in existing reinforced concrete is shown in **Fig. 3.4.29**. From this figure, the macrocell corrosion rate of steel bars increases at the higher position of concrete. Above results of field test were almost same with those obtained by laboratory test.

(a) Macrocell corrosion rate   (b) Microcell corrosion rate
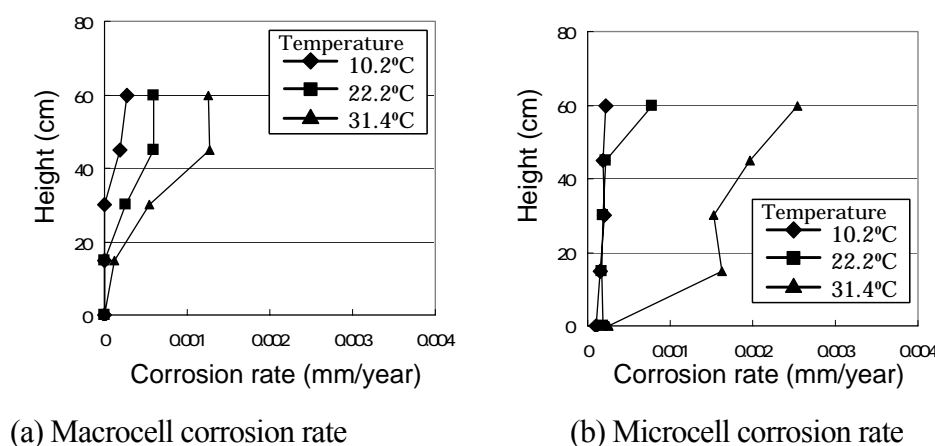
Fig. 3.4.29 Distribution of Macrocell and Microcell Corrosion Rate of Steel Bar
Embedded in Existing Reinforced Concrete

The influence of temperature on macrocell and microcell corrosion rate is shown in **Fig.3.4.30**. From this figure it can be seen that the corrosion rate of steel bar embedded in existing reinforced concrete member increases with temperature rising. The Arrhenius plots of macrocell and microcell corrosion obtained in field test is shown in **Fig. 3.4.31**. From this figure it can be seen that the logarithm of macrocell corrosion rate is proportional with the reciprocal of the absolute temperature. This tendency is also observed in case of microcell corrosion rate.

The values of slope, slice and R^2 of approximate line in Arrhenius plot of CO_2 induced corrosion in existing reinforced concrete are shown in **Table 3.4.5**. From this table it can be seen that R^2 of the approximate lines in existing reinforced concrete is smaller than that in reinforced concrete specimens. This is because there are many factors of corrosion in existing reinforced concrete. However most of data of R2 is more than 0.8 and it can be concluded that the corrosion rate of steel bar in existing reinforced concrete apparently agrees with the Arrhenius equation.

(a) Macrocell Corrosion Rate   (b) Microcell Corrosion Rate
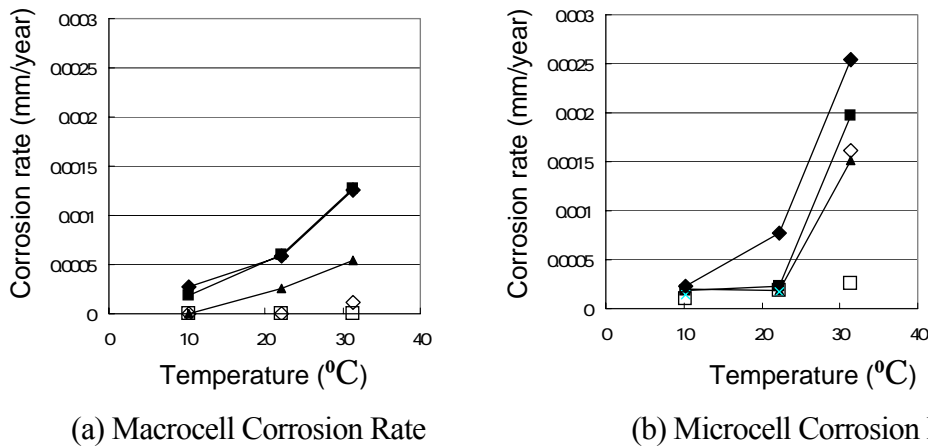
Fig. 3.4.30 Distribution of Macrocell and Microcell Corrosion Rate of Steel Bar Embedded in Existing Reinforced Concrete.

(a) Macrocell Corrosion Rate   (b) Microcell Corrosion Rate
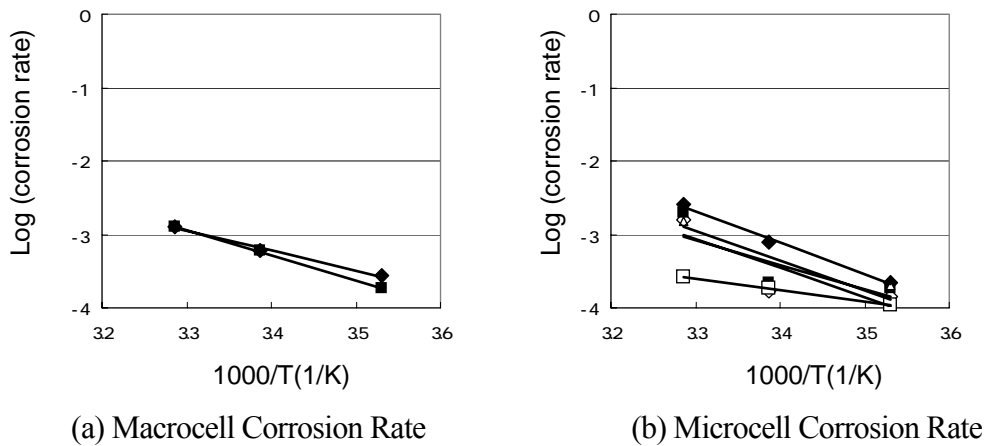
Fig. 3.4.31 Arrhenius Plot of Results of Field Test.

Table 3.4.5 Slopes, Slices and R^2 of Approximate Line in Arrhenius Plot.

Height	Macrocell corrosion			Microcell corrosion		
	Slope	Slice	R^2	Slope	Slice	R^2
60	-2.6453	5.7683	0.991	-4.2443	11.317	0.9926
45	-3.4493	8.4436	0.9991	-3.9552	10.09	0.7327
30				-3.3047	7.8238	0.6208
15				-4.017	10.196	0.7149
0				-1.5524	1.5139	0.9989

3.4.4 Summary

The rate of macrocell and microcell corrosion in concrete induced by CO_2 increases with the temperature rising. Especially the corrosion rate of steel bar in concrete induced by CO_2 becomes 1.4~3.5 times with 10 ℃ of temperature rising. Additionally the logarithm of corrosion rate induced by CO_2 is proportional to the reciprocal of absolute temperature. This fact indicates that the steel corrosion in concrete induced by CO_2 apparently agree with the Arrhenius theory.

The corrosion rate of steel bar in concrete induced by CO_2 is largely influenced by carbonation reminder and oxygen permeability. And macrocell and microcell corrosion rate in concrete with cold-joint becomes high with the bleeding ratio increasing. Moreover, higher macrocell corrosion rate generally prevail in concrete with cold-joint. This tendency is also confirmed in existing reinforced concrete after 35 years old.

3.5 Summary of Chapter 3

The conclusions derived from this chapter can be summarized as follows:

1   It was confirmed that the carbonation coefficient of concrete increased with the temperature rising. Also the rate of macrocell and microcell corrosion of steel bar in concrete induced by CO_2 increased with the temperature rising. Especially the carbonation coefficient of concrete became 1.2~1.9 times with

10 ℃ of temperature rising, while the corrosion rate of steel bar in concrete induced by CO_2 became 1.4 ~ 3.5 times with 10 ℃ of temperature rising.

2   The logarithms of above phenomenon, diffusion of substance or corrosion of steel bar in concrete, were proportional to the reciprocal of absolute temperature. This fact indicated that the deterioration of reinforced concrete due to the steel corrosion induced by CO_2 apparently agreed with the Arrhenius theory.

3   Concrete specimens containing Ordinary Portland cement had shown better performance against carbonation and corrosion at lower temperature (20°C) as compared with Blast Furnace Slag Cement. On the other hand, Blast Furnace Slag Cement concrete performed better at higher temperature (30°C and 40°C) as compared with Ordinary Portland Cement concrete and High Early Strength Cement concrete.

4   The corrosion rate of steel bar in concrete induced by CO_2 was largely influenced by carbonation reminder and oxygen permeability of concrete.

5   Macrocell and microcell corrosion rate in concrete with cold-joint became high with the bleeding ratio increasing. Moreover, higher macrocell corrosion rate generally prevailed in concrete with cold-joint. This tendency was also confirmed in existing reinforced concrete constructed 35 years ago.

References of Chapter 3

3-1)   Richardson, M.G., Fundamentals of Durable Reinforced Concrete, p. 78, (2002).

3-2)   Japan Society of Civil Engineering, Concrete standard specifications "maintenance edition", pp.81-96 (2001).

3-3)   Miyazato, S., Otsuki, N., Kimura, H., Estimation method of macrocell corrosion rate of rebar in existing concrete structures using non-destructive test. East Asia-Pacific Conference (EASEC 8), 2, p. 531-542 (2001).

Chapter 4

Discussions for Temperature Influence on Deterioration of Reinforced Concrete Based on Arrhenius Theory.

4.1 **Influence of Temperature on Diffusion or Chemical Reaction in Concrete**

4.2 **Calculation of Activation Energy**

4.3 **Significance of Activation Energy in Deterioration of Reinforced Concrete Members**

4.4 **Activation Energy of Diffusion of Substances in Concrete**

4.5 **Activation Energy of Steel Corrosion in Concrete**

4.6 **Summary of Chapter 4**

References of Chapter 4

4.1 Influence of Temperature on Diffusion or Chemical Reaction in Concrete

As shown in Chapter 1, most of the diffusion of substance and the chemical reaction is speeded up with the increase of the temperature. Most of deterioration of reinforced concrete such as steel corrosion induced by Cl^- or CO_2 also occurs based on diffusion and/or chemical reaction. Therefore it is considered that the deterioration of reinforced concrete will be speeded up with the increase of the temperature.

When the influence of temperature on the diffusion of substance and the chemical reaction is discussed, activation energy derived from Arrhenius equation is most important factor. Therefore in this chapter, the deterioration progress of reinforced

concrete is discussed based on the activation energy calculated by Arrhenius equation. First, the activation energy is calculated using Arrhenius equation. Secondly the significance of activation energy in deterioration of reinforced concrete is discussed using Arrhenius theory. Thirdly the activation energy of diffusion and corrosion in reinforced concrete discussed using the data of Chapter 2 and Chapter 3.

4.2 Calculation of Activation Energy

In general, the influences of temperature on diffusion or chemical reaction are theoretically illustrated using the Arrhenius equation as shown below.

$$k = a \exp\left(-\frac{\Delta E}{RT}\right) \qquad (4\text{-}1)$$

where, k : rate constant

a : frequency factor (Constant)

ΔE : activation energy (cal/mol)

R : ideal gas constant

T : absolute temperature (K)

By taking the logarithm of the given equation, Equation (4-1) will be transformed into Equation (4-2).

$$\log k = \left(\frac{-\Delta E}{R} \cdot \log_{10} e\right)\left(\frac{1}{T}\right) + \log a \qquad (4\text{-}2)$$

Here when chemical reactions progress, the reactants seem to shift to the products through the active state with the high energy. The difference between active state and the reactant is called the activation energy[4-1]. In the system, in which multiple chemical reactions are generated, the activation energy depends on the reaction which determines the rate of reaction. Using the Equation (4-1) and (4-2), it can be

theoretically confirmed that the rate of diffusion of substance or chemical reaction increases with temperature rising.

On the other hand, from experimental results of Chapter 2 and Chapter 3, it was confirmed that the logarithm of rate of diffusion or chemical reaction is proportional to the reciprocal of the temperature. Therefore the following relationship could be obtained.

$$\log k = A\left(\frac{1}{T}\right) + B \tag{4-3}$$

where, k : rate constant

         T : absolute temperature (K)

         A, B : experimental constant

Generally above relationship is called Arrhenius plot and the activation energy can be calculated by comparing with Equation (4-2) and (4-3).

$$\Delta E_a = -\frac{A}{\log_{10} e} \cdot R = -4.58 \times A \tag{4-4}$$

where, ΔE_a : Activation energy (kcal/mol)

         R : Gas constant 1.99×10^{-3} [kcal/K/mol]

         A : Slope of Arrhenius plot derived from experimental results (K)

4.3 Significance of Activation Energy in Deterioration of Reinforced Concrete Members

Generally the activation energies become specific value in each diffusion or reaction. However in continuous diffusion or chemical reaction phenomenon of the multiple substances the mechanism of slowest rate determines the whole rate of diffusion or reaction, and activation energy of rate-limiting mechanism is obtained from

a Arrhenius plot. This phenomenon can be explained by **Fig. 4.3.1**.
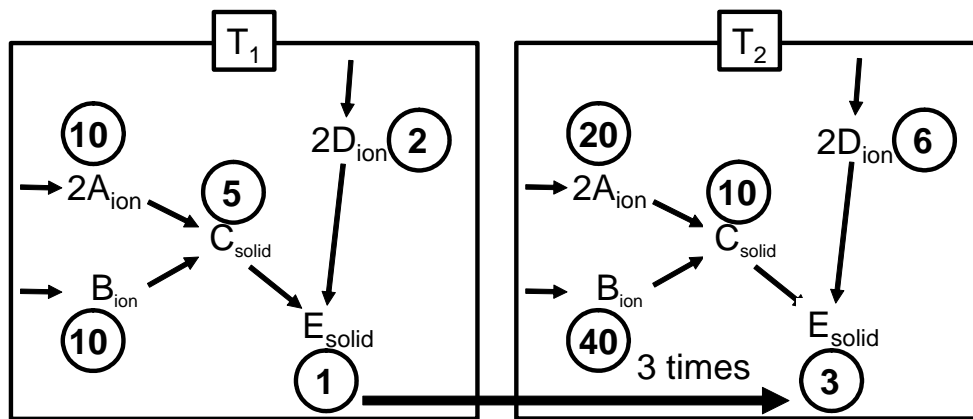
Fig. 4.3.1 Schematic Figure of Influence of Temperature on Chemical Reaction

Fig.4.3.1 shows the following chemical reaction at T_1 and T_2 of temperature condition. The number in the figure shows the quantities of substance.

$$2A_{ion} + B_{ion} \rightarrow C_{solid} \tag{4-5}$$
$$C_{solid} + 2D_{ion} \rightarrow E_{solid} \tag{4-6}$$

Here it is assumed that the quantities of substances of A_{ion}, B_{ion} and D_{ion} are 10, 10 and 2 at T_1 °C and the quantities of substances of A_{ion}, B_{ion} and D_{ion} are 20, 40 and 6 at T_2 °C respectively. These values increase with temperature rising. In this assumption the quantities of A_{ion}, B_{ion} and D_{ion} become 2, 4 and 3 times respectively with the increasing the temperature from T_1 to T_2. These magnifications are related to activation energy. Therefore activation energy becomes one of the evaluation items when the deterioration progress of reinforced concrete is discussed.

In order to confirmed the above phenomenon in reinforced concrete, the relationship between corrosion rate of steel bar and oxygen permeability is investigated as follows.

Fig. 4.3.2 shows the relationship between the corrosion rates of steel bar measured by experiment and calculated from oxygen permeability in concrete. From this figure it is confirmed that the corrosion rate of steel bar measured by experiment is almost same with that calculated from oxygen permeability. This fact indicates that the

corrosion rate of steel bar is controlled by the oxygen permeability in this concrete. On the other hand **Fig. 4.3.3** shows the relationship of activation energies of corrosion and oxygen permeability. From this figure it can be confirmed that the activation energy of corrosion of steel bar is almost same with that of oxygen permeability. Considering the above results it can be concluded that the activation energy of corrosion rate becomes almost equivalent with that of Oxygen permeability, when the corrosion rate of steel bar in concrete has been controlled by Oxygen permeability.
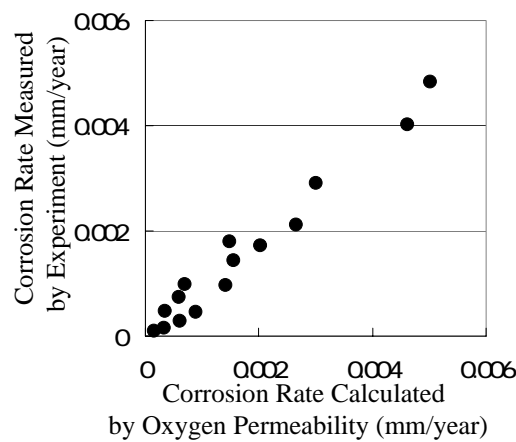
Fig. 4.3.2 Relationship between Corrosion Rates of Steel Bar Measured by Experiment and Calculated from Oxygen Permeability in Concrete.
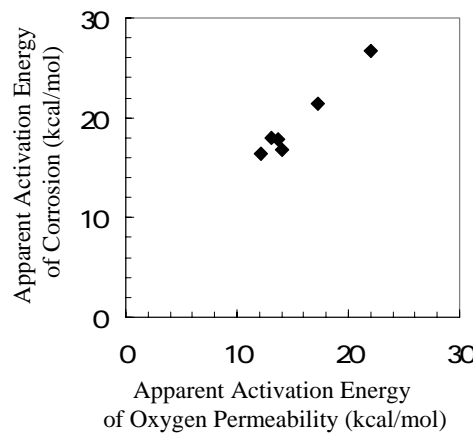
Fig. 4.3.3 Relationship of Activation Energies of Corrosion and Oxygen Permeability.

4.4 Activation Energy of Diffusion of Substances in Concrete

4.4.1 Cl⁻ Diffusivity in Concrete

The activation energy of Cl⁻ diffusivity in concrete is shown in **Table 4.4.1**. From this table it can be seen that the activation energy of Cl⁻ diffusivity is from 12.0 to 32.2 kcal/mol and it varies with the properties of concrete due to the different bleeding ratio or position of specimen.

Table 4.4.1 Activation Energies of Cl⁻ Diffusivity in Concrete.

Bleeding ratio (%)	Position	Activation energy(kcal/mol)
0.18	Top	26.3
	Side	25.4
	Bottom	20.2
	Inside	29.2
0.51	Top	16.8
	Side	24.2
	Bottom	12.0
	Inside	32.5
4.58	Top	31.0
	Side	31.5
	Bottom	20.0
	Inside	32.2

It is expected that the following phenomenon occurs in concrete during the diffusion of Cl⁻;

(1) Diffusion of Cl⁻ in pore solution of concrete.

(2) Adsorption or immobilization of Cl⁻ into cement hydrates.

According to the research of C. L. Page et. al.[4-2] the activation energy of Cl⁻ diffusivity in concrete varies with the W/C and they conclude that the activation energy is largely influenced by the tortuosity of pore structure. Otherwise according to the research of Mohara and Ishida[4-3] the immobilizing ratio of Cl⁻ in to cement hydrates is

increasing with the temperature rising. Above phenomena also depends on the different bleeding ratio or position of specimen. Therefore it is considered that the activation energy of Cl^- also varies with the distribution of pore volume or the immobilizing ratio of Cl^- into cement hydrates due to properties of concrete. Therefore the above (1) and (2) is largely influenced on the temperature influence of Cl^- diffusion in concrete.

Fig. 4.4.1 shows the relationship between activation energy of Cl^- diffusivity and bleeding ratio of concrete. From this figure it is confirmed that the activation energy of Cl^- diffusivity in concrete varies with the bleeding ratio. From this result it is considered that the temperature influence on Cl^- diffusivity in concrete varies with the property of concrete.
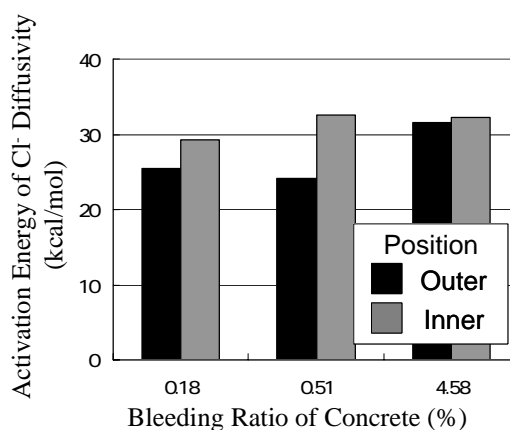
Fig. 4.4.1 Relationship between Activation Energy of Cl^- Diffusivity and Bleeding Ratio of Concrete.

4.4.2 Carbonation of Concrete

The activation energy of carbonation of concrete is shown in **Table 4.4.2**. From this table it can be seen that the activation energy of carbonation of concrete is from 3.1 to 3.9 kcal/mol and it varies with the properties of concrete due to the different cement type or W/C. This is because the carbonation reaction in concrete is highly related to the quantity of $Ca(OH)_2$ and it is depends on the type of cement or W/C. As a result it is considered that the activation energy varies with the different cement type or W/C.

Table 4.4.2 Activation Energy of Carbonation of Concrete.

Cement Type	W/C	Activation energy(kcal/mol)
OPC	0.55	3.8
	0.45	3.3
HEPC	0.55	3.4
	0.45	3.1
BFSC	0.55	3.9
	0.45	3.4

It is expected that the following phenomenon occurs in concrete during the carbonation of concrete;

(1) Diffusion of CO_2 gas in concrete.

(2) Dissolution of Ca^{2+} from cement hydrates to pore solution.

(3) Dissolution of CO_3^{2-} from air to pore solution.

(4) Reaction between Ca^{2+} and CO_3^{2-} in pore solution.

Related to the phenomenon of (1), it is expected that the diffusion of CO_2 gas in concrete increases with the temperature rising. And related to the phenomenon of (2) and (3), the influence of temperature on dissolution of Ca^{2+} or CO_2 can be expressed as shown in **Fig. 4.4.2**[4-4]. From these figures it can be seen that the solubility of $Ca(OH)_2$ and CO_2 are decreases with the temperature rising. Additionally, related to the phenomenon of (4), it can be expected that the rate of reaction between Ca^{2+} and CO_3^{2-} in pore solution increases with the temperature rising. Therefore it is considered that the diffusion of CO_2 gas increases while the degree of carbonation in certain depth of concrete is not so much progress with the temperature rising. As a result the carbonation depth increases with the temperature rising.

(a) Ca(OH)$_2$ (b) CO$_2$ gas
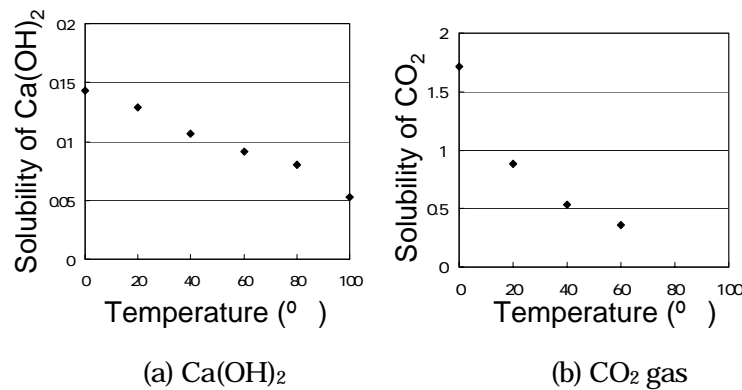
Fig. 4.4.2 Influence of temperature on dissolution of Ca(OH)$_2$ and CO$_2$ to solution.[4-4]

Fig. 4.4.3 shows the relationship between activation energy of carbonation of concrete and cement type. From this figure it is confirmed that the activation energy of carbonation of concrete varies with the type of cement. From this result it is considered that the temperature influence on carbonation of concrete varies with the property of concrete.
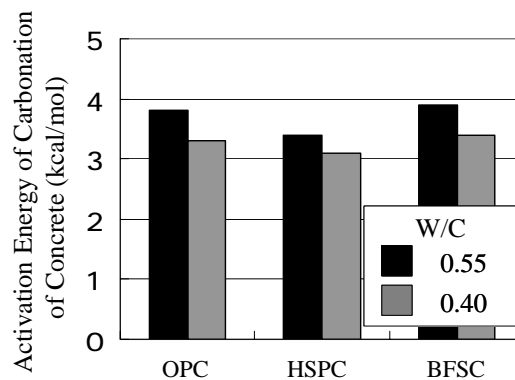
Fig. 4.4.3 Relationship between Activation Energy of Carbonation of Concrete and Cement Type.

4.4.3 Oxygen Permeability in Concrete

The activation energy of oxygen permeability is shown in **Table 4.4.3**. From this table it can be seen that the activation energy of oxygen permeability is from 10.5 to 23.8 kcal/mol and it varies with the properties of concrete due to the different cement

type and W/C. This is because the oxygen permeability in concrete is highly related to the pore structure of concrete and it is depends on the type of cement or W/C. As a result it is considered that the activation energy varies with the different cement type or W/C.

Table 4.4.3 Activation Energy of Oxygen Permeability.

Cement type	W/C	Activation energy(kcal/mol)
OPC	0.55	14.1
	0.45	13.9
HPC	0.55	13.1
	0.45	18.6
BFSC	0.55	10.5
	0.45	23.8

It is expected that the following phenomenon occurs in concrete during the diffusion of O_2 gas.

(1) Diffusion of O_2 gas in concrete.

(2) Dissolution of O_2 gas from air to pore solution.

(3) Rate of cathodic reaction at steel surface.

It can be expected that the diffusion of O_2 gas in concrete increases with the temperature rising. And the influence of temperature on dissolution of O_2 gas can be expressed as shown in **Fig. 4.4.4**[4-4]. From this figure it can be seen that the solubility of O_2 are decreases with the temperature rising. Additionally it can be expected that the rate of cathodic reaction at steel surface increases with the temperature rising. Therefore the diffusion phenomenon of O_2 increases with temperature rising while the dissolution of O_2 gas decreases.
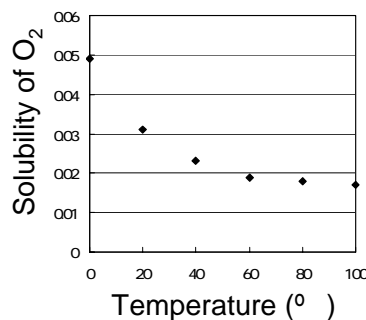
Fig. 4.4.4 Influence of temperature on dissolution of O_2 to solution[4-4)]

4.4.4 Summary

The activation energies of diffusion of harmful substance against steel corrosion in concrete such as Cl^-, CO_2 and O_2 can be obtained from 12.0 to 32.2kcal/mol, from 3.1 to 3.9kcal/mol and from 10.5 to 23.8kcal/mol respectively. It is also confirmed that these values were largely influenced by the property of concrete, especially the pore structure of concrete.

4.5 Activation Energy of Steel Corrosion in Concrete

4.5.1 Cl^- Induced Corrosion

The activation energy of Cl^- induced corrosion is as shown in **Table 4.5.1**. From this table it can be seen that the activation energy of Cl^- induced corrosion is from 5.2 to 19.4 kcal/mol and it varies with the properties of concrete due to the different W/C, bleeding ratio and position of steel bar.

Table 4.5.1 Activation Energy of Cl⁻ Induced Corrosion in Concrete Influenced by Bleeding.

(a) Vertical steel bar (kcal/mol)

Kind of steel bar		Macrocell			Microcell		
Water cement ratio =55%	Water content (kg/m³) — Position(cm)	175	225	275	175	225	275
	145	9.7	11.3	12.2	11.4	12.6	10.7
	75	19.4	10.5	7.0	13.4	12.7	14.5
	5	-	-	-	11.1	12.7	12.6
Water content =225kg/m³	W/C — Position	0.3	0.55	0.8	0.3	0.55	0.8
	145	11.7	11.3	5.2	12.7	12.6	12.6
	75	-	-	-	10.9	12.7	17.7
	5	-	-	-	10.2	12.7	16.9

(b) Horizontal steel bar (kcal/mol)

Kind of steel bar		Macrocell*			Microcell		
Water cement ratio =55%	Water content (kg/m³) — Position	175	225	275	175	225	275
	145	17.7	13.7	11.2	12.2	12.1	11.7
	75	15.1	13.5	18.2	14.5	14.2	15.1
	5	-	11.8	-	14.3	13.6	18.8
Water content =225kg/m³	W/C — Position	0.3	0.55	0.8	0.3	0.55	0.8
	145	16.0	13.7	13.1	14.3	12.1	10.3
	75	-	13.5	8.3	14.7	14.6	9.4
	5	-	11.8	9.1	17.9	13.6	5.4

* In the macrocell corrosion in horizontal steel bar, the lower part of steel bar became anode and upper part of steel bar became cathode.

Fig.4.5.1 and **Fig.4.5.2** show the influence of specific concrete resistance on the activation energy of Cl^- induced corrosion in vertical steel bar and horizontal steel bar respectively. From these figures, it can be seen that the activation energy of macrocell corrosion seems to be changed with the specific concrete resistance increasing. Especially the activation energy can be divided into 3 groups, namely (a), (b) and (c). In group (a) the activation energy is about 20kcal/mol. In group (b) the activation energy is about 9 15kcal/mol. In group (c) the activation energy is about 7kcal/mol The activation energy of macrocell corrosion varies with the specific concrete resistance, while the activation energy of microcell corrosion is almost constant

The difference of the activation energy between macrocell corrosion and microcell corrosion induced by Cl^- is examined as follows. In case of macrocell corrosion the anodic region and cathodic region separately exists. Therefore it is considered that the rate of macrocell corrosion is easily influenced by the specific concrete resistance and the rate limiting condition changes depending on the specific concrete resistance. On the other hand the microcell corrosion is not so much influenced by the concrete resistance because the anodic region and cathodic region are quite close.

From above consideration it can be concluded that the rate limiting condition of macrocell corrosion induced by Cl^- varies with the specific concrete resistance while that of microcell corrosion is constant.
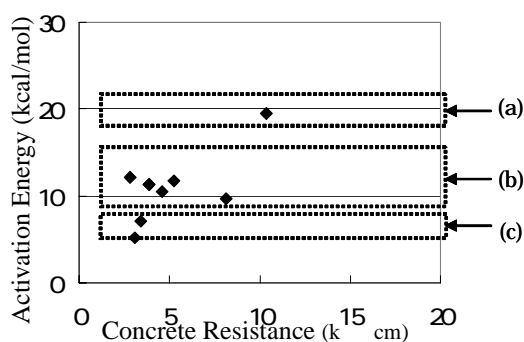
(a) Macrocell Corrosion
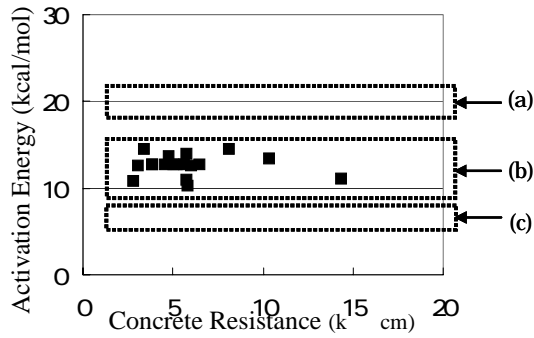
(b) Microcell Corrosion

Fig. 4.5.1 Influence of Specific Concrete Resistance on Activation Energy of Cl⁻
Induced Corrosion in Vertical Steel Bar.
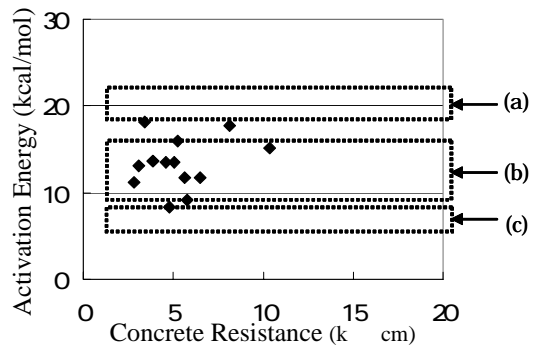
(a) Macrocell corrosion
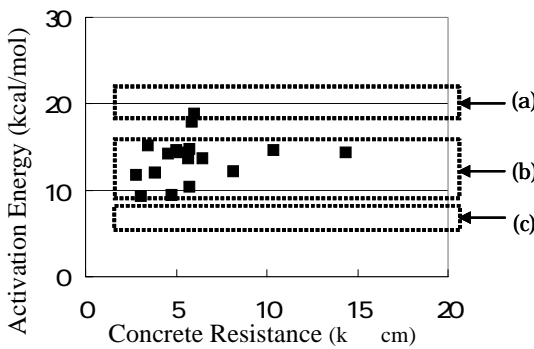
(b) Microcell corrosion

Fig. 4.5.2 Influence of Specific Concrete Resistance on Activation Energy of Cl⁻
Induced Corrosion in Horizontal Steel Bar

4.5.2 CO_2 Induced Corrosion

The activation energy of CO_2 induced corrosion is as shown in **Table 4.5.2**. From this table it can be seen that the activation energy of CO_2 induced corrosion is from 7.2 to 44.5 kcal/mol and it varies with the properties of concrete due to the different W/C and position of steel bar.

Table 4.5.2 Activation Energy of CO_2 Induced Corrosion in Concrete with Cold-joint (kcal/mol)

W/C / Position (cm)	Macrocell			Microcell		
	0.3	0.55	0.8	0.3	0.55	0.8
165	28.9	13.4	18.6	26.4	36.3	26.2
142.5	15.6	16.6	16.8	35.8	21.2	7.2
117.5	-	-	-	14.3	28.9	10.0
92.5	-	-	-	29.3	27.9	18.1
67.5	-	-	-	44.4	14.2	14.6
42.5	-	-	-	44.5	15.8	12.8

Fig.4.5.3 shows the influence of concrete resistance on the activation energy of CO_2 induced corrosion. From these figures, it can be seen that the activation energy of macrocell corrosion increases with the concrete resistance increases. As shown in the previous section the activation energy of macrocell corrosion seems to be easily influenced by concrete resistance. On the other hand the microcell corrosion is scattering. This is because the value of microcell corrosion rate in carbonated concrete is relatively small and the data contains the measurement scattering.
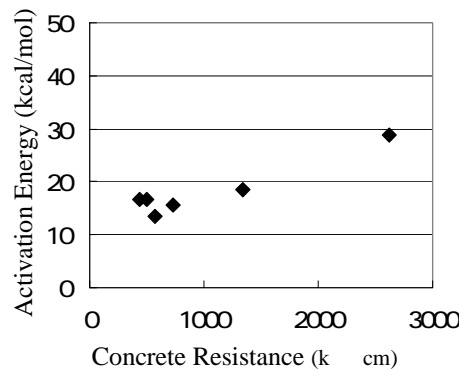
(a) Macrocell corrosion
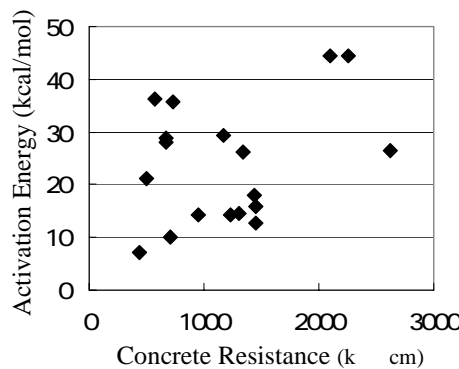
(b) Microcell corrosion

Fig. 4.5.3 Influence of Specific Concrete Resistance on Activation Energy
(CO_2 Induced Corrosion)

4.5.3 Influential Factor on Activation Energy of Corrosion in Concrete

Fig.4.5.4 shows the relationship between activation energy (Cl^- induced corrosion and CO_2 induced corrosion) and specific concrete resistance. From this figure it can be seen that the activation energy varies with the specific concrete resistance. Especially in case of high concrete resistance, the activation energy seems to be scattering and relatively large.

It is considered that there are two reasons on this matter. First reason is that the rate-limiting condition of corrosion is changes with the specific concrete resistance. The corrosion reaction is one of the electrochemical reactions and it is largely influenced by the solution resistance. In case of corrosion of steel bar embedded in

concrete the solution resistance means concrete resistance. If the concrete resistance changes, the rate-limiting condition also changes. In order to confirm the above, the relationship between the activation energy of corrosion and oxygen permeability is shown in **Fig. 4.5.5** (microcell). From this figure it can be seen that the activation energy of corrosion of steel bar is almost same with that of oxygen permeability. This means that the rate-controlling factor of corrosion rate is mainly the quantity of O_2 around the steel bar and the activation energy of corrosion reaction increases with that of O_2 permeability increasing.

Second reason is the problem of measurement method. From the **Fig.4.5.4** the activation energy of macrocell corrosion is not so much scattering while that of microcell corrosion is scattering. In case of macrocell corrosion the Am meter is used and the macrocell corrosion current directly is directory measured. On the other hand in case of microcell corrosion the alternating current impedance method is used. In this measurement the small value has the measured scattering. **Fig. 4.5.6** shows the relationship between the corrosion rate and specific concrete resistance of all data obtained in this study. From this figure it can be seen that (1) the microcell corrosion rate is smaller than macrocell corrosion rate in any concrete resistance, (2) the microcell corrosion rate of high resistance of concrete seems to be scattered.

Fig. 4.5.4 Influence of Concrete Resistance on Activation Energy of Corrosion.
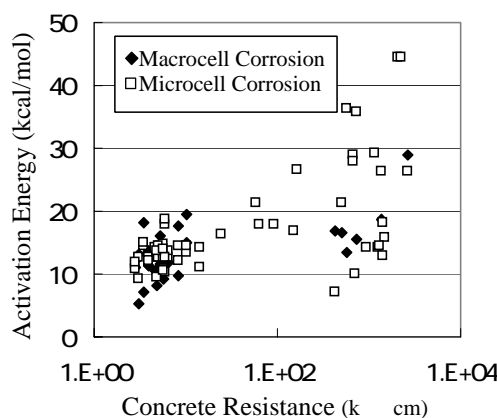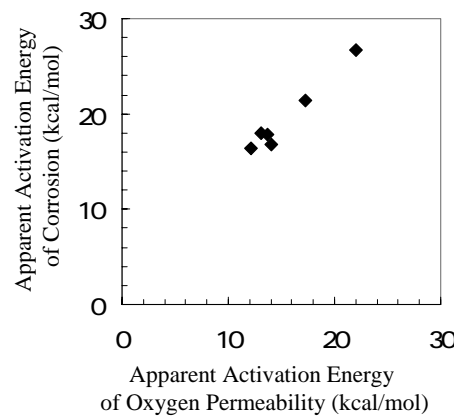
Fig. 4.5.5 Relationship of Activation Energy of Corrosion and Oxygen Permeability.
(Carbonated Concrete, Microcell Corrosion)
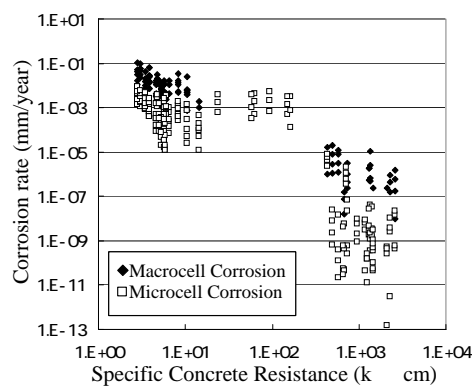
Fig. 4.5.6 Relationship between Corrosion Rate and Concrete Resistance.

4.5.4 Summary

The activation energy of steel corrosion in concrete induced by Cl^- and CO_2 can be obtained from 5.2 to 19.4 kcal/mol and from 7.2 to 44.5 kcal/mol respectively. These activation energies seemed to be changed with the property of concrete or the kind of substance. And it was confirmed that the macrocell corrosion rate and the microcell corrosion rate had different temperature dependency. Especially, the rate of macrocell corrosion seemed to be easily influenced by concrete resistance and the activation energy increased with the concrete resistance increasing. Additionally the activation energy of corrosion of steel bar was almost same with that of oxygen

permeability when the corrosion rate of steel bar in concrete controlled by oxygen permeability.

4.6 Summary of Chapter 4

The conclusions derived from this chapter can be summarized as follows:

1   The activation energies of deterioration phenomenon of reinforced concrete were calculated based on Arrhenius theory. As a result, the activation energies of diffusion of harmful substance against steel corrosion in concrete such as Cl^-, CO_2 and O_2 obtained were 12.0 to 32.2kcal/mol, 3.1 to 3.9kcal/mol and 0.5 to 23.8kcal/mol respectively. It was also confirmed that these values were largely influenced by the property of concrete, especially the pore structure of concrete.

2   The activation energy of steel corrosion in concrete induced by Cl^- and CO_2 obtained were 5.2 to 19.4 kcal/mol and 7.2 to 44.5 kcal/mol respectively. These activation energies seemed to be changed because the rate-limiting condition changed with the increase of specific concrete resistance. Especially, the activation energy of corrosion of steel bar was almost same with that of oxygen permeability. This indicated that the rate-controlling factor of corrosion rate was mainly the quantity of O_2 around the steel bar and the activation energy of corrosion reaction increases with that of O_2 permeability increasing.

3   It was confirmed that the macrocell corrosion rate and the microcell corrosion rate had different temperature dependency. Especially, the rate of macrocell corrosion seemed to be easily influenced by concrete resistance and the activation energy increased with the concrete resistance increasing.

4   The activation energy of corrosion of steel bar was almost same with that of oxygen permeability when the corrosion rate of steel bar in concrete controlled by oxygen permeability.

References of Chapter 4

4-1) Ohki, M., Ohsawa, T., Tanaka, M., Tihara, H., Chemical Dictionary, p. 275 (1994).

4-2) Page, C. L., Lambert, P., Kinetics of Oxygen Diffusion in Hardened Cement Pastes, Journal of Materials Science, 22, pp.942-946 (1987).

4-3) Mohara, K., Ishida, T., A grasp of chloride behavior under the high temperature environment in concrete, Proceedings of the 58th Annual Conference of the Japan Society of Civil Engineers, V-031 (2003).

4-4) National Astronomical Observatory of Japan, Rikanenpyo (2004).

Chapter 5

Prediction of Deterioration Progress of Reinforced Concrete Due to Steel Corrosion Considering Temperature Effect.

5.1 Deterioration Progress of Reinforced Concrete

It is not always guaranteed that required performance of the structure is maintained in concrete structure during the scheduled service period. In the meantime, the maintenance administrators of the concrete structure should check the performance of the structure in the scheduled service period. Therefore the maintenance administrators must appropriately maintain the reinforced concrete structures based on the maintenance procedure such as inspection, degradation prediction, evaluation and judgment, countermeasure as shown in **Fig.5.1.1**.[5-1].
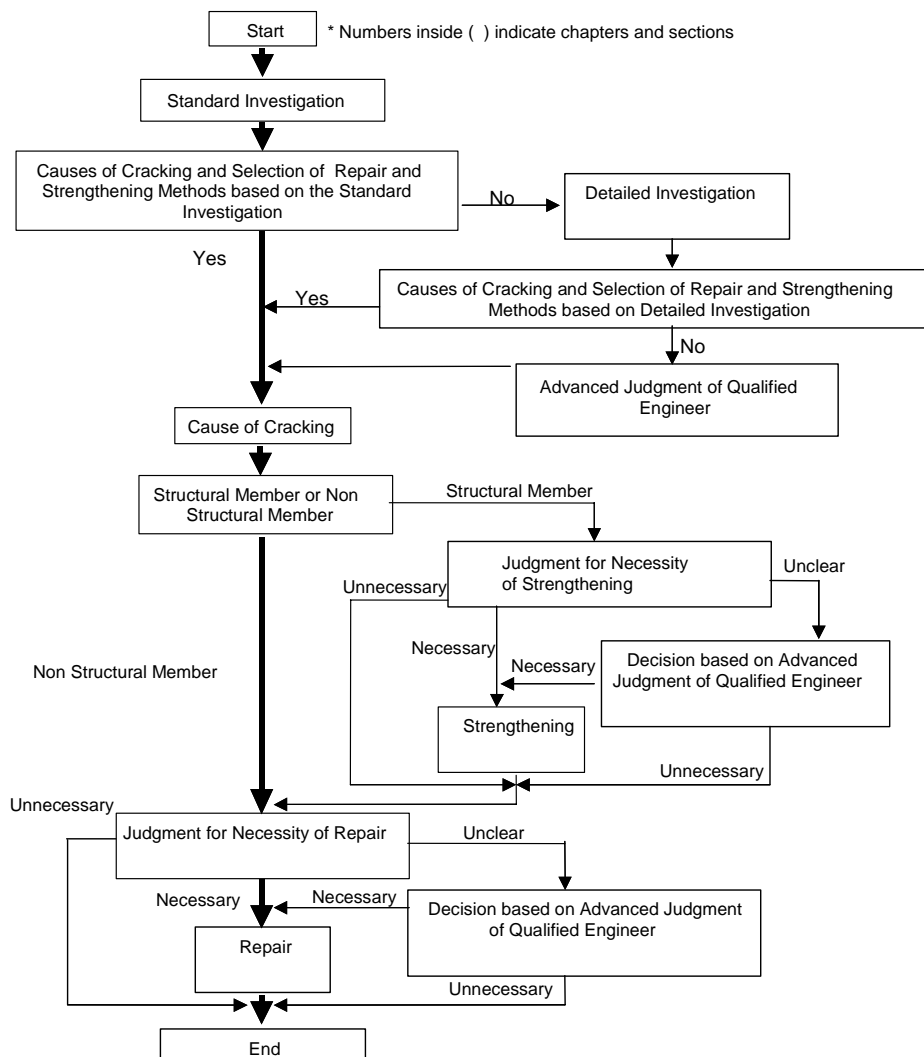
Fig.5.1.1 Concept of Investigation, Repair and Strengthening of Cracks.[5-1)]

The information that how the performance deterioration of the structure changes under the environment and where the structure is used must be grasped in order to carry out the appropriate and systematic maintenance for the concrete structure. In this case, it is necessary to do the degradation prediction of the structure based on the result of inspection. Appropriate prediction needs the evaluation and judgment of performance based on the following matters; (a) the evaluation and judgment of whether it has satisfied a demand level of concrete structure during the scheduled service period, (b) the estimation in the persistence in-service period of the structure and (c) the evaluation and judgment of necessity of detailed inspection and the repair.

The deterioration induced by steel corrosion in concrete such as Cl^- induced corrosion and CO_2 induced corrosion progress through 4 deterioration stages as follows; incubation stage, progress stage, acceleration stage and deterioration stage as shown in **Fig.5.1.2**[5-2].
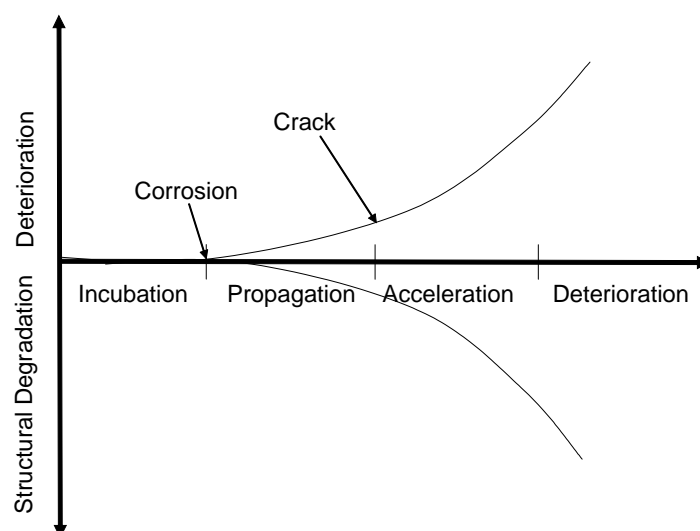
Fig.5.1.2 Deterioration Progress in Reinforced Concrete[5-2]

Considering results of previous chapters, it is considered that the deterioration progress of reinforced concrete such as Cl^- induced corrosion or CO_2 induced corrosion are affected by temperature. And the temperature of the environment is regionally and seasonally different from the cities. Therefore it is necessary to consider the regional and seasonal temperature effect on deterioration progress of reinforced concrete appropriately. In this chapter the influence of temperature on above deterioration progress of reinforced concrete is discussed using Arrhenius theory.

5.2 Influence of Temperature on Deterioration Progress of Reinforced Concrete

5.2.1 Relationship between Magnification of Rate of Reaction and Activation Energy

The influence of temperature on the deterioration progress of the reinforced concrete structure is discussed as shown below.

As shown before, the Arrhenius equation can be expressed as shown in Equation (5-1).

$$k = a \exp\left(-\frac{\Delta E}{R \cdot T}\right) \tag{5-1}$$

Therefore the rate constant of reaction at T_1 and T_2 can be obtained by Equation (5-2) and (5-3) respectively.

$$k_{T_1} = a \exp\left(-\frac{\Delta E}{R \cdot T_1}\right) \tag{5-2}$$

$$k_{T_2} = a \exp\left(-\frac{\Delta E}{R \cdot T_2}\right) \tag{5-3}$$

From above equations, the relationship between the rate of reactions at T_1 and T_2 can be expressed as shown in Equation (5-4).

$$\frac{V_{T_2}}{V_{T1}} = \frac{k_{T_2} \cdot C}{k_{T_1} \cdot C} = \frac{a \exp\left(-\Delta E/R \cdot T_2\right)}{a \exp\left(-\Delta E/R \cdot T_1\right)} = \exp\left[\frac{\Delta E}{R}\left(\frac{1}{T_1} - \frac{1}{T_2}\right)\right] \tag{5-4}$$

From this equation it can be said that the deterioration progress of the reinforced concrete structure at T_2 becomes $\exp\left[\frac{\Delta E}{R}\left(\frac{1}{T_1} - \frac{1}{T_2}\right)\right]$ times of that at T_1. The relationship between magnification of rate of reaction and activation Energy is shown in **Fig. 5.2.1**. From this the influence of temperature on the deterioration progress of reinforced concrete structures using activation energy can be understood.
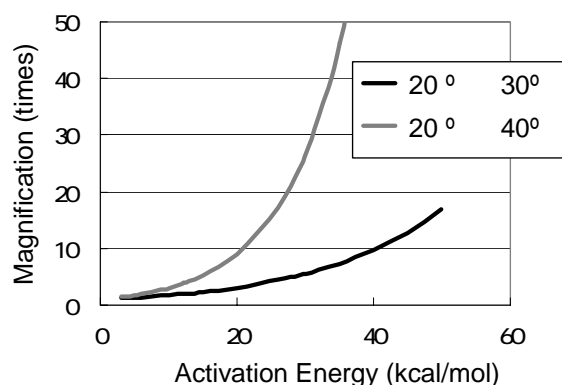
Fig. 5.2.1 Relationship between Magnification of Rate of Reaction and Activation Energy.

5.2.2 Influence of Temperature on Deterioration Progress of Concrete

Table 5.2.1 shows the magnification of deterioration progress of reinforced concrete based on the Arrhenius equation. From this table it can be seen that the temperature dependencies of deterioration progress of reinforced concrete are different from the kinds of deterioration. Also it can be seen that the deterioration of reinforced concrete under 40℃ progress faster than that under 30℃.

Table 5.2.1 Magnification of Deterioration Progress of Reinforced Concrete against 20°C.

	Deterioration Periods	Cl⁻ induced corrosion		CO₂ induced corrosion	
30℃ /20℃	Incubation	2.0 ~ 4.4 times (Cl⁻ diffusivity)		1.2 ~ 1.3 times (Carbonation coefficient)	
	Propagation	1.3~3.1 times (Macrocell Corrosion)	1.3~3.1 times (Microcell Corrosion)	1.3~3.1 times (Macrocell Corrosion)	1.3~3.1 times (Microcell Corrosion)
	Acceleration				
	Deterioration				
40℃ /20℃	Incubation	3.7 ~ 17.3 times (Cl⁻ diffusivity)		1.4 ~ 1.6 times (Carbonation coefficient)	
	Propagation	1.7 ~ 9.0 times (Macrocell Corrosion)	3.0 ~ 9.0 times (Microcell Corrosion)	4.2 ~24.0times (Macrocell Corrosion)	5.2 ~26.8times (Microcell Corrosion)
	Acceleration				
	Deterioration				

5.3 Deterioration Progress of Reinforced Concrete Due to Cl^- Induced Corrosion Considering Regional and Seasonal Temperature

The temperature is the regionally or seasonally different in each city. Therefore the deterioration progress of reinforced concrete is also different. In this section the deterioration progress of Cl^- induced corrosion and CO_2 induced corrosion in reinforced concrete considering the regional and the seasonal temperature is discussed based on the Arrhenius theory. The reinforced concrete considered in this section has 0.55 of water cement ratio and 175 kg/m^3 of water content. The input data of reinforced concrete is shown in **Table 5.3.1**. Also the input temperatures of several cities are shown in **Table 5.3.2**.

Table 5.3.1 Input Data of Reinforced Concrete

W/C	0.55			
W (kg/m^3)	175			
Kind of deterioration	Cl^- induced corrosion		CO_2 induced corrosion	
Activation energy of diffusivity of aggressive substance (kcal/mol)	16.8		3.8	
Activation energy of steel corrosion (kcal/mol)	Macrocell	Microcell	Macrocell	Microcell
	9.7	11.4	21.2	26.2
Environmental condition	Tidal zone			
Decision Factor for Period of Deterioration				
Incubation Period	Before the Cl^- concentration reaches to the threshold level (Cl^- concentration =1.2kg/m^3).			
Propagation Period	Before the corrosion crack occurs (Corrosion quantity =10mg/cm^2).			
Deterioration Period	Before the loading capacity of reinforced concrete member decreases up to 70 % of sounding member (Corrosion quantity =500mg/cm^2).			

Table 5.3.2 Average Temperature of Cities

	Name of City		Jan	Feb	Mar	Apr	May	Jun	Jul	Aug	Sep	Oct	Nov	Dec	Ave.
1	Asia Japan	Naha	16.6	16.6	18.6	21.3	23.8	26.6	28.5	28.2	27.2	24.9	21.7	18.4	22.7
2		Miyako	17.7	17.8	19.7	22.3	24.6	27.1	28.5	28.1	27.1	25.1	22.3	19.4	23.3
3		Fukuoka	6.4	6.9	9.9	14.8	19.1	22.6	26.9	27.6	23.9	18.7	13.4	8.7	16.6
4		Kagoshima	8.3	9.3	12.1	16.8	20.2	23.6	27.9	28.2	25.8	20.8	15.6	10.4	18.3
5		Kohchi	6.1	6.9	10.5	15.5	19.3	22.7	26.4	27.2	24.1	18.8	13.4	8.2	16.6
6		Hiroshima	5.3	5.7	9.0	14.6	18.9	22.8	26.9	27.9	23.9	18.0	12.3	7.5	16.1
7		Matsue	4.2	4.3	7.3	12.7	17.3	21.1	25.2	26.3	22.1	16.4	11.3	6.7	14.6
8		Kyoto	4.6	4.8	8.1	14.1	18.8	22.7	26.7	27.8	23.6	17.5	11.9	6.9	15.6
9		Gifu	4.3	4.7	8.2	14.1	18.6	22.5	26.2	27.5	23.5	17.7	11.9	6.6	15.5
10		Koufu	2.5	3.7	7.6	13.5	18.0	21.6	25.1	26.2	22.2	16.1	10.1	4.5	14.3
11		Tokyo	5.8	6.1	8.9	14.4	18.7	21.8	25.4	27.1	23.5	18.2	13.0	8.4	15.9
12		Niigata	2.6	2.5	5.4	11.2	16.1	20.4	24.5	26.2	22.0	16.0	10.2	5.3	13.5
13		Sendai	1.5	1.7	4.5	10.1	14.9	18.3	22.1	24.1	20.4	14.8	9.1	4.3	12.2
14		Wakkanai	-5.0	-5.1	-1.4	4.2	8.6	12.4	16.9	19.5	16.6	10.8	3.3	-2.0	6.6
15		Nemuro	-4.0	-4.7	-1.7	3.2	7.3	10.5	14.4	17.3	15.5	11.1	5.0	-0.5	6.1
16	Asia	Beijing	-3.6	1.6	8.2	14.0	21.5	25.4	25.2	25.2	21.3	13.8	3.6	-0.8	13.0
17		Shanghai	3.5	6.7	8.7	14.2	18.6	24.3	26.7	25.9	23.8	18.2	13.4	5.8	15.8
18		Dalian	-3.6	-0.3	5.2	10.5	17.4	19.2	21.9	24.1	21.6	13.4	5.3	-0.2	11.2
19		Guangzhou	11.9	16.5	18.5	21.5	25.8	27.5	29.5	29.2	27.3	23.5	20.1	15.2	22.2
20		Nanking	1.6	3.5	8.5	14.8	20.9	24.2	27.3	27.4	22.6	16.6	10.3	3.4	15.1
21		Hong Kong	15.8	15.9	18.5	22.2	25.9	27.8	28.8	28.4	27.6	25.2	21.4	17.6	22.9
22		Taipei	15.3	15.7	17.7	21.6	24.8	27.0	29.0	28.8	27.1	24.1	20.7	17.2	22.4
23		Seoul	-3.4	-1.1	4.5	11.8	17.4	21.5	24.6	25.4	20.6	14.3	6.6	-0.4	11.8
24		Singapore	25.5	26.1	26.5	26.9	27.1	27.1	26.8	26.7	26.6	26.5	26.0	25.5	26.4
25		Manila	25.7	26.2	27.5	29.0	29.4	28.6	27.9	27.3	27.4	27.6	27.5	26.2	27.5
26		Kuala Lumpur	26.1	26.5	26.8	27.0	27.2	27.0	26.6	26.7	26.4	26.5	26.1	26.1	26.6
27		Bangkok	25.6	27.2	28.6	29.6	29.3	28.7	28.1	27.9	27.6	27.5	26.7	25.5	27.7
28		Ho Chi Minh	26.7	27.6	28.4	29.7	29.1	27.8	27.6	28.0	27.3	27.1	27.9	27.1	27.9
29		Hanoi	17.8	18.9	18.5	25.4	27.7	28.7	28.4	28.3	27.0	24.3	23.2	19.7	24.0
30		Jakarta	26.2	26.6	27.1	27.7	27.8	27.7	27.4	27.3	27.6	27.7	27.4	27.0	27.3
31		New Delhi	14.2	17.2	22.7	18.9	32.8	33.8	31.0	29.6	29.2	26.2	20.5	15.7	24.3
32	U.S.A. continent	New York	0.1	0.8	5.1	11.2	16.8	22.0	24.8	23.8	20.2	14.8	8.6	1.9	12.5
33		Los Angeles	12.3	13.1	14.0	15.9	17.8	19.6	22.3	22.9	22.1	19.4	15.9	13.1	17.4
34		San Francisco	10.7	10.1	12.9	12.9	14.0	15.5	15.7	17.0	16.8	14.4	10.2	9.0	13.3
35		Chicago	-4.3	-2.6	2.7	9.9	15.6	21.4	23.7	23.2	18.8	13.0	4.7	-1.9	10.4
36		Houston	11.2	12.9	16.0	20.8	24.2	27.3	28.5	28.6	26.2	21.6	16.2	12.6	20.5
37		Honolulu	22.4	22.4	22.8	23.8	24.9	26.1	26.7	27.1	26.9	26.1	24.7	23.2	24.8
38		Atlanta	5.8	7.2	10.6	16.2	20.6	24.2	25.6	25.3	22.4	16.9	10.8	6.4	16.0
39		Montreal	-9.8	-8.9	-2.2	5.6	13.1	18.4	21.0	19.8	15.2	8.9	2.2	-6.6	6.4
40		Vancouver	2.9	5.1	6.0	8.5	11.8	14.8	16.9	16.8	14.3	10.3	6.2	4.1	9.8
41		Mexico City.	12.9	14.5	17.0	18.0	18.1	17.2	16.0	16.3	15.7	15.1	14.0	12.9	15.6
42		Sao Paulo	23.6	25.6	22.4	24.2	20.3	17.5	18.6	18.3	21.0	21.8	22.8	24.1	21.7
43	Europe	London	3.6	4.1	5.6	7.9	11.1	14.3	16.1	15.9	13.7	10.7	6.4	4.4	9.5
44		Paris	3.3	4.0	6.6	9.6	13.3	16.4	18.2	17.8	15.3	11.2	6.6	4.3	10.6
45		Milan	1.1	3.6	7.8	12.1	16.6	20.5	22.9	21.8	18.2	12.4	6.6	2.1	12.1
46		Roma	7.9	8.8	10.5	13.2	17.2	21.2	23.6	23.6	20.9	16.3	12.3	9.0	15.4
47		Vienna	-0.8	1.1	4.9	10.0	14.5	18.1	19.7	19.0	15.3	9.9	4.9	1.1	9.8
48		Brussel	2.3	3.1	5.8	8.8	13.0	15.8	17.2	17.0	14.5	10.7	6.0	3.6	9.8
49		Amsterdam	5.2	1.5	7.3	8.1	12.4	15.2	21.1	17.6	13.6	9.2	10.2	5.4	10.6
50		Dusseldorf	4.8	2.1	7.9	9.0	13.3	16.5	22.7	18.6	14.1	9.5	10.0	5.7	11.2
51		Geneva	1.1	2.3	5.9	9.7	14.2	17.7	20.1	18.9	15.8	10.8	5.8	2.4	10.4
52		Stockholm	-3.0	-3.6	-0.5	4.1	9.9	15.4	16.9	16.0	11.7	7.1	2.2	-0.8	6.3
53		Moscow	-9.5	-8.4	-3.3	5.1	12.4	16.8	18.4	16.5	10.9	4.8	-1.7	-6.0	4.7
54	Oceania	Sydney	22.3	22.4	21.5	18.9	15.6	13.4	12.4	13.4	15.3	17.7	19.6	21.5	17.8
55		Melbourne	19.2	19.2	17.7	14.5	11.4	9.1	8.3	9.6	12.0	14.5	16.0	17.7	14.1

5.3.1 Relationship between Magnification of Deterioration Progress and Temperature

The magnifications of deterioration progress of reinforced concrete in several cities around the world considering the regional and seasonal temperature are shown in **Fig. 5.3.1** to **Fig 5.3.4**. Each bars in these figures shows the month (from January to December). From these figures it can be seen that the deterioration progress of reinforced concrete is quite different from the cities. Also it can be easily imagined the deterioration progress is different even if the average temperature is same. This is because the rate of deterioration progress exponentially increases with temperature increasing.

From above results, it is considered that the deterioration progress of reinforced concrete is quite different from the city. Therefore it is necessary to consider the influence of temperature on deterioration of reinforced concrete when the life cycle of reinforced concrete structures is estimated. The deterioration progress of reinforced concrete induced by Cl$^-$ is discussed in following sections based on Arrhenius theory.
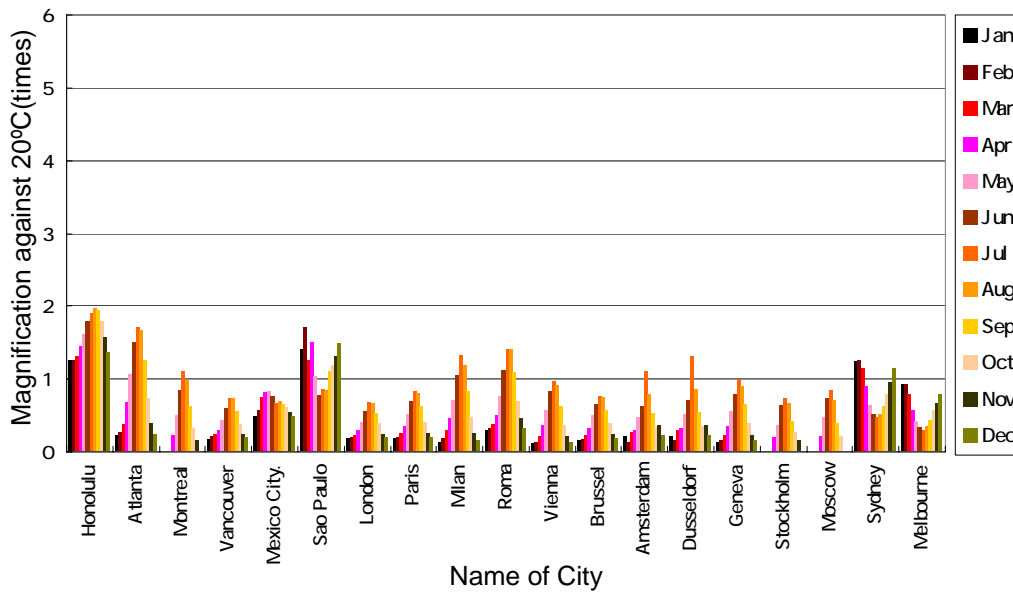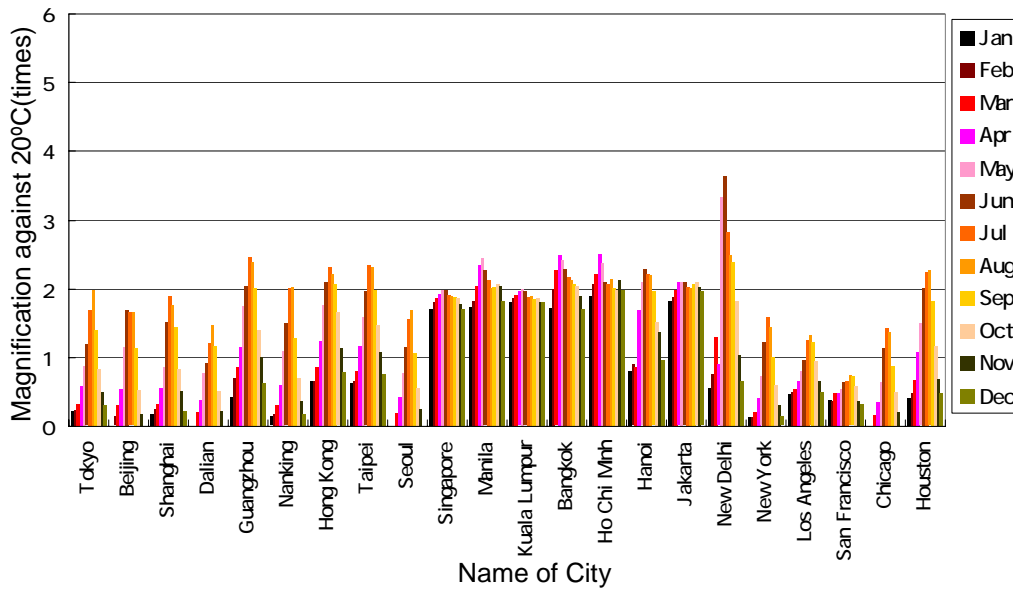
(a) Cl⁻ Diffusivity

Fig. 5.3.1 Magnification of Deterioration Progress of Cl⁻ Induced Corrosion around the World.
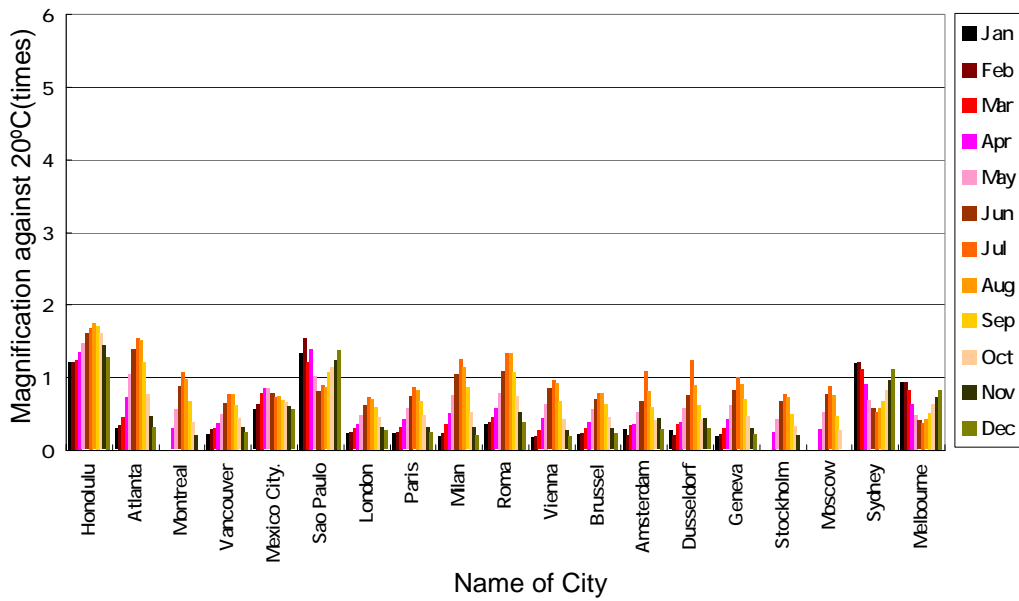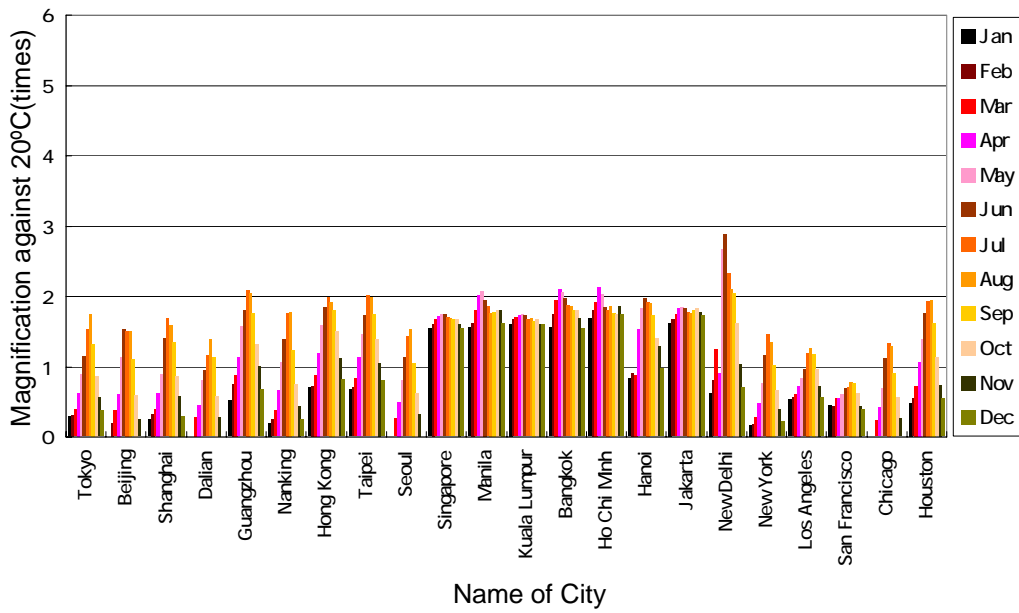
(b) Macrocell Corrosion

Fig. 5.3.1 Magnification of Deterioration Progress of Cl⁻ Induced Corrosion around the
World
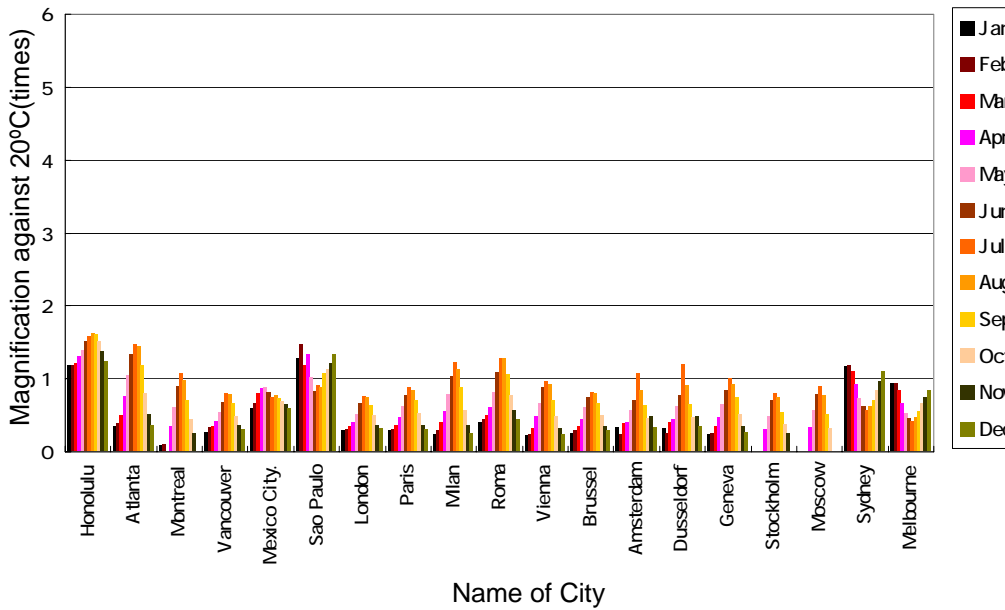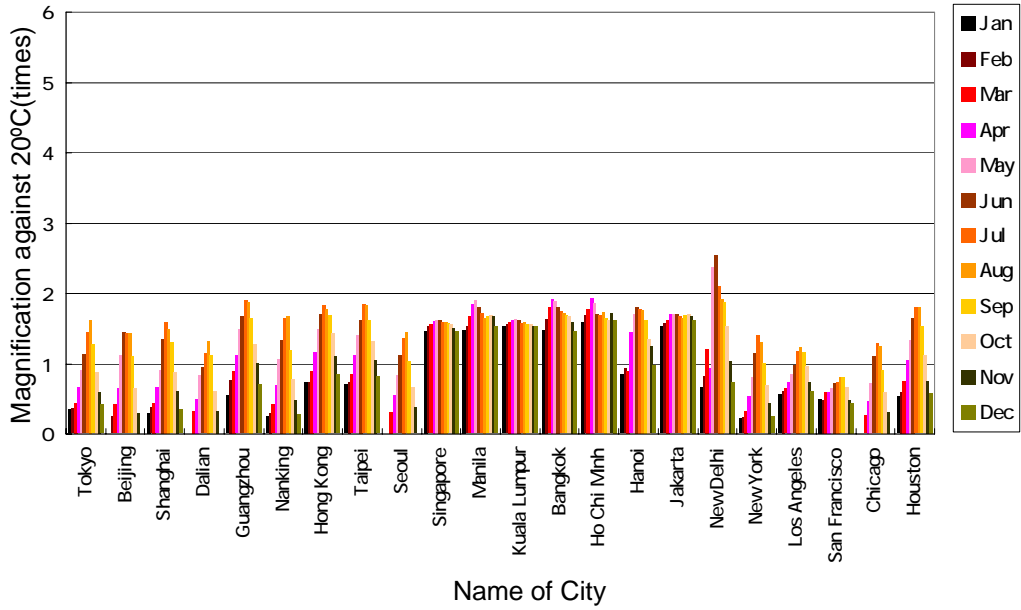
(c) Microcell Corrosion

Fig. 5.3.1 Magnification of Deterioration Progress of Cl⁻ Induced Corrosion around the World.
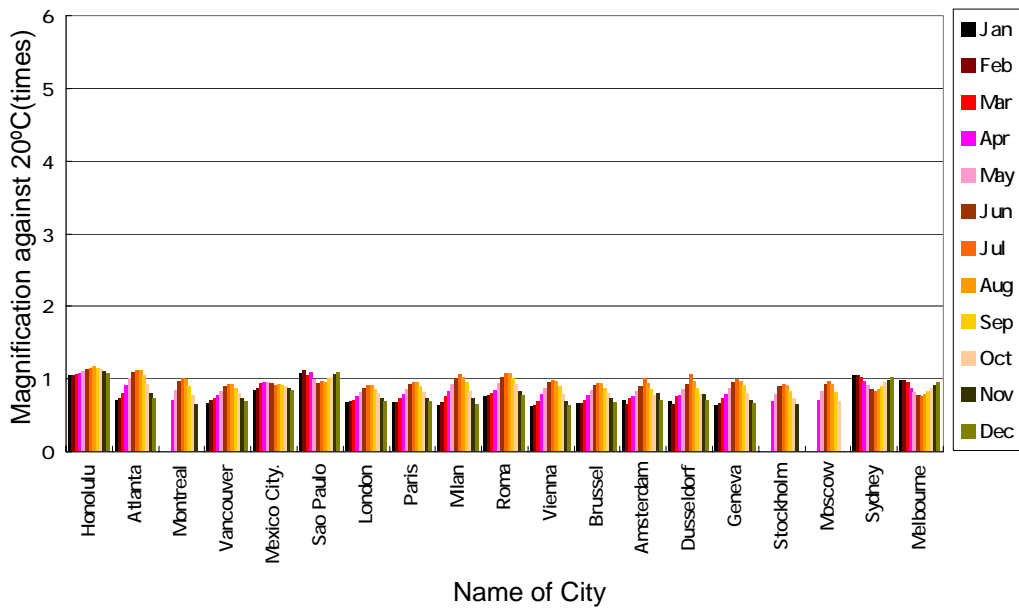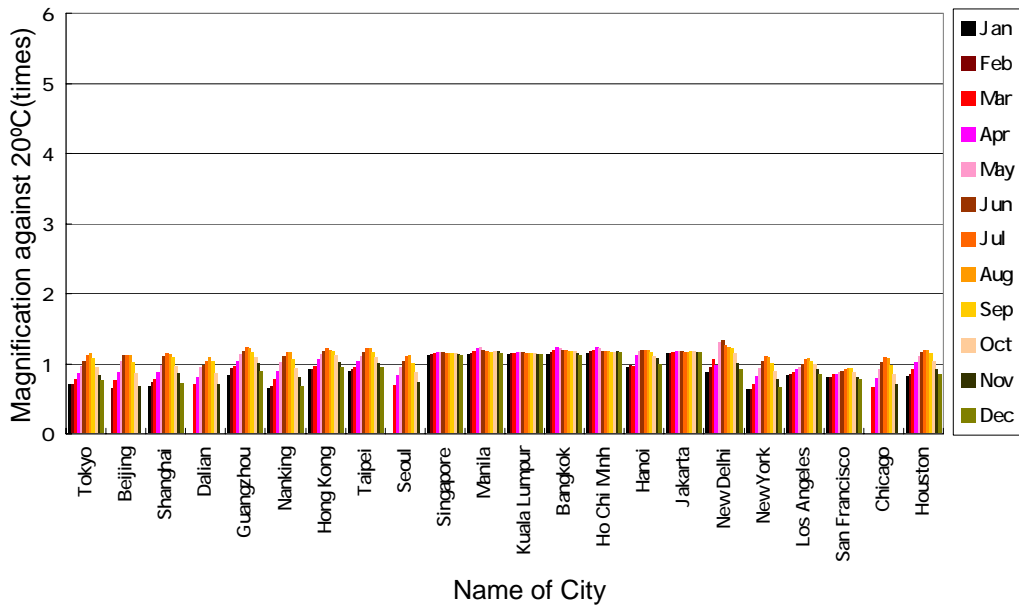
(a) Carbonation Coefficient

Fig. 5.3.2 Magnification of Deterioration Progress of CO_2 Induced Corrosion around the World.
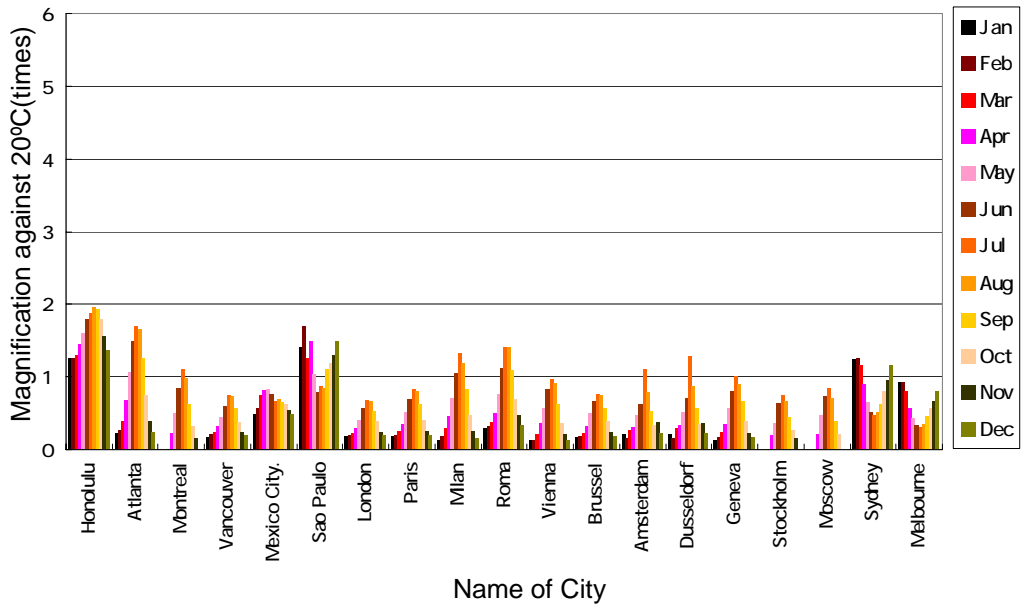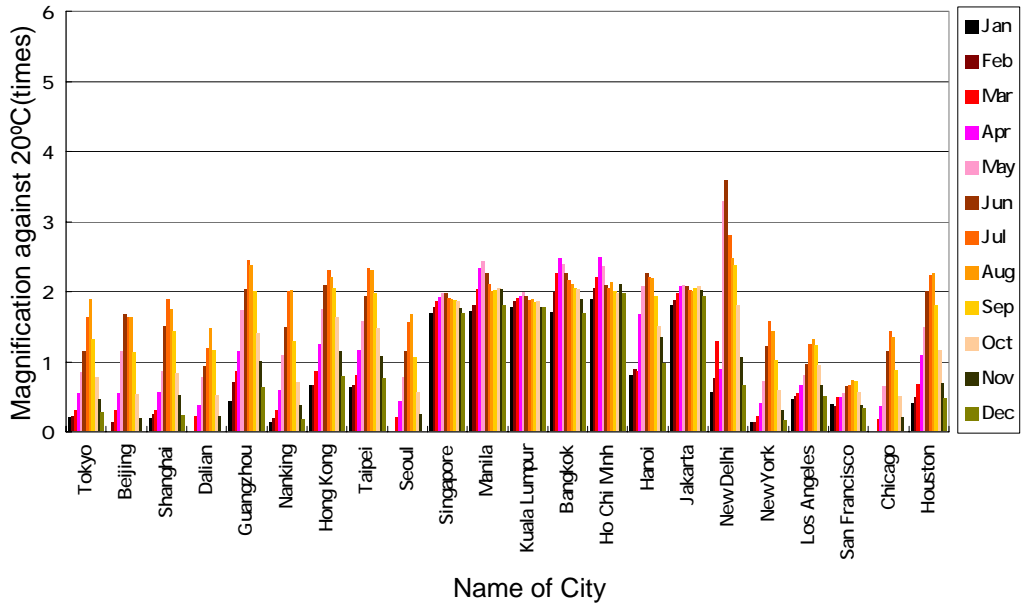
(b) Macrocell Corrosion

Fig. 5.3.2 Magnification of Deterioration Progress of CO_2 Induced Corrosion around the World.
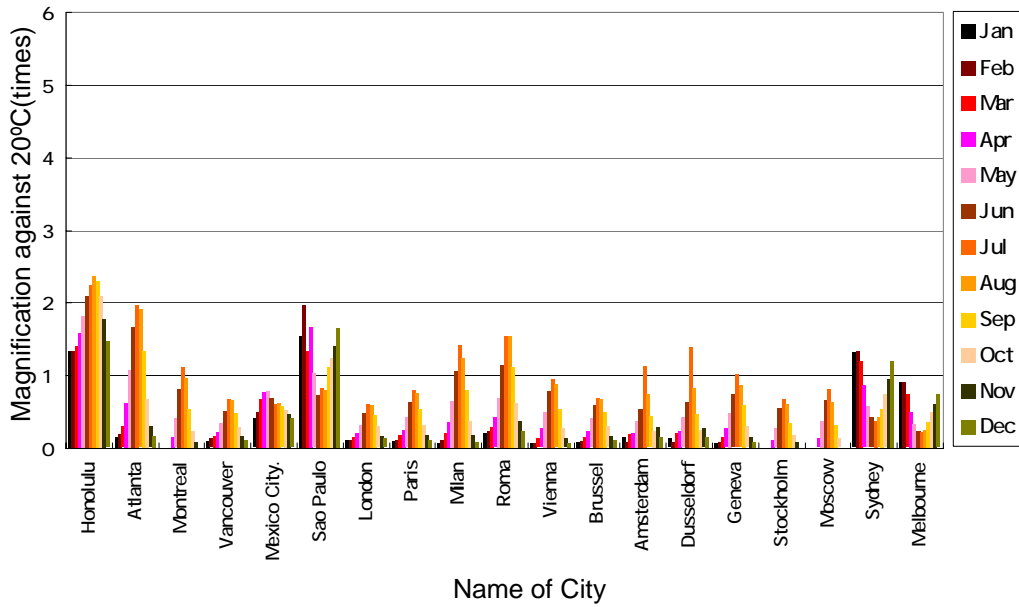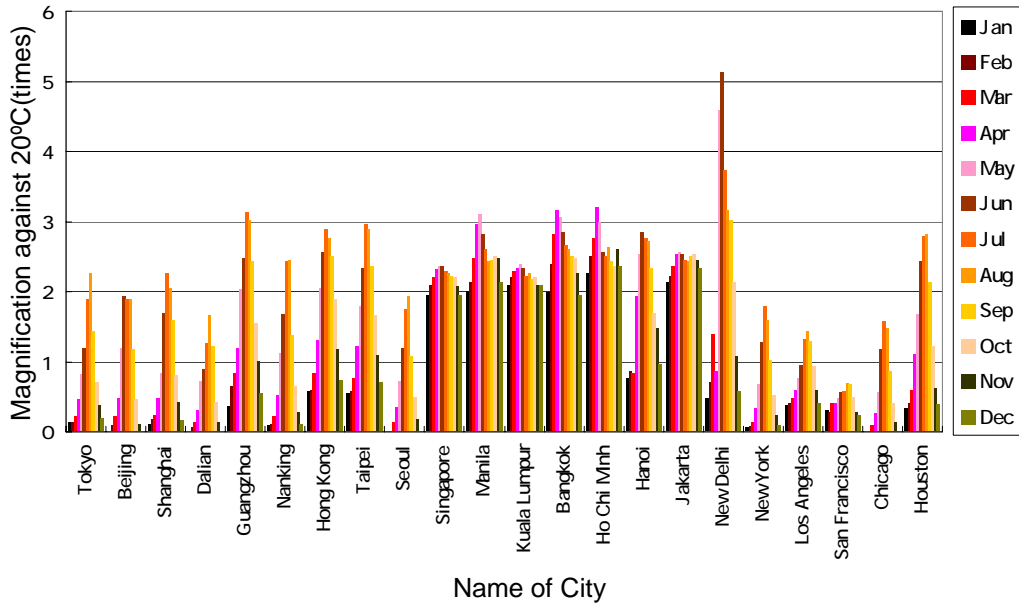
(c) Microcell Corrosion

Fig. 5.3.2 Magnification of Deterioration Progress of CO_2 Induced Corrosion around the World.
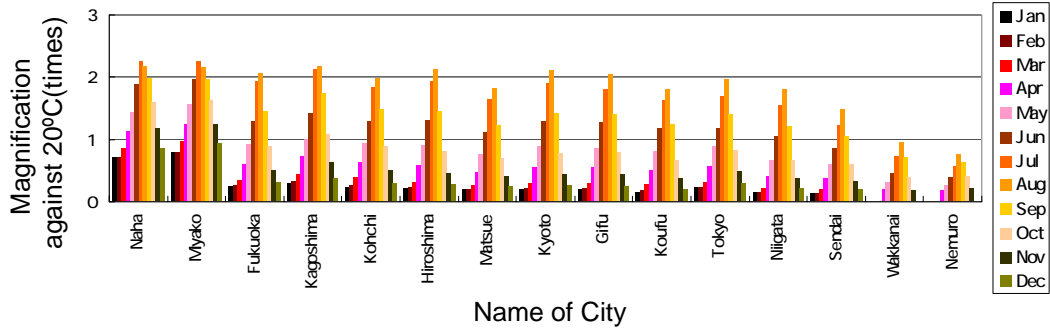
(a) Cl⁻ Diffusivity
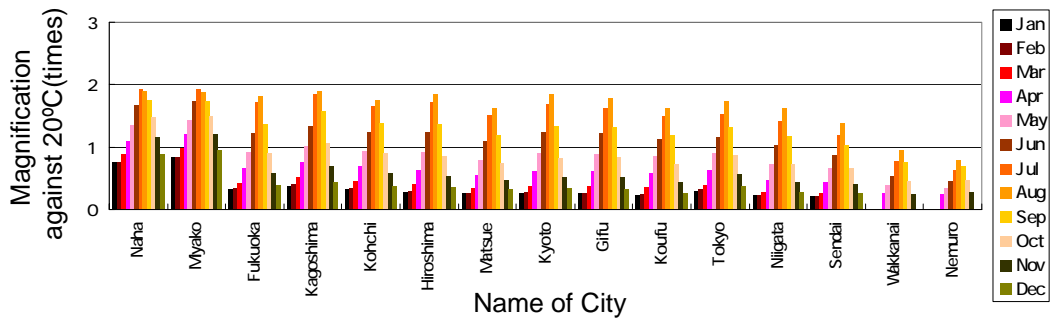
(b) Macrocell Corrosion
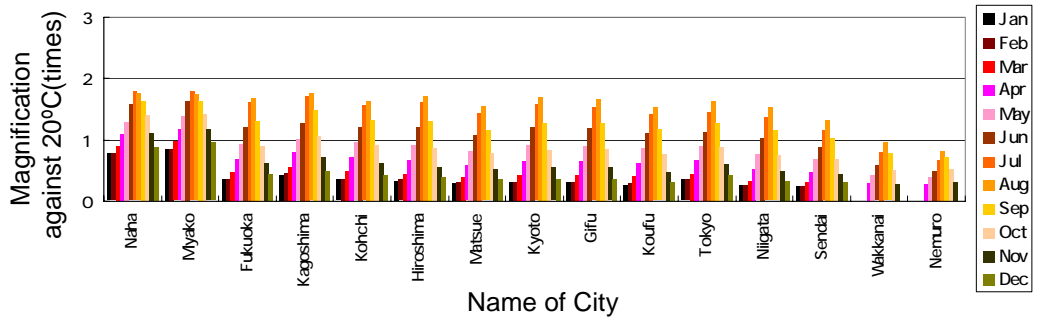
(c) Microcell Corrosion

Fig. 5.3.3 Magnification of Deterioration Progress of Cl⁻ Induced Corrosion in Japan.
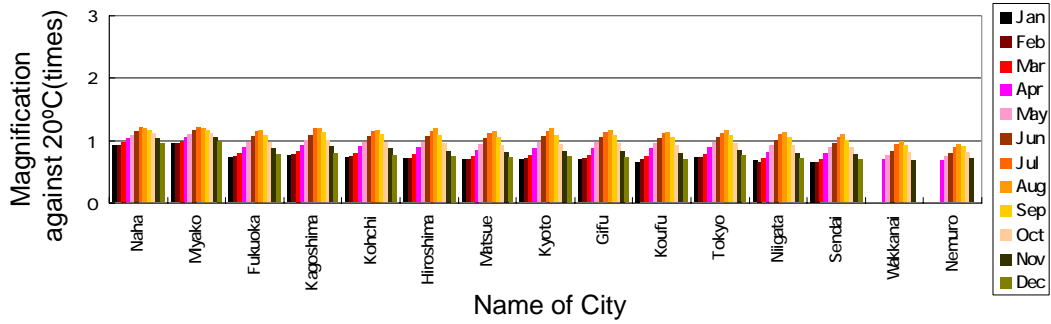
(a) Carbonation Coefficient
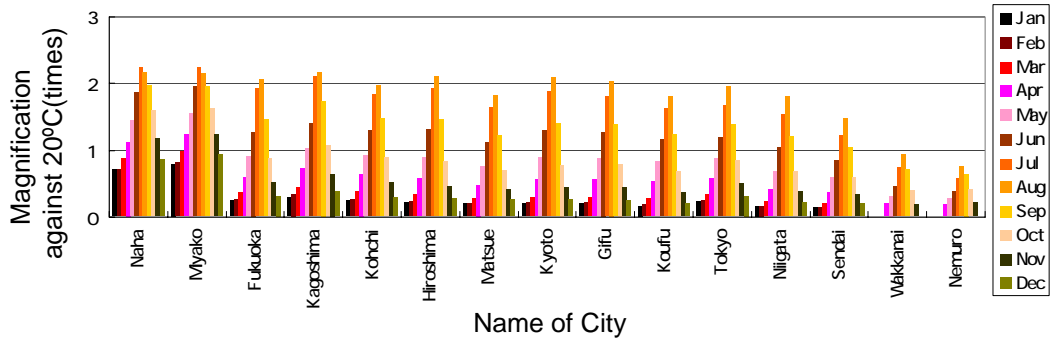
(b) Macrocell Corrosion
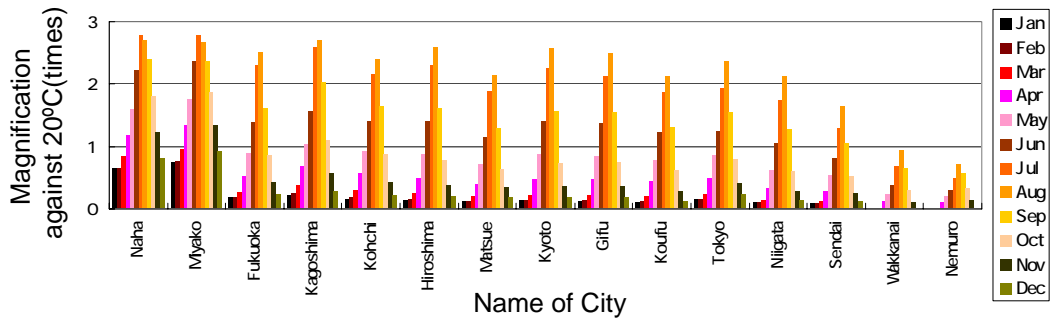
(c) Microcell Corrosion

Fig. 5.3.4 Magnification of Deterioration Progress of CO_2 Induced Corrosion in Japan.

5.3.2 Cl⁻ Diffusion in Concrete Considering Regional and Seasonal Temperature

In this section the rate of Cl⁻ diffusion in reinforced concrete considering the temperature effect is investigated using a numerical analysis. In this numerical analysis Nernst-Planck equation considering with Debye-Hückel equation and electro-neutrality condition is used. By considering these equation and condition, the influence of co-existing ions in pore solution of concrete can be simulated. The effectiveness of this numerical analysis is already confirmed in the literature survey held by Minagawa et. al.[5-3]. In this study the above numerical analysis is modified in order to consider the effect of the temperature. The method and results of prediction for Cl⁻ diffusion in concrete considering temperature effect are discussed as following.

(1) Method of prediction
(a) Assumption

It is difficult to solve ion migration in concrete strictly. Hence, in order to establish a prediction method for the Cl⁻ diffusion considering temperature effect, ion migration and adsorption of the Cl⁻ are modeled under the following assumptions:

1   Concrete is a macroscopically homogeneous material.

2   Ion migration in concrete follows the Nernst-Planck equation[5-4] for electrochemical mass transfer. Namely, the driving force for ion motion in concrete is developed by the concentration gradient and electrostatic potential gradient.

3   The influence of ionic strength on diffusion can be considered using the Debye-Hückel equation[5-5].

4   The migration of multiple ions depends on the electro-neutrality condition.

5   All pores in concrete can be thought of as continuous capillaries filled with pore solution.

6   The adsorption of Cl⁻ can be evaluated by Cl⁻ speciation model constructed by Maruya et. al[5-7].

7   It is assumed that six types of ion are contained in pore solution. That is, only Ca^{2+}, Na^+, K^+, Cl^-, Mg^{2+}, SO_4^{2-}, H^+, OH^-.

(b) Nernst-Planck equation

In this study, it is assumed that ion migration in concrete follows the Nernst-Planck equation. This, which is commonly used in solution chemistry, is formulated as follows:

$$J_i = -k \cdot T \cdot B_i \cdot \left(1 + \frac{\partial \ln \gamma_i}{\partial \ln C_i}\right) \cdot \frac{\partial C_i}{\partial x} - e \cdot Z_i \cdot B_i \cdot C_i \cdot \frac{\partial \phi}{\partial x} \tag{5-5}$$

where, i : ionic species

J : flux (mol/cm^2/sec)

k : Boltzman number (=1.38×10^{-23}J/K)

T : temperature (=297K)

B : absolute mobility (cm/sec/dyne)

γ : activity coefficient

C : concentration of ions (mol/cm^3)

x : distance from the exposure surface (cm)

e : elementary electric charge (=1.60×10^{-19}C)

Z : ionic charge number

ϕ : electrostatic potential (V)

The first term describes diffusion, in which the driving force is the concentration gradient, and it is referred to as the 'diffusion term'. The second term describes the electro-migration, which is driven by the electrostatic potential gradient. This member is referred to as the 'electro-migration term'. Note that Equation (5-5) shows that the ion migration index of diffusion and electro-migration is the absolute mobility B_i only.

Incidentally, in an aqueous solution of multiple ions, such as concrete pore solution, diffusion is influenced by the co-existence of ions. The activity coefficient γ is a coefficient that account for this influence, and it is given by the Debye-Hückel equation as follows:

$$\log \gamma_i = -\frac{u \cdot Z^2 \cdot \sqrt{I}}{1 + v \cdot a_i \sqrt{I}} \tag{5-6}$$

where, a_i : ion size parameter (cm)

I : ionic strength (mol/l), u is a constant (=0.5115 dm$^{3/2}$/ mol$^{1/2}$)

v : constant (=0.3921×108 dm$^{3/2}$/mol$^{1/2}$).

Ionic strength is defined by the following equation:

$$I = \frac{1}{2} \sum_i \left(Z_i^2 \cdot C_i \right) \qquad (5\text{-}7)$$

The accuracy of the Debye-Hückel equation depends on the accuracy of the estimate of ion size parameter a_i. However, Equation (5-6) can be simplified engineeringly as shown in Equation (5-8), because the ion size parameters ai of many ions are about 3 Å [5-8].

$$\log \gamma_i = -\frac{0.51 \cdot Z_i^2 \cdot \sqrt{I}}{1 + \sqrt{I}} \qquad (5\text{-}8)$$

Equation (5-8) is partially differentiated about Ci after substituting Equation (5-7). As a result, the following equation can be introduced:

$$\frac{\partial \ln \gamma_i}{\partial \ln C_i} = \ln 10 \times C_i \times \frac{-0.51 \cdot Z_i^2}{2 \cdot \sqrt{I} \cdot \left(1 + \sqrt{I} \right)^2} \qquad (5\text{-}9)$$

Equation (5-9) is part of Equation (5-5). Therefore, by substituting Equation (5-9) and Equation (5-7) into Equation (5-5), the flux shown in Equation (5-5) can be described as a function of ion concentration and electrostatic potential.

(c) Electro-neutrality condition

The paragraph above explains that the ion migration equation is described by ion concentration and electric potential. In this method, the ion concentration distribution is calculated from the initial ion concentration distribution. Hence, the ion concentration is the known parameter. However, the electric potential gradient can be calculated by considering the electro-neutrality condition.

The electro-neutrality condition means that cations and anions maintain electrical neutrality in passing through an arbitrary section. This condition, described by ionic charge number and flux in Equation (5-10), shows that the multiple ions in concrete migrate while maintaining a charge balance.

$$\sum_i \left(Z_i \cdot J_i \right) = 0 \qquad (5\text{-}10)$$

The flux of each ion shown in Equation (5-5) is substituted into Equation (5-10). As a result, the electrostatic potential gradient is given by the following equation:

$$\frac{\partial \phi}{\partial x} = -\frac{\sum_i \left(Z_i \cdot \left(1 + \frac{\partial \ln \gamma_i}{\partial \ln C_i} \right) \cdot B_i \cdot \frac{\partial C_i}{\partial x} \right)}{\sum_i \left(Z_i^2 \cdot B_i \cdot C_i \right)} \cdot \frac{k \cdot T}{e} \tag{5-11}$$

If Equation (5-11) is used, the electric potential gradient can be described by ion concentration, also. Therefore, the flux of an ion species (ion) is a function of the concentrations of several kinds of ion as follows:

$$J_{ion} = -k \cdot T \cdot B_{ion} \cdot \left(1 + \ln 10 \times C_{ion} \times \frac{-0.51 \cdot Z_{ion}^4}{4 \cdot \sqrt{I} \cdot \left(1 + \sqrt{I} \right)^2} \right) \cdot \frac{\partial C_{ion}}{\partial x} + k \cdot T \cdot Z_{ion} \cdot B_{ion} \cdot C_{ion} \cdot \frac{\sum_i \left(Z_i \cdot \left(1 + \frac{\partial \ln \gamma_i}{\partial \ln C_i} \right) \cdot B_i \cdot \frac{\partial C_i}{\partial x} \right)}{\sum_i \left(Z_i^2 \cdot B_i \cdot C_i \right)} \tag{5-12}$$

(d) Calculation of diffusion coefficient

The engineering absolute mobility of ion is shown in **Table 5.3.3**. These values are obtained by the ion migration cell test.[5-6)]

Table 5.3.3 Engineering Absolute Mobility[5-6)]

Ion species	Engineering Absolute Mobility (cm^2/sec/dyne)
Ca^{2+}	8.80 x 10^{12}
Na^+	1.47 x 10^{13}
K^+	2.21 x 10^{12}
Mg^{2+}	9.87 x 10^{12}
Cl^-	2.10 x 10^{13}
SO_4^{2-}	7.77 x 10^{12}
OH^-	5.90 x 10^{13}
H^+	1.09 x 10^{14}

Here, from Equation (5-12), the flux of ion can be written as follows;

$$J_{ion} = -\left(k \cdot T \cdot B_{ion} \cdot \left(1 - \ln 10 \times C_{ion} \cdot \frac{0.51 \cdot Z_{ion}^4}{4\sqrt{I} \cdot \left(1 + \sqrt{I}\right)^2} \right) - Z_{ion} \cdot B_{ionl} \cdot C_{ion} \cdot \frac{k \cdot T \cdot \sum_n \left(Z_n \cdot \left(1 - \ln 10 \times C_n \cdot \frac{0.51 \cdot Z_n^4}{4\sqrt{I} \cdot \left(1 + \sqrt{I}\right)^2} \right) \cdot B_n \cdot \frac{\frac{\partial C_n}{\partial x}}{\frac{\partial C_{ionl}}{\partial x}} \right)}{\sum_n \left(Z_n^2 \cdot B_n \cdot C_n \right)} \right) \cdot \frac{\partial C_{ion}}{\partial x}$$

(5-13)

By comparing Equation (5-14) and Fick's low, the diffusion coefficient of Cl⁻ at 20 ℃ can be written as follows;

(5-14)

$$D_{ion,20} = k \cdot (20 + 273) \cdot \left(\left(1 - \ln 10 \times C_{ion} \cdot \frac{0.51 \cdot Z_{ion}^4}{4\sqrt{I} \cdot \left(1 + \sqrt{I}\right)^2} \right) - Z_{ion} \cdot C_{ion} \cdot \frac{\sum_n \left(Z_n \cdot \left(1 - \ln 10 \times C_n \cdot \frac{0.51 \cdot Z_n^4}{4\sqrt{I} \cdot \left(1 + \sqrt{I}\right)^2} \right) \cdot B_n \cdot \frac{\frac{\partial C_n}{\partial x}}{\frac{\partial C_{ion}}{\partial x}} \right)}{\sum_n \left(Z_n^2 \cdot B_n \cdot C_n \right)} \right) \cdot B_{ion}$$

Also the diffusion coefficient of ion at different temperature can be written as follows;

$$D_{ion,T_2} = \exp\left[\frac{\Delta E}{R}\left(\frac{1}{(20 + 273)} - \frac{1}{T_2} \right) \right] \cdot D_{ion,20}$$

(5-15)

where, $D_{ion,T}$: diffusion coefficient (cm²/sec)

  ΔE : activation energy of Cl⁻ diffusion (=16.8 kcal/mol)

  R : gas constant (=1.99 cal/K/mol)

  T : absolute temperature (K)

Therefore the ion flux can be obtained as follows;

$$J_{Cl} = -\left\{ k \cdot T \cdot B_{Cl} \cdot \left(1 - \ln 10 \times C_{Cl} \cdot \frac{0.51 \cdot Z_{Cl}^4}{4\sqrt{I} \cdot \left(1 + \sqrt{I}\right)^2}\right) - Z_{Cl} \cdot B_{Cl} \cdot C_{Cl} \cdot \frac{k \cdot T \cdot \sum_n \left(Z_n \cdot \left(1 - \ln 10 \times C_n \cdot \frac{0.51 \cdot Z_n^4}{4\sqrt{I} \cdot \left(1 + \sqrt{I}\right)^2}\right) \cdot B_n \cdot \frac{\partial C_n}{\partial x} \cdot \frac{\partial C_{Cl}}{\partial x}\right)}{\sum_n \left(Z_n^2 \cdot B_n \cdot C_n\right)} \right\} \cdot$$

$$\exp\left[\frac{\Delta E}{R}\left(\frac{1}{(20+273)} - \frac{1}{T_2}\right)\right] \cdot \frac{\partial C_{Cl}}{\partial x} \quad (5\text{-}16)$$

(e) Cl⁻ speciation model

Cl⁻ which permeates in concrete are fixed in solid phase. In order to calculate the Cl⁻ diffusion in concrete it is necessary to use the reliable model of Cl⁻ adsorption phenomenon to the wall of cement phase. In this study the Maruya's model is used as the Cl⁻ adsorption model[5-7]. In this model 3 kinds of Cl are defined as follows; (1) fixed Cl in the cement phase, (2) fixed Cl⁻ on the wall of cement phase, (3) free Cl⁻. Here the migration of Cl⁻ occur only free Cl⁻. This quantity of free Cl⁻ can be calculated from the following equations.

$$C_{fixed} = \alpha_{fixed} \cdot C_{tot} \quad (5\text{-}17)$$

$$C_{free} = C_{tot} - C_{fixed} \quad (5\text{-}18)$$

where, C_{tot} : quantity of total Cl (wt% of cement)

C_{fixed} : quantity of fixed Cl (wt% of cement)

C_{free} : quantity of free Cl⁻ (wt% of cement)

α_{fixed} : immobilization coefficient

The value of α_{fixed} depends on the quantity of total Cl and kinds of binder and the α_{fixed} of ordinary Portland cement can be expressed by Equation (5-19).

$$\left. \begin{array}{ll} \alpha_{fixed} = 1 & C_{tot} \leq 0.5 \\ \alpha_{fixed} = 1 - 0.5 \cdot \left(C_{tot} - 0.5\right)^{0.39} & 0.5 \leq C_{tot} \leq 4.5 \\ \alpha_{fixed} = 0.141 & 4.5 \leq C_{tot} \leq 10.0 \end{array} \right\} \quad (5\text{-}19)$$

(g) Boundary conditions

The boundaries of this method are interface-m, which is the exposure surface, and interface-0, which is the deepest part of the concrete.

The ion concentration at interface m is assumed to be equal to the external environment. Also, the engineering absolute mobility at outer interface is assumed to be equal to that of absolute mobility in the dilute solution. In other words, at outer interface, the pore ratio ε and the tortuosity factor τ are assumed to equal 1. Incidentally, the ion concentration gradient, required when calculating the flux at interface-m, is defined as shown in **Fig. 5.3.5**. Also, ion migration does not occur at the interface-0.
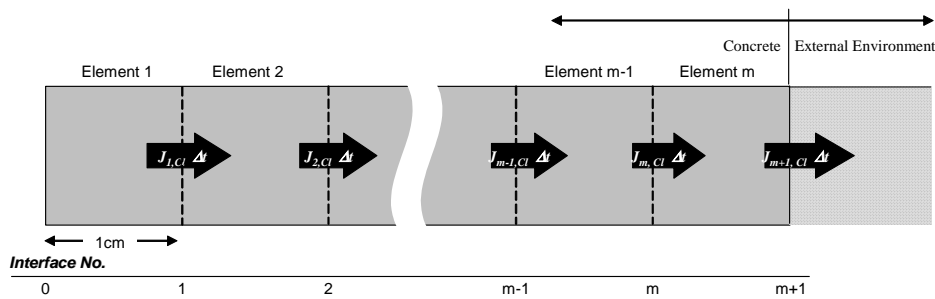
Fig. 5.3.5 Boundary Condition.

(2) Influence of temperature on Cl⁻ distribution considering regional and seasonal temperature effects

Fig. 5.3.6 shows the prediction results of Cl⁻ distribution after 1, 5, 10, 20 years in several cities in Japan. From these figures it can be seen that the distributions of Cl⁻ concentration in several cities are influenced by regional or seasonal temperature. For example the rate of Cl⁻ diffusion of Naha-city (average temp: 22.7℃) is more than 2 times of Nemuro-city (average temp.: 6.1℃). From this result it can be realized that it is necessary to apply the appropriate maintenance method to reinforced concrete member considering the influence of temperature on Cl⁻ diffusion.

(a) Naha

(b) Miyako-Island

(c) Fukuoka

(d) Kagoshima

(e) Kochi

(f) Hiroshima

(g) Matsue

(h) Kyoto

(i) Gifu

(j) Kofu

(k) Tokyo

(l) Niigata

(m) Sendai

(n) Wakkanai

(o) Nemuro
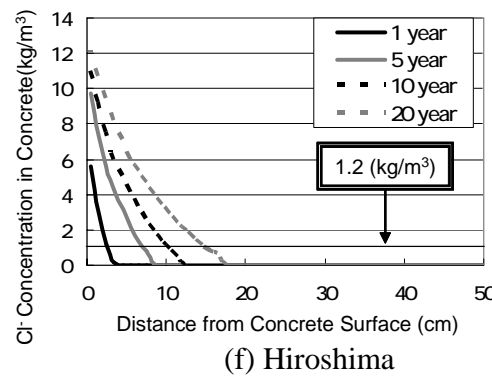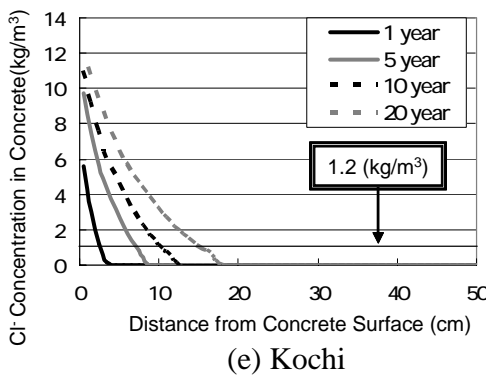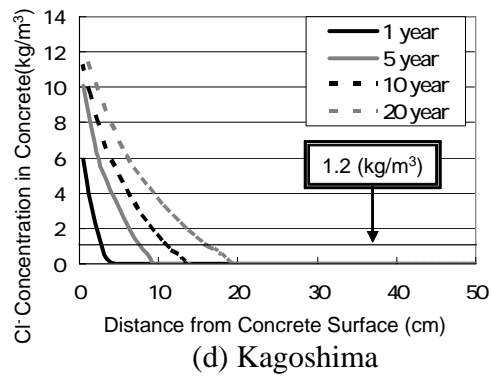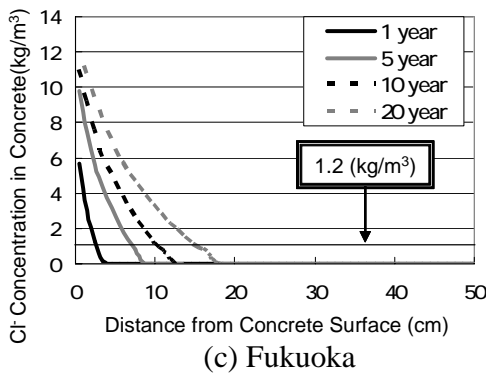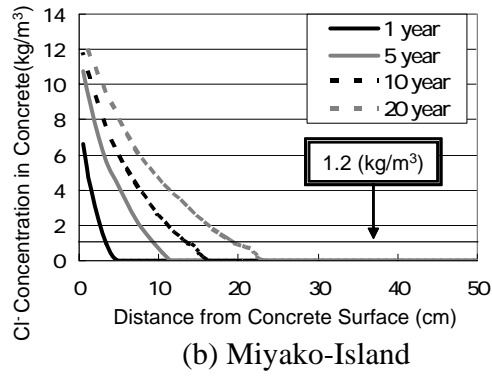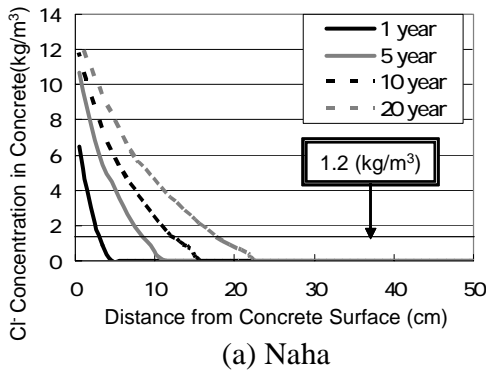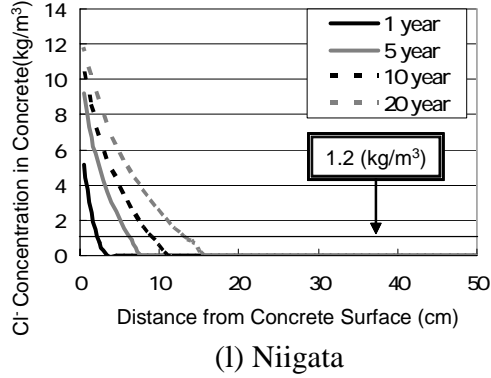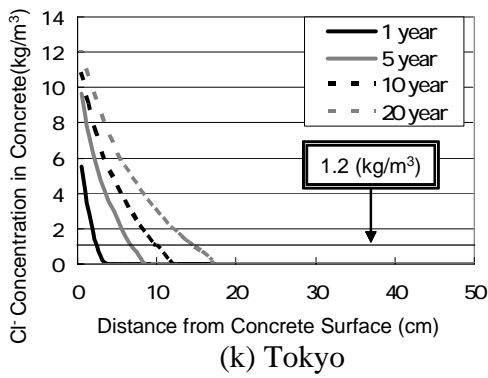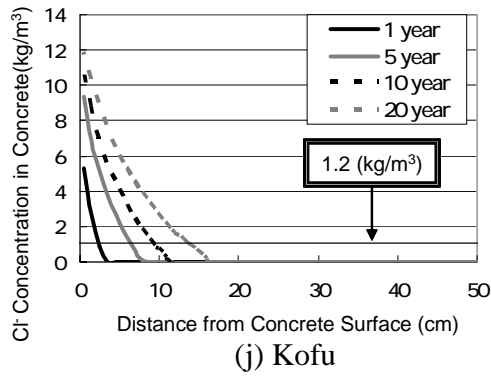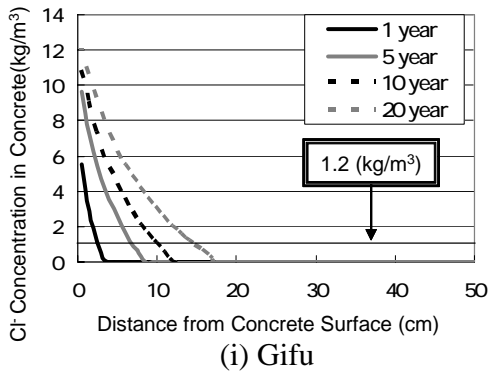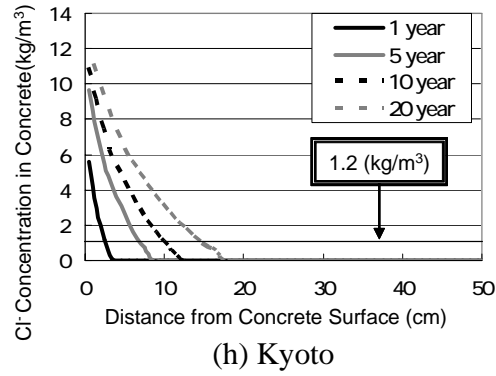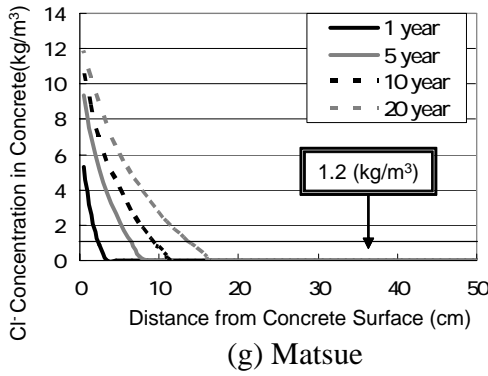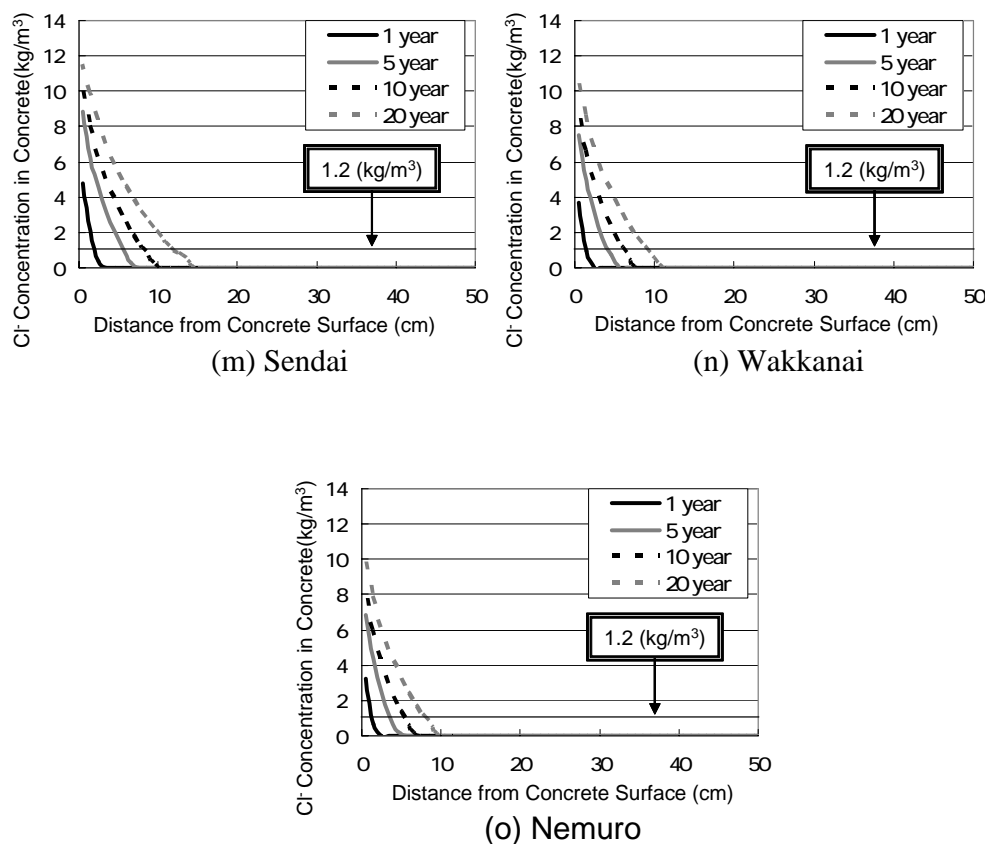
Fig. 5.3.6 Prediction Results of Cl⁻ Distribution

5.3.3 Cl⁻ Induced Corrosion in Concrete Considering Regional and Seasonal Temperature

In this section the rate of steel corrosion in reinforced concrete induced by Cl⁻ considering the temperature effect is investigated. The total quantity of corrosion is calculated by the sum of the quantity of corrosion in each month. The method and results of prediction for total quantity of steel corrosion in concrete considering temperature effect are discussed as following.

(1) Method of prediction

Considering the influence of temperature on deterioration of reinforced concrete, the rate of corrosion of steel bar (macrocell and microcell) in concrete is different from each month. Especially it is confirmed that the influence of temperature on macrocell and microcell corrosion is different in previous chapters. Therefore when

the deterioration progress of steel corrosion is predicted, it is necessary to consider the influence of temperature on macrocell and microcell corrosion rate respectively.

In case of prediction of progress of corrosion in concrete it is necessary to know the basic rate of corrosion at a temperature. In this section the corrosion rate at 20 ℃ shown in **Table 5.3.4** are used. In case of the corrosion rate of steel bar in concrete before cracking, the experimental results obtained in Chapter 2 are used. On the other hand in case of the corrosion rate after cracking, the experimental results obtained by Miyazato[5-9] are used.

The total quantity of corrosion is calculated by the sum of the quantity of corrosion in each month. Here it is reported that the total quantity of corrosion for crack propagation equals to 10 mg/cm^2. Also it is reported that the bending property of reinforced concrete becomes 70% of initial property when 15 % of the steel bar decreases due to corrosion.[5-9] In this case the quantity of corrosion becomes about 510 mg/cm^2 (diameter of steel bar: 19mm). In this study above values are used in order to determine the periods of cracking and structural deterioration.

Table 5.3.4 Corrosion Rate of Steel Bar in Concrete at 20 ℃.

	Corrosion rate at 20 ℃ (mm/year)	
	Macrocell	Microcell
Before cracking	0.00555	0.000264
After cracking	0.02	0.06

(2) Influence of temperature on Cl$^-$ induced corrosion in concrete considering regional and seasonal temperature effects

Fig. 5.3.7 shows the prediction results of the total quantity of corrosion. From these figures it can be seen that the total quantity of corrosion in several cities is influenced by regional or seasonal temperature. For example the rate of Cl$^-$ induced corrosion of Naha-city (average temp: 22.7℃) is more than 3 times of that of Nemuro-city (average temp.: 6.1℃). From this result it can be seen that it is necessary to apply the appropriate maintenance method to reinforced concrete member considering the influence of temperature on rate of corrosion induced by Cl$^-$.
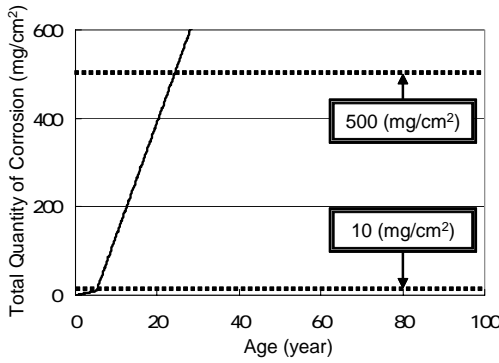
(a) Naha
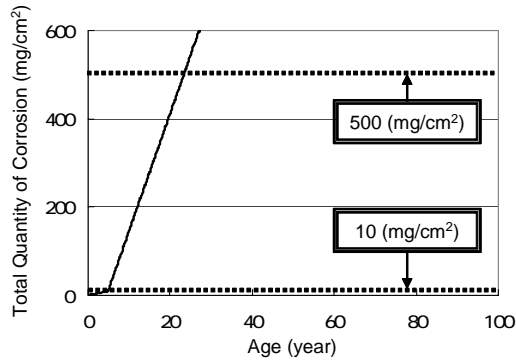
(b) Miyako Island
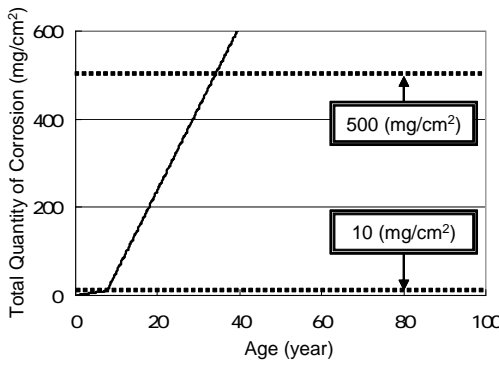
(c) Fukuoka
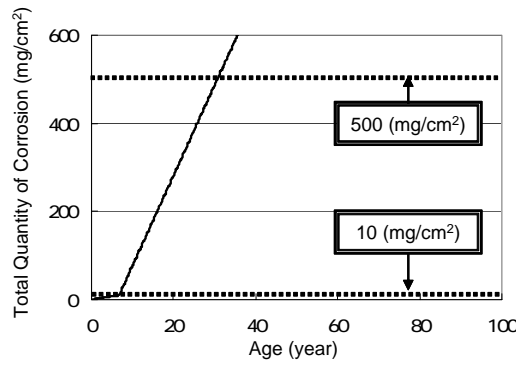
(d) Kagoshima
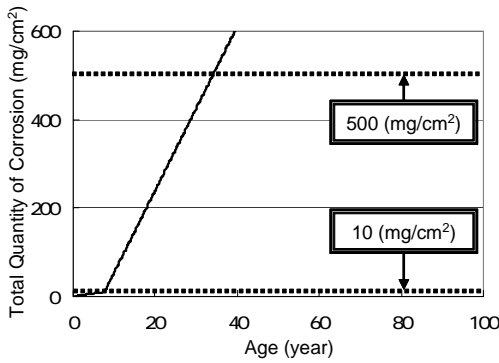
(e) Kohchi
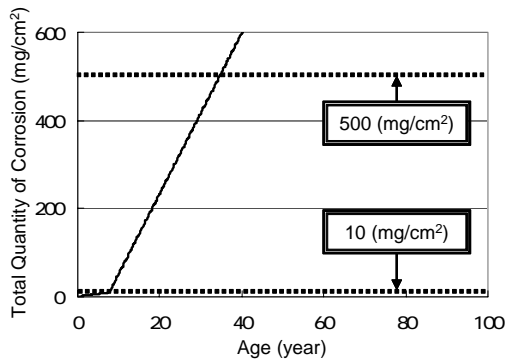
(f) Hiroshima
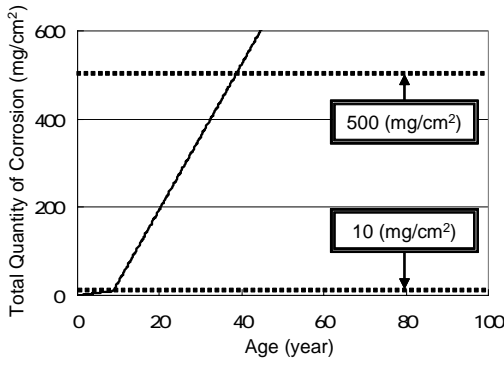
(g) Matsue
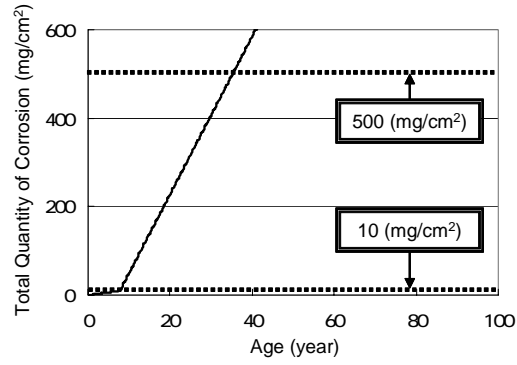
(h) Kyoto
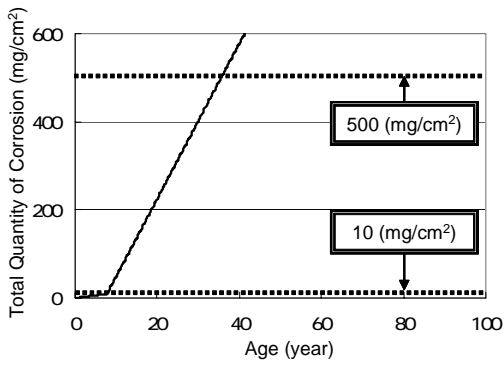
(i) Gifu

(j) Kouhu

(k) Tokyo

(l) Niigata

(m) Sendai

(n) Wakkanai

(o) Nemuro
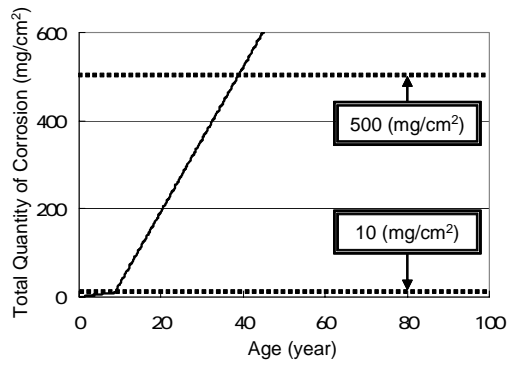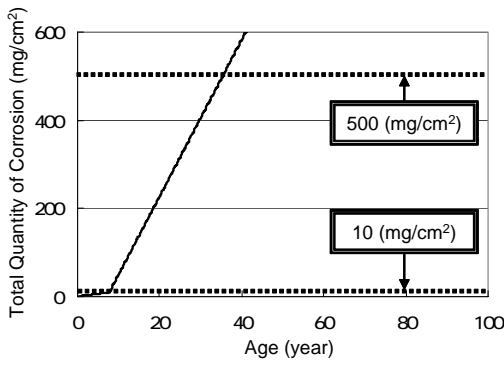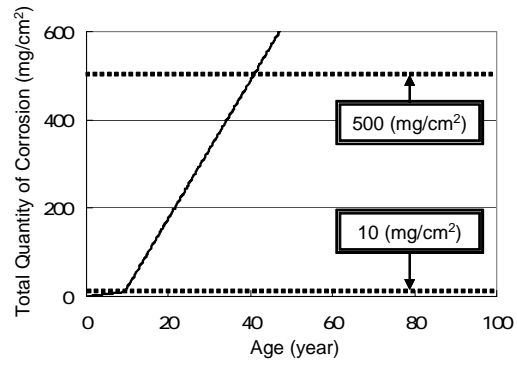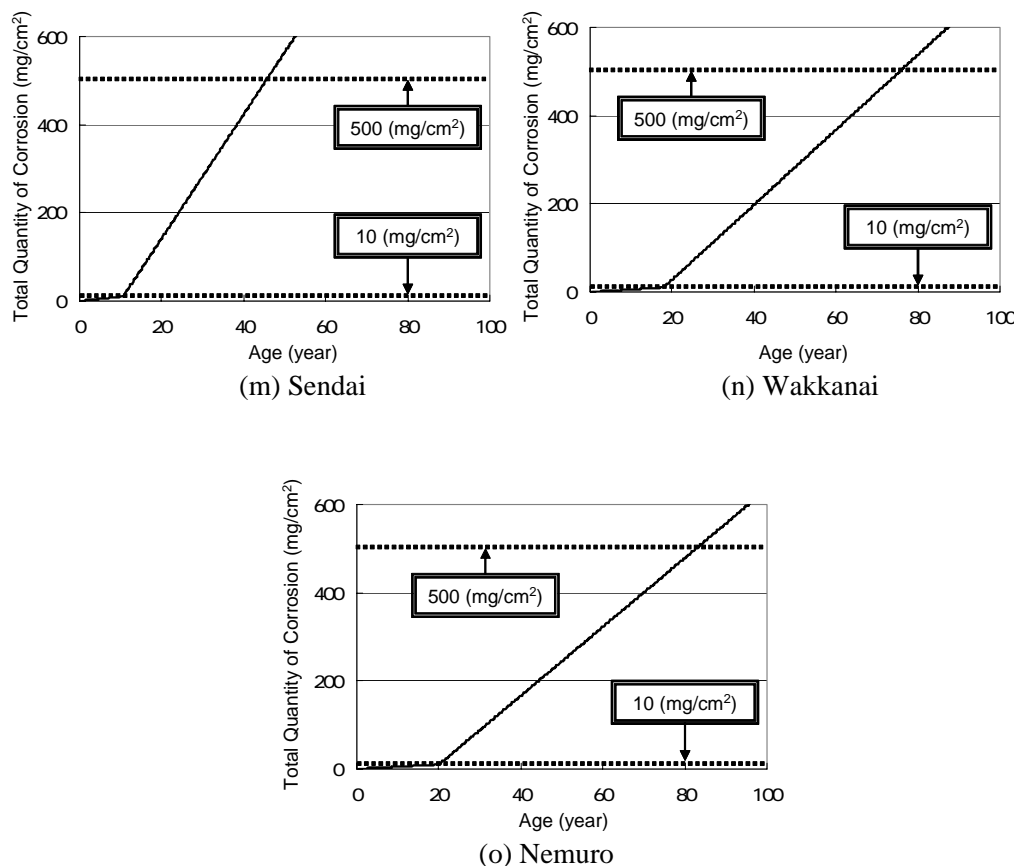
Fig. 5.3.7 Prediction Results of Total Quantity of Corrosion

5.3.4 Discussion of Deterioration Progress Considering Regional and Seasonal Temperature

In this section the deterioration period (incubation, propagation, acceleration periods) are calculated using the results of **5.3.2** and **5.3.3**. In case of determination of deterioration progress of reinforced concrete, the threshold values used in this section are shown in **Table 5.3.5**. Here the water cement ratio, water content in mixture proportion and concrete cover are set at 55%, 175kg/m^3 and 7.0cm respectively. The environmental condition considered in this prediction is tidal zone which is the most sever environment for chloride attack.

Table 5.3.5 Threshold Values for Determination of Deterioration Periods.

Incubation period	Concentration of Cl$^-$ (kg/m^3)	1.2
Propagation period	Total quantity of corrosion at cracking (mg/cm^2)	10
Acceleration period	Total quantity of corrosion at　70% of initial loading capacity (mg/cm^2)	510

Table 5.3.6 shows the deterioration period of reinforced concrete induced by Cl$^-$ in several cities. From this table it can be seen that the period of inculcation, propagation and acceleration is quite different from cities. The shortest period of deterioration is about 20 years such as Ho Chi Minh, Bangkok or Manila and these cities are located in South-East Asia. On the other hand the longest period is more than 100 years such as Stockholm, Nemuro and Moscow.

Fig. 5.3.8 shows the relationship between life time of reinforced concrete and average temperature. From this figure it is confirmed that the period of inculcation, propagation and acceleration varied with the regional and seasonal temperature, and the life time of reinforced concrete exponentially decreased with the temperature of the city increasing. Therefore when the reinforced concrete structure is designed or maintained it is necessary to consider the temperature effect.

And it is indicated that the cities in South-East Asian countries is most severe environment against steel corrosion in concrete from the viewpoint of temperature effect and the life time of reinforced concrete in South-East Asia becomes 70% of that in mild temperature environment (20ºC).

Table 5.3.6 Deterioration Period of Reinforced Concrete at Several Cities.

	Name of City		Average Temp.	Incubation Period	Propergation Period	Acceleration Period	life Time
			°C	year	year	year	year
1		Naha	22.7	4.0	5.2	19.7	28.9
2		Miyako	23.3	3.7	4.9	18.6	27.2
3		Fukuoka	16.6	6.2	7.7	26.5	40.4
4		Kagoshima	18.3	5.4	6.8	23.9	36.1
5		Kohchi	16.6	6.2	7.7	26.5	40.4
6		Hiroshima	16.1	6.3	7.8	26.8	40.9
7		Matsue	14.6	7.4	8.8	29.6	45.7
8	Asia Japan	Kyoto	15.6	6.4	7.8	27.6	41.8
9		Gifu	15.5	6.5	7.8	27.8	42.1
10		Koufu	14.3	7.5	8.8	29.9	46.2
11		Tokyo	15.9	6.5	7.8	27.7	42.0
12		Niigata	13.5	7.7	9.3	31.5	48.5
13		Sendai	12.2	9.3	10.7	34.8	54.7
14		Wakkanai	6.6	15.6	17.9	57.7	91.2
15		Nemuro	6.1	19.1	20.0	62.8	101.9
16		Beijing	13.0	7.5	8.8	31.8	48.2
17		Shanghai	15.8	6.7	7.7	27.4	41.8
18		Dalian	11.2	9.4	11.4	38.7	59.5
19		Guangzhou	22.2	4.0	5.2	19.4	28.6
20		Nanking	15.1	6.5	7.7	27.7	41.9
21		Hong Kong	22.9	3.8	4.9	18.7	27.4
22		Taipei	22.4	4.0	5.2	19.3	28.5
23	Asia	Seoul	11.8	8.8	10.5	36.4	55.7
24		Singapore	26.4	3.0	4.0	15.6	22.6
25		Manila	27.5	2.6	3.7	14.6	20.9
26		Kuala Lumpur	26.6	2.8	4.0	15.5	22.3
27		Bangkok	27.7	2.6	3.6	14.4	20.6
28		Ho Chi Minh	27.9	2.5	3.6	14.3	20.4
29		Hanoi	24.0	3.6	4.7	17.7	26.0
30		Jakarta	27.3	2.7	3.8	14.8	21.3
31		New Delhi	24.3	3.6	4.3	16.6	24.5
32		New York	12.5	8.4	9.6	33.0	51.0
33		Los Angeles	17.4	6.6	7.8	27.7	42.1
34		San Francisco	13.3	10.4	11.1	35.8	57.3
35		Chicago	10.4	10.0	11.6	39.7	61.3
36		Houston	20.5	4.4	5.7	21.3	31.4
37	U.S.A. continent	Honolulu	24.8	3.5	4.6	17.3	25.4
38		Atlanta	16.0	6.5	7.8	27.6	41.8
39		Montreal	6.4	13.5	15.6	49.5	78.6
40		Vancouver	9.8	13.7	14.2	43.8	71.7
41		Mexico City.	15.6	8.3	9.3	30.9	48.5
42		Sao Paulo	21.7	4.6	5.7	20.8	31.1
43		London	9.5	14.6	14.7	45.1	74.4
44		Paris	10.6	12.0	13.0	41.3	66.3
45		Milan	12.1	9.5	10.6	35.3	55.4
46		Roma	15.4	7.7	8.7	29.7	46.1
47		Vienna	9.8	12.0	12.8	41.5	66.3
48	Europe	Brussel	9.8	13.7	13.8	43.4	70.9
49		Amsterdam	10.6	12.4	12.9	41.1	66.4
50		Dusseldorf	11.2	11.3	12.3	39.0	62.6
51		Geneva	10.4	11.6	12.7	40.5	64.8
52		Stockholm	6.3	18.8	19.8	62.7	101.3
53		Moscow	4.7	18.5	19.7	63.8	102.0
54	Oceania	Sydney	17.8	6.3	7.5	26.3	40.1
55		Melbourne	14.1	9.1	10.2	33.4	52.7
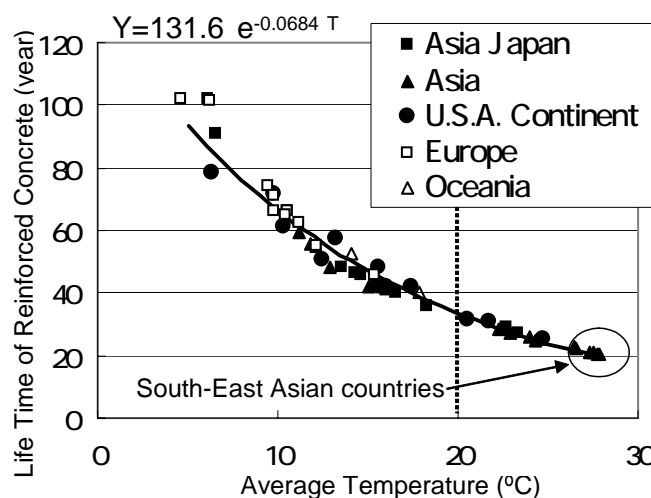
Fig. 5.3.8 Relationship between Life Time of Reinforced Concrete and Average Temperature.

5.4 Summary of Chapter 5

The conclusions derived from this chapter can be summarized as follows:

1. It was confirmed that the period of inculcation, propagation and acceleration varied with the regional and seasonal temperature, and the life time of reinforced concrete exponentially decreased with the temperature of the city increasing.

2. It was indicated that the environment in the cities of South-East Asian countries was the most severe environment against steel corrosion in concrete from the viewpoint of temperature effect and the life time of reinforced concrete in South-East Asia became 70% of that in mild temperature environment (20ºC).

3. From the Arrhenius equation it could be said that the deterioration progress of the reinforced concrete structure at T_2 became $\exp\left[\dfrac{\Delta E}{R}\left(\dfrac{1}{T_1}-\dfrac{1}{T_2}\right)\right]$ times of that at T_1.

Using this relation, the influence of temperature on the deterioration progress of reinforced concrete structures could be expressed. Additionally it was indicated that the temperature dependencies of deterioration progress of reinforced concrete were different from the kinds of deterioration (Cl^- induced corrosion or CO_2 induced corrosion) as shown in **Table 5.4.1**

Table 5.4.1 Magnification of Deterioration Progress of Reinforced Concrete against 20°C

	Cl⁻ induced corrosion		CO₂ induced corrosion	
30ºC /20ºC	2.0 ~ 4.4 times (Cl⁻ diffusivity)		1.2 ~ 1.3 times (Carbonation coefficient)	
30ºC /20ºC	1.3~3.1 times (Macrocell Corrosion)	1.3~3.1 times (Microcell Corrosion)	1.3~3.1 times (Macrocell Corrosion)	1.3~3.1 times (Microcell Corrosion)
40ºC /20ºC	3.7 ~ 17.3 times (Cl⁻ diffusivity)		1.4 ~ 1.6 times (Carbonation coefficient)	
40ºC /20ºC	1.7 ~ 9.0 times (Macrocell Corrosion)	3.0 ~ 9.0 times (Microcell Corrosion)	4.2 ~24.0times (Macrocell Corrosion)	5.2 ~26.8times (Microcell Corrosion)

4   The distributions of Cl⁻ concentration in several cities were influenced by regional or seasonal temperature. For example the rate of Cl⁻ diffusion of Naha-city (average temp: 22.7ºC) was more than 2 times of Nemuro-city (average temp.: 6.1ºC). From this result it can be realized that it was necessary to apply the appropriate maintenance method to reinforced concrete member considering the influence of temperature on Cl⁻ diffusion.

5   The total quantity of corrosion in several cities was influenced by regional or seasonal temperature. For example the rate of Cl⁻ induced corrosion of Naha-city (average temp: 22.7ºC) was more than 3 times of that of Nemuro-city (average temp.: 6.1ºC). From this result it can be realized that it was necessary to apply the appropriate maintenance method to reinforced concrete member considering the influence of temperature on rate of corrosion induced by Cl⁻.

References of Chapter 5

5-1)   Japan Concrete Institute, Practical Guideline for Investigation, Repair and Strengthening of Cracked Concrete Structures, (2003).

5-2)   Japan Society of Civil Engineering Concrete Committee, Standard

Specification for Concrete [Maintenance Edition], (2001).

5-3)   Minagawa, H., Otsuki, N., Miyazato, S., Nishida, T., Establishment of Numerical Analysis Method For the Prediction of Leaching of Calcium from Concrete Considering Migration of Multiple Ions, Concrete Library of JSCE No.40,pp.253-268 (2002).

5-4)   Hladik, J., Physics of Electrolytes Volume 1, Transport processes in Solid Electrolytes and in Electrode, Academic Press, London, pp.418-420 (1972).

5-5)   Robinson R.A., and Stokes, R.H., Electrolyte Solutions, Butterworths, London, p.78. (1955).

5-6)   Minagawa, H. Evaluation of Ion Migration and Prediction of Deterioration of Concrete for Chloride Attack and Ca Leaching, Doctoral Thesis of Tokyo Institute of Technology, (2004).

5-7)   Maruya, T., Tangtermsirikul, S., Matsuoka, Y., Simulation of Chloride Movement in Hardened Concrete, Journal of Materials, Concrete Structures and Pavements, Japan Society of Civil Engineers, No.442/V-16, pp.81-90 (1992).

5-8)   Tsuchiya, M., Toda, S., Haraguchi, H., Analytical chemistry I, Maruzen-Shuppan, pp. 136-137 (1988).

5-9)   Miyazato, S., Study on Macrocell Corrosion Induced by Chloride attack or Carbonation at Defect in Reinforced Concrete, Doctoral Thesis of Tokyo Institute of Technology, (2001).

Chapter 6

Conclusions.

The main objectives of this study became as follows; (1) To investigate the influence of temperature on the rate of diffusion of substance and steel corrosion in concrete induced by Cl^- or CO_2, (2) To study the influence of temperature on deterioration of reinforced concrete using the activation energy calculated by Arrhenius theory using the result of the objective (1), and (3) To predict the deterioration progress of reinforced concrete considering the temperature effect.

As a result of this study, it was confirmed that the Cl^- diffusivity and carbonation coefficient of concrete increased with the temperature rising. Also the rate of macrocell and microcell steel corrosion in concrete induced by Cl^- and CO_2 increased with the temperature rising. Additionally it was confirmed that the logarithms of this phenomenon, diffusion of substance or steel corrosion in concrete, were proportional to the reciprocal of absolute temperature. This fact indicated that the deterioration of reinforced concrete due to the steel corrosion induced by Cl^- or CO_2 apparently agreed with the Arrhenius theory.

After considering the above results, the activation energies of deterioration phenomenon of reinforced concrete were calculated based on Arrhenius theory. As a result, the activation energies of diffusion of harmful substance against steel corrosion in concrete such as Cl^-, CO_2 and O_2 obtained were 12.0 to 32.2kcal/mol, 3.1 to 3.9kcal/mol and 10.5 to 23.8kcal/mol respectively. It was also confirmed that these values were largely influenced by the property of concrete, especially the pore

structure of concrete derived from mix proportion. On the other hand, the activation energy of steel corrosion in concrete induced by Cl^- and CO_2 obtained were 5.2 to 19.4 kcal/mol and 7.2 to 44.5 kcal/mol respectively. These activation energies seemed to be changed with the property of concrete or the kind of substance. And it was confirmed that the rates of macrocell corrosion and the microcell corrosion had different temperature dependency. Especially, it was considered that the rate of macrocell corrosion seemed to be easily influenced by concrete resistance and the activation energy increased with the concrete resistance increasing. Also it was confirmed that the activation energy of corrosion of steel bar was almost same with that of oxygen permeability when the corrosion rate of steel bar in concrete controlled by oxygen permeability.

Finally, the deterioration progress of reinforced concrete due to steel corrosion induced by Cl^- was discussed using the data of temperature of various cities in the world. According to the results, it was confirmed that the period of inculcation, propagation and acceleration varied with the regional and seasonal temperature, and the life time of reinforced concrete exponentially decreased with the temperature of the city increasing. Especially it was indicated that the environment in the cities of South-East Asian countries was the most severe environment against steel corrosion in concrete from the viewpoint of temperature effect. The life time of reinforced concrete in South-East Asia became 70% of that in mild temperature environment (20℃).

Conclusions Obtained in Each Chapter

Conclusions of Chapter 2

1   It was confirmed that the Cl^- diffusivity of concrete increased with the temperature rising. Also the rate of macrocell and microcell corrosion of steel bar in concrete induced by Cl^- increased with the temperature rising. Especially the Cl^- diffusivity became almost 1.6 ~7.5 times, while the corrosion rate of steel bar in concrete induced by Cl- became almost 1.2 ~3.5 times with 10 ℃ of temperature rising.

2   The logarithms of these phenomena, diffusion of substance or corrosion of steel

bar in concrete, were proportional to the reciprocal of absolute temperature. This fact indicated that the deterioration of reinforced concrete due to the steel corrosion induced by Cl^- apparently agreed with the Arrhenius theory.

3 The Cl^- diffusivity in concrete increased with the higher position of concrete. This tendency became larger in case of concrete with high bleeding.

4 Macrocell and microcell corrosion rate in concrete influenced by bleeding became high with the bleeding ratio increasing. Moreover, higher macrocell corrosion rate generally prevailed in concrete influenced by bleeding.

Conclusions of Chapter 3

1 It was confirmed that the carbonation coefficient of concrete increased with the temperature rising. Also the rate of macrocell and microcell corrosion of steel bar in concrete induced by CO_2 increased with the temperature rising. Especially the carbonation coefficient of concrete became 1.2~1.9 times with 10 ℃ of temperature rising, while the corrosion rate of steel bar in concrete induced by CO_2 became 1.4 ~ 3.5 times with 10 ℃ of temperature rising.

2 The logarithms of above phenomenon, diffusion of substance or corrosion of steel bar in concrete, were proportional to the reciprocal of absolute temperature. This fact indicated that the deterioration of reinforced concrete due to the steel corrosion induced by CO_2 apparently agreed with the Arrhenius theory.

3 Concrete specimens containing Ordinary Portland cement had shown better performance against carbonation and corrosion at lower temperature (20°C) as compared with Blast Furnace Slag Cement. On the other hand, Blast Furnace Slag Cement concrete performed better at higher temperature (30°C and 40°C) as compared with Ordinary Portland Cement concrete and High Early Strength Cement concrete.

4 The corrosion rate of steel bar in concrete induced by CO_2 was largely influenced by carbonation reminder and oxygen permeability of concrete.

5 Macrocell and microcell corrosion rate in concrete with cold-joint became high with the bleeding ratio increasing. Moreover, higher macrocell corrosion rate generally prevailed in concrete with cold-joint. This tendency was also confirmed in existing reinforced concrete constructed 35 years ago.

Conclusions of Chapter 4

1 The activation energies of deterioration phenomenon of reinforced concrete were

calculated based on Arrhenius theory. As a result, the activation energies of diffusion of harmful substance against steel corrosion in concrete such as Cl^-, CO_2 and O_2 obtained were 12.0 to 32.2kcal/mol, 3.1 to 3.9kcal/mol and 0.5 to 23.8kcal/mol respectively. It was also confirmed that these values were largely influenced by the property of concrete, especially the pore structure of concrete.

2   The activation energy of steel corrosion in concrete induced by Cl^- and CO_2 obtained were 5.2 to 19.4 kcal/mol and 7.2 to 44.5 kcal/mol respectively. These activation energies seemed to be changed because the rate-limiting condition changed with the increase of specific concrete resistance. Especially, the activation energy of corrosion of steel bar was almost same with that of oxygen permeability. This indicated that the rate-controlling factor of corrosion rate was mainly the quantity of O_2 around the steel bar and the activation energy of corrosion reaction increases with that of O_2 permeability increasing.

3   It was confirmed that the macrocell corrosion rate and the microcell corrosion rate had different temperature dependency. Especially, the rate of macrocell corrosion seemed to be easily influenced by concrete resistance and the activation energy increased with the concrete resistance increasing.

4   The activation energy of corrosion of steel bar was almost same with that of oxygen permeability when the corrosion rate of steel bar in concrete controlled by oxygen permeability.

Conclusions of Chapter 5

1   It was confirmed that the period of inculcation, propagation and acceleration varied with the regional and seasonal temperature, and the life time of reinforced concrete exponentially decreased with the temperature of the city increasing.

2   It was indicated that the environment in the cities of South-East Asian countries was the most severe environment against steel corrosion in concrete from the viewpoint of temperature effect. The life time of reinforced concrete in South-East Asia became 70% of that in mild temperature environment (20ºC).

3   From the Arrhenius equation it could be said that the deterioration progress of the reinforced concrete at T_2 became $\exp\left[\dfrac{\Delta E}{R}\left(\dfrac{1}{T_1}-\dfrac{1}{T_2}\right)\right]$ times of that at T_1. Using this relation, the influence of temperature on the deterioration progress of reinforced concrete could be expressed. Additionally it was indicated that the temperature dependencies of deterioration progress of reinforced concrete were different from

the kinds of deterioration (Cl^- induced corrosion or CO_2 induced corrosion) as shown in **Table 6.1**

4   The distributions of Cl^- concentration in several cities were influenced by regional or seasonal temperature. For example the rate of Cl^- diffusion of Naha-city (average temp: 22.7ºC) was more than 2 times of Nemuro-city (average temp.: 6.1ºC). From this result it can be realized that it was necessary to apply the appropriate maintenance method to reinforced concrete member considering the influence of temperature on Cl^- diffusion.

5   The total quantity of corrosion in several cities was influenced by regional or seasonal temperature. For example the rate of Cl^- induced corrosion of Naha-city (average temp: 22.7ºC) was more than 3 times of that of Nemuro-city (average temp.: 6.1ºC). From this result it can be realized that it was necessary to apply the appropriate maintenance method to reinforced concrete member considering the influence of temperature on rate of corrosion induced by Cl^-.

Table 6.1 Magnification of Deterioration Progress of Reinforced Concrete against 20°C.

	Cl^- induced corrosion		CO_2 induced corrosion	
30ºC /20ºC	2.0 ~ 4.4 times (Cl^- diffusivity)		1.2 ~ 1.3 times (Carbonation coefficient)	
	1.3~3.1 times (Macrocell Corrosion)	1.3~3.1 times (Microcell Corrosion)	1.3~3.1 times (Macrocell Corrosion)	1.3~3.1 times (Microcell Corrosion)
40ºC /20ºC	3.7 ~ 17.3 times (Cl^- diffusivity)		1.4 ~ 1.6 times (Carbonation coefficient)	
	1.7 ~ 9.0 times (Macrocell Corrosion)	3.0 ~ 9.0 times (Microcell Corrosion)	4.2 ~24.0times (Macrocell Corrosion)	5.2 ~26.8times (Microcell Corrosion)

Publications of Journals Related to This Study

Takahiro Nishida, Nobuaki Otsuki, Akihiro Kinagai, CORROSION RATE OF STEEL BAR AT JOINT AND ITS CONTROL METHOD IN REINFORCED CONCRETE MEMBERS INDUCED BY CARBONATION, Journal of the Society of Materials Science, Vol.52, No.9, pp.1067-1074, (in Japanese) 2003.9.

Takahiro Nishida, Nobuaki Otsuki, Jyunpei Hamamoto, Kyoku Chin, TEMPERATURE DEPENDENCY OF CORROSION RATE OF STEEL BARS IN CONCRETE INFLUENCED BY MATERIAL SEGREGATION, Journal of Materials, Concrete Structures And Pavements, JSCE, V-66, No.781, pp.75-87, (in Japanese) 2005.2.

Takahiro Nishida, Nobuaki Otsuki, Masakazu Ikeda, Champapanh Bouavieng, Masaaki Terashi, PROPOSAL OF A NUMERICAL PREDICTION METHOD FOR CA LEACHING FROM SOIL IMPROVED BY DEEP MIXING METHOD, Journal of Materials, Concrete Structures And Pavements, JSCE, VI-66, No784, pp.205-216, (in Japanese) 2005.3.

Nobuaki Otsuki, Takahiro Nishida, Shinichi Miyazato, Koichi Soeda, EVALUATION OF STEEL CORROSION IN EXISTING CONCRETE MEMBERS USING CALCULATION METHOD FOR MACROCELL CORROSION RATE, Jounal of Structural And Construction Engineering, Transactions of AIJ, No.577, pp.15-20, (in Japanese) 2004.3.

Nobuaki Otsuki, Shinichi Maruyama, Takahiro Nishida, Melito A. Baccay, INFLUENCE OF TEMPERATURE ON CORROSION RATE OF STEEL BAR IN CARBONATED CONCRETE MEMBERS, Journal of the Society of Materials Science, Vol.53, No.1, pp.108-113, (in Japanese) 2004.1.

Nobuaki Otsuki, Wanchai Yodsudjai, Takahiro Nishida, Hiroyuki Yamane, NEW TEST METHODS FOR MEASURING STRENGTH AND CHLORIDE ION DIFFUSION COEFFICIENT OF MINUTE REGIONS IN CONCRETE, ACI Materials Journal, Vol.101, No.2, pp.146-153, 2004.3.

Hiroshi Minagawa, Nobuaki Otsuki, Shinichi Miyazato, Takahiro Nishida, ESTABLISHMENT OF NUMERICAL ANALYSIS METHOD FOR THE PREDICTION OF LEACHING OF CALCIUM FROM CONCRETE CONSIDERING MIGRATION OF MULTIPLE IONS, Journal of Materials, Concrete Structures And Pavements, JSCE, Vol.50, No.697, pp.85-96, (in Japanese) 2002.2.

Publications of International Conference or Symposium Related to This Study

Takahiro Nishida, Nobuaki Otsuki, Jyunpei Hamamoto, Melito Baccay A., INFLUENCE OF TEMPERATURE ON STEEL CORROSION IN REINFORCED CONCRETE AFFECTED BY SEGREGATION, Proceedings of Third International Conference on Construction Materials Parformance, (ConMat'05), (under reviewing) 2005.

Takahiro Nishida, Nobuaki Otsuki, Jyunpei Hamamoto, Melito A. Baccay, INFLUENCE OF TEMPERATURE ON STEEL CORROSION IN REINFORCED CONCRETE AFFECTED BY SEGREGATION, Proceedings of the Symposium on Environmental Issues Related to Infrastructure Development JSPS Manila, pp.533-542, 2003.8.

Nobuaki Otsuki, Takahiro Nishida, Melito Alibuyog Baccay, Akihiro Konagai, CORROSION RATE OF STEEL BAR NEAR COLD-JOINT AND ITS CONTROL METHOD IN REINFORCED CONCRETE MEMBER INDUCED BY CARBONATION, Proceedings of the Fourth Regional Symposium on Infrastructure Development in Civil Engineering (RSID4) Bangkok, Vol.4, pp.471-481, 2003.4.

Shinichi Maruyama, Nobuaki Otsuki, Konagai Akihiro, Takahiro Nishida, INFLUENCE OF TEMPERATURE AND RELATIVE HUMIDITY ON CORROSION RATE OF STEEL BAR AT COLD JOINT IN CARBONATED CONCRETE MEMBERS, Proceedings of the JSPS-DOST Regional Symposium on Construction Materials & Testing, pp.87-94, 2002.9.

Nobuaki Otsuki, Wanchai Yodsudjai, Marietta C. L. Castillo, Takahiro Nishida, Shinichi Maruyama, INFLUENCE

OF TEMPERATURE ON CHLORIDE ION DIFFUSION AND CORROSION RATE OF STEEL BARS IN CONCRETE, Proceedings of the International Scientific Workshop Cement And Concrete Technology Vietnam, pp.20-26, 2003.12.

Marieta Cristine Castillo, Wanchai Yodsudjai, Nobuaki Otsuki, Takahiro Nishida, INFLUENCE OF EXPOSURE TEMPERATURE ON THE CHLORIDE ION DIFFUSIVITY IN THE MINUTE REGION OF THE CEMENT MORTAR MATRIX, Proceedings of the Symposium on Environmental Issues Related to Infrastructure Development JSPS Manila, pp.447-454, 2003.8.

Other Publications of Journals and Reviewed Papers

Takahiro Nishida, Nobuaki Otsuki, Ryosuke Onitsuka, Wanchai Yodsudjai, Jyunji Yokokura, STUDY ON STRENGTH AND PERMEABILITY OF CONCRETE USING LOW QUALITY COARSE AGGREGATES FROM CIRCUM-PACIFIC REGION, Journal of Materials, Concrete Structures And Pavements, JSCE, Vol.61, No.746, pp.103-114, (in Japanese) 2003.11.

Nobuaki Otsuki, Takahiro Nishida, Shinichi Miyazato, Hiroshi Minagawa, CLARIFICATION OF ELECTRODEPOSITION MECHANISM AND SELECTION OF BEST ELECTRODEPOSITION CONDITIONS TO REINFORCED CONCRETE ON LAND, Journal of the Society of Materials Science, Vol.51, No.5, pp.573-580, (in Japanese) 2002.5.

Nobuaki Otsuki, Takahiro Nishida, Hiroshi Minagawa, Wanchai Yodsudjai, INVESTIGATION OF DURABILITY OF REINFORCED CONCRETE MEMBER ON LAND REPAIRED BY ELECTRODEPOSITION METHOD, Journal of the Society of Materials Science, Vol.51, No.11, pp.1278-1283, (in Japanese) 2002.11.

Nobuaki Otsuki, Wanchai Yodsudjai, Takahiro Nishida, Hiroyuki Yamane, DEVELOPED METHOD FOR MEASURING FLEXURAL STRENGTH AND MODULUS OF ELASTICITY OF MICRO REGIONS IN NORMAL AND RECYCLED AGGREGATE CONCRETES, Magazine of Concrete Research (England), Vol55, No.5, pp.439-448, 2003.1.

Hiroshi Minagawa, Nobuaki Otsuki, Shinichi Miyazato, Takahiro Nishida, FUNDAMENTAL STUDY ON PREDICTION OF CONCRETE DETERIORATION CAUSED BY CALCIUM LEACHING OVER 100 YEARS, Journal of Materials, Concrete Structures And Pavements, JSCE, Vol.50, No.662, pp.41-49, (in Japanese) 2001.5.

Nobuaki Otsuki, Jae-Suk. Ryou, Shinichi Miyazato, Takahiro Nishida, AN EXPERIMENTAL STUDY ON THE EFFECTIVENESS OF ELECTRODEPOSITION METHOD FOR RC, Concrete Research and Technology, Vol.11, No.1, pp.85-93, (in Japanese) 2000.1.

Nobuaki Otsuki, Shinichi Miyazato, Jae-Suk Ryou, Takahiro Nishida, Makoto Hisada, AN APPLICATION OF ELECTRODEPOSITION METHOD FOR REPAIR OF MORTAR DAMAGED BY DRY SHRINKAGE CRACKS, Journal of the Society of Materials Science, Vol.49, No.2, pp.215-221, (in Japanese) 2000.2.

Melito A. Baccay, Takahiro Nishida, Nobuaki Otsuki, Junpei Hamamoto, Kyoku Chin, INFLUENCE OF BLEEDING ON MINUTE PROPERTIES AND STEEL CORROSION IN CONCRETE, Journal of Advanced Concrete Technology, Vol.2, No.2, pp.187-199, 2004.6.

Takahiro Nishida, Nobuaki Otsuki, Renze Zheng, Melito Alibuyog, SELECTION OF APPROPRIATE ELECTRODEPOSITION CONDITIONS FOR CLOSING CRACKS IN REINFORCED CONCRETE MEMBER INDUCED BY CHLORIDE ATTACK, Proceedings of 4th International Conference on Concrete Under Severe Conditions: Environment and Loading 04, Vol.4, pp.393-400, 2004.7.

Takahiro Nishida, Masaaki Terashi, Nobuaki Otsuki, Kanta Ohishi, PREDICTION METHOD FOR CA LEACHING AND RELATED PROPERTY CHANGE OF CEMENT TREATED SOIL, Proceeding of Third International Conference on Grouting & Ground Treatment, Vol.3, No.2, pp.658-669, 2003.2.

Takahiro Nishida, Nobuaki Otsuki, Hiroshi Minagawa, Wanchai Yodsudjai, INVESTIGATION OF APPLICATION

OF ELECTRODEPOSITION METHOD TO CRACK REPAIR OF EXISTING REINFORCED CONCRETE, Proceedings of the Japan Concrete Institute, Vol24, No.1, pp.1443-1448, (in Japanese) 2002.6.

Wanchai Yodsudjai, Nobuaki Otsuki, Takahiro Nishida, Ryosuke Onitsuka, Evaluation of Micro-Region in Various Concrete with Newly Developed Micro-Bending Method, Proceedings of the Japan Concrete Institute, Vol.24, No.1, pp.255-260, 2002.6.

Awards

Japan Concrete Institute, Paper Award of Japan Concrete Institute, 2005, Japan.

Teshima Commemorative Foundation, The Teshima Commemoration Invention Prize, 2004, Japan.

The Japan Society of Materials Science, Science Encouraging Prize, 2004, Japan.

ACI-Singapore Chapter, ACI-Singapore Chapter Award, 2004, Singapore.

The Japan Society of Materials Science, Excellent Presentation Prize, 2003, Japan.

ACI-Singapore Chapter, Ready-Mixed Concrete Association of Singapore Concrete Award, 2002, Singapore.

ACI-Singapore Chapter, ACI-Singapore Chapter Award, 2001, Japan.

ACI-Singapore Chapter, Young Concrete Researcher Award, 2000, Singapore.

Japan Society of Civil Engineers, 2nd International Summer Symposium Excellent Presentation Prize, 2000, Japan.